Fjord sedimentation during the rapid retreat of tidewater glaciers: observations and modeling

Katherine V. Boldt

A dissertation

submitted in partial fulfillment of the

requirements for the degree of

Doctor of Philosophy

University of Washington

2014

Reading Committee:

Charles Nittrouer, Co-Chair

Bernard Hallet, Co-Chair

Thomas Pratt

Program Authorized to Offer Degree:

Oceanography

University of Washington

Abstract

Fjord sedimentation during the rapid retreat of tidewater glaciers: observations and modeling

Katherine V. Boldt

Co-Chairs of the Supervisory Committee:
Professor Charles Nittrouer
Oceanography
Professor Bernard Hallet
Earth and Space Sciences

Ice-ocean interactions remain poorly understood despite the growing recognition that they play significant roles in the complex behavior of glaciers that reach the oceans, which is of broad interest because it contributes substantially to the challenge of predicting global sea-level rise. This research focuses on the dynamics of sediment accumulation near the calving fronts of tidewater glaciers across a climatic continuum from polar to temperate conditions. Rates and spatial patterns of sediment accumulation merit close attention because they can affect glacier stability by reducing the water depth that controls the calving rate, the surface area available for submarine melting, and the ability of tidewater glaciers to advance into deep water. The sediments produced by these glaciers are also of considerable interest because they record changes in glacial, environmental, and tectonic conditions.

In light of the recent, well documented changes in climate and glacier extent along the Antarctic Peninsula through much of the last century, a detailed study was developed to understand how modern sediments have recorded these regional changes. Sediment

accumulation rates for sixteen cores collected in fjords across a 15° N-S transect from the Antarctic Peninsula to southern Chile were calculated using the decay of naturally occurring radioisotope ^{210}Pb. Records from the Antarctic Peninsula show surprisingly constant rates of sediment accumulation (1-7 mm yr^{-1}) throughout the past century despite rapid warming, increase in surface melt, and glacial retreat. Cores from the South Shetland Islands, on the other hand, reveal accelerated sediment accumulation over the past few decades, likely due to warming and an increase in surface melt in this region, which straddles the boundary between subpolar and temperate conditions. In the temperate fjords of southern Chile, sediment accumulates faster (11-24 mm yr^{-1}). This increase in sediment accumulation with decreasing latitude reflects the gradient from subpolar to temperate climates, and is consistent with glacial erosion being much faster in the very wet, temperate climate of southern Chile than along the colder Antarctic Peninsula.

Links between rates of glacier retreat, ice motion, sediment flux, and the evolution of glacial sediment deposits in a temperate setting are explored using a large existing dataset for Columbia Glacier, Alaska and new oceanographic data from the fjord recently exposed by its retreat. High-resolution seismic data indicate that 3.2×10^8 m^3 of sediment has accumulated over the last three decades; this volume corresponds to erosion at 5.1 ± 1.8 mm yr^{-1} averaged over the entire ~1000 km^2 area of the glacier. A numerical model is developed to relate known patterns of sedimentation and changes in the glacier terminus position to the accumulation of sediment in the fjord during the 30-year period of retreat. The model, which represents both primary sedimentation and secondary reworking, is used to produce a history of the sediment flux from the glacier that is compatible with the observed post-retreat sediment deposit thickness and architecture. The bathymetric history and model results corroborate that the sediment flux increased sixfold within the 1997-2000 period; interestingly this increase is not correlated with concurrent changes in glacier dynamics. It is suggested that the increase resulted from the sediment transport capacity of subglacial rivers increasing due to the retreat-related steepening of the glacier surface over a deep subglacial basin. That major variations in the sediment flux can be controlled by changes in subglacial sediment storage, in addition to changes in climate and the erosion rate, adds richness and complexity to the interpretation of the glacimarine sediment record.

The sediment-flux model is also applied to Jorge Montt Glacier, a Patagonian tidewater glacier with very similar behavior to Columbia Glacier, but without the detailed record of its retreat history and other complementary glaciological data. Sediment volume calculations for both glaciers indicate that the effective erosion rate necessary to sustain the mean sediment fluxes during their respective periods of retreat is surprisingly similar, ~5 mm yr^{-1}, despite differences in the geographic, tectonic, and geologic settings. For both rapidly retreating glaciers, the numerical model yields a sediment-flux history that produces sediment packages generally consistent with observed bathymetry and internal stratigraphic architecture. On the time scale of retreat, temporal variations in the modeled sediment flux from both glaciers are not related to concurrent variations in ice velocity, as expected. Rather, changes in the sediment flux are attributed to the tendency for sediment to be flushed from subglacial basins due to the progressive steepening of the glacier terminus during retreat. In both fjords, model results corroborate that sediment accumulates rapidly (>1 m yr^{-1}) near the ice front. In addition, the model suggests that gravity-driven processes are essential for delivering and redistributing sediment within the fjords to create the observed bathymetry and internal stratigraphic architecture.

Acknowledgments

My deepest gratitude goes to my advisors, Bernard Hallet and Chuck Nittrouer, whose guidance, knowledge, and support were essential to my development as a scientist. I also thank my committee members, Tom Pratt, Andrea Ogston, Michele Koppes, Rebecca Woodgate, and Cecilia Bitz, who have provided an immense amount of insight and encouragement, both personally and professionally.

The work presented here would not have been possible without assistance, collaboration, and commitment from the following colleagues: Michele Koppes, John Anderson, Julia Wellner, Brittany Forrest, Dave Janka, Tom Pratt, Adam Barker, Shaun Finn, Tad Pfeffer, Shad O'Neel, Robert McNabb, Carlos Moffat, JC and Allen Szydlowski and their company *Waters of Patagonia*, Andres Rivera, and Dick Sylwester. Eric Steig and the Quaternary Research Center at the University of Washington provided generous financial support.

I thank my many lab mates over the years, Rip Hale, Dan Nowacki, Aaron Fricke, Emily Eidam, Kristen Lee, and Tina Drexler, for sharing their scientific creativity and insights, as well as their friendship. I am also grateful for the invaluable services and support provided by the engineering and administrative staff at the School of Oceanography.

The continued love and support from my family and friends made this dissertation possible.

Table of Contents

List of Figures

List of Tables

Chapter 1: Introduction

1.1 Broader Context

The recent loss of ice from glaciers and ice sheets worldwide is often used as dramatic and visible evidence of global climate change. Their societal and environmental implications grow as sea levels rise and water resources are impacted, and as these changes continue to outpace projections. Some of the most rapid mass loss has occurred in the dynamic glaciers reaching the sea from Greenland, Antarctica, and Alaska (Arendt et al., 2002; Howat et al., 2007; Rignot et al., 2011). Together, the shrinkage of these glaciers accounts for ~80% of global sea-level rise due to ice loss and highlights a direct connection between the cryosphere and the global ocean (Jacob et al., 2012). The mechanism by which ocean heat affects the stability of these glaciers is not well known, however, and uncertainty in the dynamic response of these large glaciers limits projections of sea-level rise (Lemke et al., 2007; Meier et al., 2007; Pfeffer et al., 2008; Straneo et al., 2013).

Much contemporary research is devoted to understanding the causes and implications of the changes along ice-sheet and glacier margins (e.g., Holland et al., 2008; Joughin et al., 2012; Sutherland and Straneo, 2012). A series of retreat mechanisms likely accounts for these rapid changes, including: 1) surface melt thins the ice and allows flotation; 2) surface melt increases water-induced fracturing and calving; 3) warmer ocean water melts more ice below sea level; and 4) decreased sea ice reduces buttressing support (Figure 1.1) (e.g., Vieli and Nick, 2011). Each of these mechanisms accelerates with increasing temperatures of the air and/or water.

Documenting these mechanisms requires further research and has been highlighted as a major scientific priority in recent climate change reports (e.g., IPCC, 2013; Straneo et al., 2013).

A facet of the ice-ocean interface that has received relatively less attention is the role of glacially derived sediment in the stability of these glaciers. Terminal-moraine sediments have long been recognized to control the advance of tidewater glaciers by decreasing the water depth at the terminus, allowing the glacier to advance into deep water (Alley, 1991; Powell, 1991; Hunter et al., 1996b; Nick et al., 2007; Goff et al., 2012). The advance rate is governed by how quickly the glacier can erode and redeposit sediment to the seaward side of the moraine (Figure 1.2) (Meier and Post, 1987). Models of continental-scale ice sheets also highlight the critical role of the sediment shoal in allowing ice to advance into deep ocean water over tens of millions of years, even in the absence of direct climatic forcing (Pollard and DeConto, 2007).

Large, recent fluctuations in the termini of outlet glaciers draining the a significant portion of the Greenland and Antarctic Ice Sheets provide considerable impetus for understanding the processes controlling the stability of these ice masses on much shorter (< 100 yr) time scales. Modern fjords constitute ideal natural laboratories for illuminating these underlying processes, as many retreating tidewater glaciers are relatively accessible for oceanographic studies. Moreover, they produce relatively large meltwater and sedimentary signals (e.g., Hallet et al., 1996; Koppes and Hallet, 2002; 2006) that are related to subglacial processes on diverse time scales ranging from events lasting minutes to many decades (e.g., Cowan et al., 1988; 1997; 1999; Jaeger and Nittrouer, 1999a). In addition, studies of sedimentary processes along the ice-ocean interface will help refine poorly constrained parameters, such as the sediment production rate, to more accurately model ice behavior over cycles of advance and retreat (Nick et al., 2007). Establishing a direct link between ice behavior, the formation of sediment shoals, and ice-proximal sediment deposits will help increase the accuracy and resolution of interpretations from glacimarine sediment archives on longer time scales (Cowan et al., 1997; Anderson et al., 2002; Andresen et al., 2011).

1.2 Climate, Ice, and the Ocean

Climate exerts a first-order control on the extent and behavior of glaciers worldwide by modulating the thermal regime of the ice, as well as the rates and patterns of accumulation and ablation on the glacier surface. While the synchronous retreat of ice masses worldwide suggests causation from the global climate (Oerlemans, 2005), no simple relationship exists between climate and the extent of glaciers (e.g., Nick et al., 2007; McNabb and Hock, 2014). The response of glaciers to climate change depends on many factors. The greatest changes occur for tidewater glaciers, as the sensitivity of the terminus position to changes in climate is especially complicated due to additional mass loss by calving and submarine melting (van der Veen, 1996; De Woul and Hock, 2005; Post et al., 2011).

When tidewater glaciers are in their advanced and stable position, climate or ocean changes can trigger instabilities at the termini, causing rapid retreat in deep water (Figure 1.2). Tidewater glaciers tend to exhibit some of the fastest ice speeds and rates of retreat worldwide, as exemplified by the large, recent changes along the margins of the Greenland Ice Sheet (Rignot and Kanagaratnam, 2006; Howat et al., 2007; Joughin et al., 2008). The simple interpretation of this rapid retreat as direct evidence of a warming climate can be misleading, however, as it is highly nonlinear with respect to climate and can be “relatively independent of direct climate forcing” (Meier and Post, 1987; Pfeffer, 2007; Post et al., 2011; McNabb and Hock, 2014). The external forcing is strongly modulated by internal glacier dynamics as well as by the rate of calving, but the relationship between these two processes remains poorly understood. Models of calving suggest that the calving rate increases linearly with water depth; thus glacier retreat into deeper water promotes calving and accelerates mass loss, which in turn exacerbates the retreat (Brown et al., 1982; Benn et al., 2007).

While the nonlinear relationship between climate, calving, sediment release and accumulation, and the stability of tidewater glaciers remains a problem for glaciologists modeling the future behavior of ice sheets (Benn et al., 2007), climate can clearly impact the stability of these glaciers through submarine melting of the terminus and sub-aerial melting of the ice surface (Motyka et al., 2003; 2013; Rignot et al., 2010; Straneo et al., 2010). The acceleration and thinning of Greenland's outlet glaciers coincided with a warming of offshore waters (Murray et al., 2010; Straneo et al., 2011), which lead to the hypothesis that warm ocean water reaching glacier termini triggered the dynamic response of many outlet glaciers (Holland et al., 2008; Motyka et al., 2011), and that submarine melting may account for a significant portion of the mass balance of outlet glaciers (Rignot et al., 2010). Currently, more questions than answers remain in this nascent field; efforts to resolve the complexities of this interaction will fill an important scientific gap in understanding processes along the ice-ocean margin.

1.3 Subglacial Processes

While the physics governing the motion of glaciers is relatively well known, a detailed understanding of basal processes, which control critical glacier dynamics and erosion by glaciers, remains elusive due to the complexity of the ice-rock interface and the difficulty in obtaining direct measurements to validate theoretical results. When the base of a glacier is at the melting temperature, the ice can slide along its bed due to the process of regelation and enhanced viscous deformation around roughness elements on the glacier bed. The sliding speed, u_{slide}, depends on the basal drag, τ_d, and the effective pressure at the bed, P_e:

$$u_{slide} = k * \tau_d^p * P_e^{-q} \qquad (1.1),$$

where k is a sliding rate factor inversely related to the bed roughness; the effective pressure, P_e, is the difference between the ice overburden pressure, $P_i=\rho_i gH$, and the local water pressure, P_w; and p and q are empirical constants. Pressurized subglacial water decreases the effective pressure, which increases the sliding speed, and it is only by sliding that the glacier can erode the underlying substrate. Determining how water pressure affects the sliding speed, however, requires direct measurements of the subglacial water system, as well as knowledge of the basal shear stress, bed roughness, and sediment properties, among others. Studies of subglacial water pressure from borehole measurements typically reveal considerable spatial and temporal variation (Harper et al., 2005; Fudge et al., 2008); estimates of sliding velocity range across four orders of magnitude (Cuffey and Paterson, 2010).

From a theoretical perspective, erosion by both abrasion and quarrying depend on the sliding speed (Hallet, 1979; Iverson, 1991). Thus, to understand the production and release of glacially eroded sediment, the nature of the subglacial hydrologic system must also be considered. The efficiency of the subglacial drainage system evolves seasonally as varying amounts of meltwater reach the bed. In early spring, water drains from the surface and creates a system of water-filled cavities at the bed, which increases the subglacial water pressure and accelerates sliding. As the cavities become linked, the drainage system evolves into a more channelized flow moving from the terminus upglacier until the subglacial system can efficiently transport meltwater, at which point sliding slows (Nienow et al., 1998; Anderson et al., 2004). Once an efficient drainage system develops, only large and episodic meltwater events (e.g., a large rainstorm) that overwhelm the capacity of the system can sufficiently increase the water pressure to allow faster sliding, which promotes subglacial erosion (Iken and Bindschadler, 1986; Bartholomew et al., 2010; Schoof, 2010). Accelerations in sliding (often inferred from direct measurements of accelerated surface ice motion), have been correlated with increases in meltwater discharge, and sediment production and transport in various settings (Humphrey and Raymond, 1994; Merrand and Hallet, 1996; Swift et al., 2002; Riihimaki et al., 2005).

1.4 Glacimarine Sedimentary Processes

Sediment deposits near tidewater glacier termini merit close attention because the dynamics of these glaciers are at least partially modulated by the sediments they produce, and the sediments also contain valuable information about past glacier behavior. These glaciers frequently discharge into nearly closed fjords, forming a well preserved sediment record of glacier fluctuations, associated climatic changes, erosion, and sediment-transfer events (Syvitski, 1989; Cowan et al., 2010). A number of studies have related known environmental conditions to sedimentary signatures in fjord seabeds (e.g., sedimentary structure, seismic stratigraphy, accumulation rates) (e.g., Griffith and Anderson, 1989; Domack et al., 1994; Cowan et al., 1997; Milliken et al., 2009), and a continuing research objective is to increase the accuracy and resolution of such paleoenvironmental interpretations. Studies of fjords from Svalbard, Alaska, Patagonia, and Antarctica stress the first-order importance of climate in controlling glacial-marine sedimentation by determining the thermal regime of the glacier and the amount of meltwater produced (Griffith and Anderson, 1989; Powell, 1991; DaSilva et al., 1997; Elverhøi et al., 1998).

For the relatively well studied temperate tidewater glaciers of Alaska, glacial meltwater transports the majority of glacially derived sediment to fjords (Figure 1.3) (Powell and Molnia, 1989; Cowan and Powell, 1991; Hunter et al., 1996a). If the density of the sediment-rich fresh water exceeds the density of the ambient seawater, the fresh water will move seaward as a gravity flow, driven by its excess density (Figure 1.4) (Mulder and Alexander, 2001; Mulder et al., 2003). If the fresh water density is low, meltwater delivered at the base of the glacier will rise buoyantly as a turbulent plume, mix with the ambient seawater (Powell and Molnia, 1989; Syvitski, 1989), and sediment suspended in the plume will settle to the seabed (Cowan and Powell, 1990, 1991; Hunter et al., 1996a). The large meltwater discharge in temperate glacimarine systems results in some of the highest rates of grounding-line sediment accumulation worldwide; they can exceed tens of meters per year (e.g. Molnia, 1983; Cowan and Powell, 1991). These rates have been shown to decrease rapidly with distance from the terminus (e.g., Powell and Molnia, 1989; Cowan and Powell, 1991; Jaeger and Nittrouer, 1999a). Fjord sediments from temperate glaciers commonly comprise interlaminated sands, muds, and ice-rafted debris, and often preserve a high-resolution history of glacier behavior and sediment production over a range of timescales (tidal, diurnal, seasonal, individual event) (e.g., Mackiewicz et al., 1984; Domack et al., 1994; Cowan et al., 1997; 1999; Jaeger and Nittrouer, 1999b).

In polar and subpolar settings, controls on sedimentation are believed to be somewhat different. The production of sediment by glacial erosion is expected to decrease progressively as surface melt vanishes, because little or no water reaches the bed from the glacier surface to facilitate glacier sliding, erosion, and the transport of sediment. Significant sediment production by bedrock erosion likely vanishes as soon as the basal ice temperature drops below the melting point (e.g., Cuffey et al., 1999). Thus, in polar regions, rates of sediment production are likely to nearly vanish as surface temperatures drop well below 0°C (Griffith and Anderson, 1989; Hooke and Elverhøi, 1996; Powell et al., 1996). For subpolar glaciers, the majority of sediment is thought to be transported through fjords in bottom and intermediate-depth plumes of cold water, which appear to originate at the grounding line (e.g., Domack and Williams, 1990; Domack et al., 1994).

1.5 Dissertation Objectives and Organization

The overall goals of this study are to determine and understand modern rates of sediment accumulation in fjords of tidewater glaciers across a range of climates, and to shed light on the glacial characteristics that control sediment delivery to fjords. Specifically, sediment accumulation in fjords is examined across a climatic continuum from temperate to subpolar conditions, and two temperate fjords are then studied in detail to define the history of sediment delivery to the fjords, and to understand the processes controlling both the delivery and accumulation of fjord sediments. In general, observations from the fjord water column and seabed are combined with existing observations of glacier behavior, and numerical models are used to integrate these observations, enhancing understanding of sediment processes in these fjords on time scales of days to decades.

The results of this research are divided into three sections. The first section, Chapter 2, focuses on how modern rates of sediment accumulation vary from temperate conditions in Patagonia to subpolar conditions in the Antarctic Peninsula, and addresses whether recent environmental changes are preserved in the fjord sediment record. In the second section, Chapter 3, the detailed history of sediment delivery to Columbia Fjord in Alaska is examined, the model of glacimarine sedimentation is developed, and the temporal changes in sediment delivery are interpreted in light of an exceptionally complete dataset documenting the recent behavior of this glacier. In Chapter 4, complementary observations of fjord sediment deposits are compared to modeled sediment-flux histories for two rapidly retreating tidewater glaciers: Colombia Glacier, Alaska and Jorge Montt Glacier, Patagonia. The physical implications of these results for fjord sediment dynamics and deposits are then explored.

Chapters 2, 3, and 4 were written for publication in peer-reviewed journals. Chapter 2 is published in Journal of Geophysical Research- Earth Surface with coauthors Charles Nittrouer, Bernard Hallet, Michele Koppes, Brittany Forrest, Julia Wellner, and John Anderson (Boldt et al., 2013). Chapters 3 and 4 are in preparation. Bernard Hallet and Thomas Pratt coauthored Chapter 3. Chapter 4 was written in collaboration with Bernard Hallet, Charles Nittrouer, Michele Koppes, Carlos Moffat, and Thomas Pratt. The concluding section, Chapter 5, summarizes the primary contributions of this dissertation.

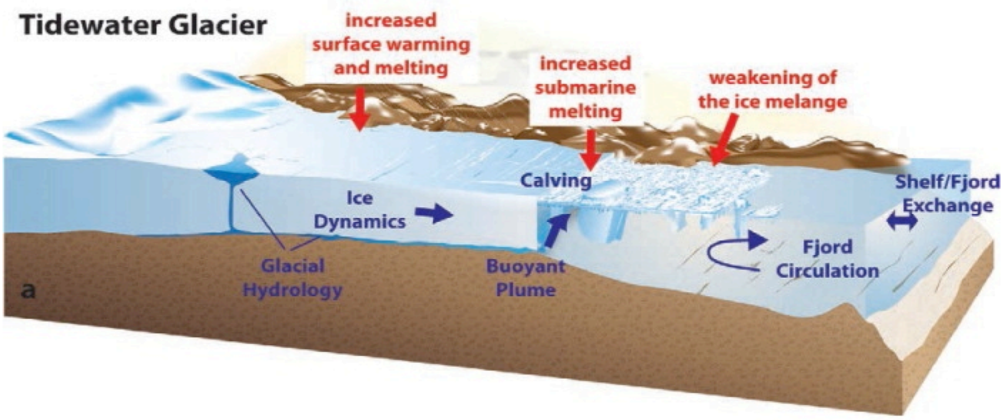

Figure 1.1. Processes Affecting Tidewater Glaciers
Several mechanisms controlling the recent retreat of glaciers worldwide have been proposed (shown in red). Specific processes that need further direct study are highlighted in blue (from Straneo et al., 2013).

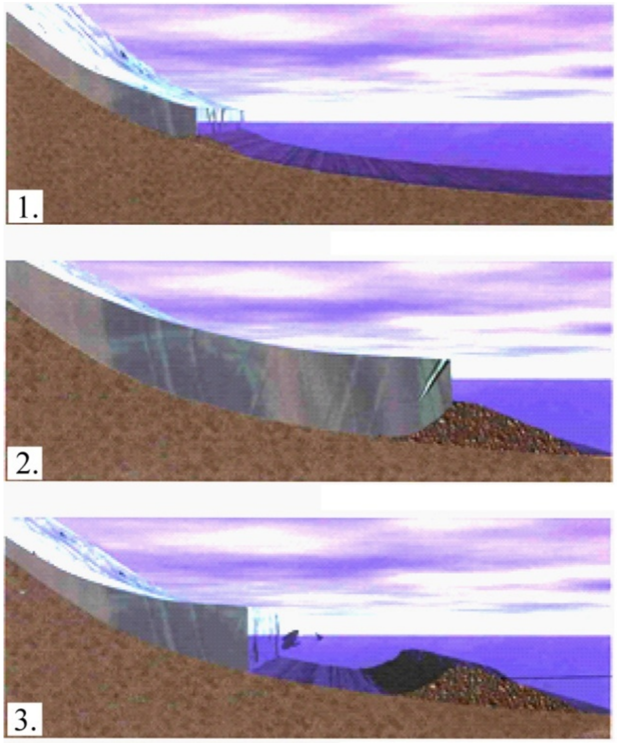

Figure 1.2. Tidewater Glacier Cycle
The role of a terminal moraine in controlling the behavior of tidewater glaciers, which are thought to advance when their morainal shoal decreases exposure to ocean water (cases 1 and 2), and to rapidly retreat to a stable position above sea level when they separate from the moraine (case 3) (modified from Ben and Evans, 2010).

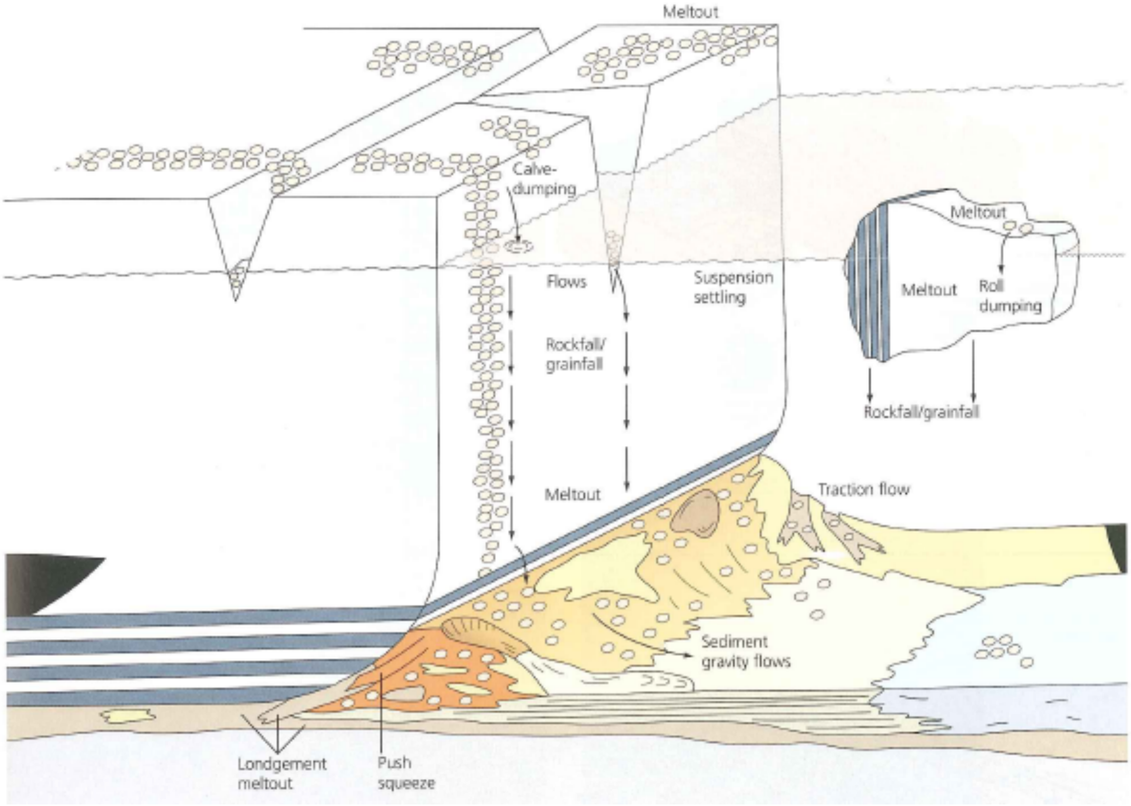

Figure 1.3. Glacimarine Sedimentary Processes
Glaciers deliver sediment supraglacially, englacially, and subglacially, and these sediments are transported to and within fjords by many mechanisms (from Benn and Evans, 2010).

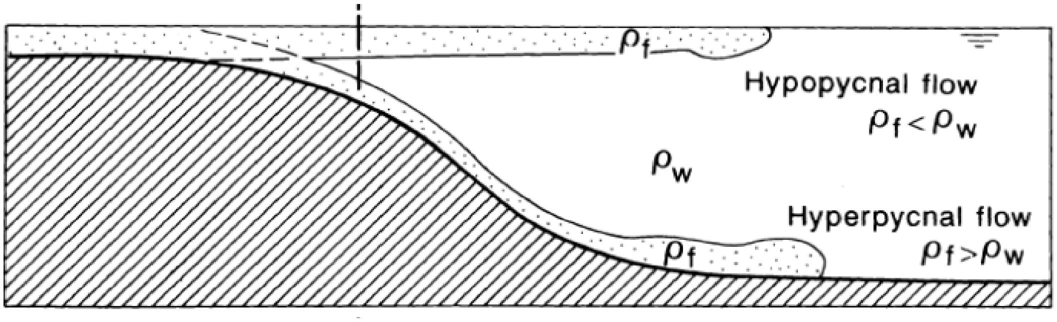

Figure 1.4. Role of Plume Density
The primary transport mechanism of sediment within a plume depends on the densities of the sediment-laden freshwater, ρ_f, and the ambient seawater ρ_w (from Mulder and Alexander, 2001).

Chapter 2: Modern rates of glacial sediment accumulation in fjords from the Antarctic Peninsula to southern Chile

2.1 Introduction

Glacial erosion and sediment production are of interest to diverse scientific communities concerned with 1) the interaction of climatic, tectonic, and surface processes that influences the evolution of mountain ranges (e.g., Egholm et al., 2009; Thomson et al., 2010), and 2) the interpretation of environmental and tectonic signals archived in sediments produced by glaciers (e.g., Griffith and Anderson, 1989; Domack and McClennen, 1996; Michalchuk et al., 2009; Cowan et al., 2010; Koppes et al., 2010). Sediment production from temperate glaciers is among the greatest worldwide (Hallet et al., 1996), demonstrating the efficacy of glaciers in eroding highlands and producing large volumes of sediment (Koppes and Montgomery, 2009), which accumulate in nearshore marine environments (e.g., Jaeger et al., 1998; Jaeger and Nittrouer, 1999a). For example, the onset of widespread glaciation and concomitant increase in sedimentation induced by a change to a cooler, more variable climate in the late Cenozoic (Hay et al., 1988; Zhang et al., 2001) is often viewed as responsible for the creation of clastic wedges up to five kilometers thick on high-latitude continental margins (e.g., Syvitski, 1991; Vorren et al., 1991; Elverhøi et al., 1998; Berger et al., 2008).

One objective of contemporary glacimarine research is to understand the fidelity of recent and past climate-change signals preserved in the sedimentary record, and how these records are altered by time and changing boundary conditions (e.g., Milliken et al., 2009; Koppes et al., 2010; Fernandez et al., 2011; Simms et al., 2011). Climate controls the extent and thermal regime of glaciers, as well as the amount of meltwater produced (e.g., Griffith and Anderson, 1989; DaSilva et al., 1997), with increased meltwater generally promoting glacier erosion by reducing the basal effective pressure (e.g., Cuffey and Paterson, 2010). When abundant, glacial meltwater transports the majority of glacially derived sediment to fjords, where most of this sediment remains trapped (e.g., Powell and Molnia, 1989; Cowan and Powell, 1991; Hallet et al., 1996; Hunter et al., 1996a). The large meltwater discharge in temperate glacimarine systems results in proximal rates of sediment accumulation that can reach tens of meters per year (e.g., Molnia, 1983; Cowan and Powell, 1991). In colder settings, the production of sediment by glacial erosion is expected to decrease progressively as surface melt vanishes, because little or no water reaches the bed from the glacier surface to facilitate sliding, erosion, and sediment transport. Moreover, significant sediment production likely vanishes as soon as the basal ice temperature drops below the freezing point (e.g., Cuffey et al., 1999). Thus, for polar and subpolar regions, subglacial sediment production and delivery to fjords are both expected to drop with decreasing air temperature, especially as it drops below 0˚C (Griffith and Anderson, 1989; Hooke and Elverhøi, 1996; Powell et al., 1996).

An abrupt decrease in sediment accumulation rates from the temperate glaciers in Chile to subpolar and polar glaciers along the Antarctic Peninsula, has been well recognized and attributed to climatically controlled differences in glacier dynamics (Harden et al., 1992; Domack and McClennen, 1996; DaSilva et al., 1997). Analyses of continental-margin sediments from this region provides considerable insight into the history of glacial and climate changes over time scales of 10^3 years and longer (e.g., Domack et al., 2001; Anderson et al., 2002; Boyd et al., 2008; Milliken et al., 2009; Simms et al., 2011; Majewski et al., 2012). In addition, substantial radiochemical work along Antarctic margins provides important biological and sedimentological chronologies from which to examine how modern climate transitions are impacting the sediment record (Ledford-Hoffman et al., 1986; DeMaster et al., 1991; Harden et al., 1992; Leventer et al., 1996; Monien et al., 2011). Quantitative definition of modern accumulation rates complements existing measurements of longer-term sediment accumulation in high-latitude environments (Boyd et al., 2008; Milliken et al., 2009; Fernandez et al., 2011), and reveals how recent climate change has affected accumulation rates in the recent glacimarine sedimentary record (e.g., Gilbert and Domack, 2003; Majewski et al., 2012).

Herein, contemporary sediment accumulation rates from 12 fjords along the western side of the Antarctic Peninsula (WAP), the South Shetland Islands, Tierra del Fuego, and the Southern Patagonia Icefield are measured (Figure 2.1a), with sediments derived from diverse glaciers ranging from subpolar to temperate. For each glacier system, accumulation rates within proximal basins in the fjords were determined using ^{210}Pb analyses, which provide information about sediment accumulation over decadal to centennial timescales. The objectives include: 1) adding to the limited knowledge about recent sediment accumulation in this region (e.g., Harris et al., 1999) and determining the signature of recent rapid warming and glacier retreat in the sediment record (Vaughan et al., 2003; Cook et al., 2005; Pritchard and Vaughan, 2007); 2) comparing sediment accumulation rates among systems across a range of climatic and glaciologic settings, and defining quantitatively the well recognized general northerly increase in sediment accumulation rates in the southern hemisphere (Harden et al., 1992; Domack and McClennen, 1996; DaSilva et al., 1997); and 3) comparing the rates and modes of deposition in the study region with those measured using similar records in a range of other glacimarine settings (e.g., Cowan and Powell, 1991; Jaeger and Nittrouer, 1999a). The accumulation rates presented here are the focus of current work to define sediment yields for individual glaciers at the head of each fjord, and to compare the empirical yields with the dynamic characteristics of each glacier system; this work is part of a broader study on the factors controlling rates of glacial erosion and sediment accumulation across climatic regimes (Boyd et al., 2008; Milliken et al., 2009; Fernandez et al., 2011).

2.2 Geographic and Climatic Setting

The sediments analyzed span 15° of latitude from southern Chile to the Antarctic Peninsula (Figure 2.1a), where the climate varies from the relatively cold and dry setting along the WAP, to a transitional climate in the South Shetland Islands, and to the warm and wet conditions of southern Chile. This transect provides an ideal setting to study the climatic factors influencing modern glacimarine sedimentation because of the substantial ranges of temperature and precipitation that significantly influence glacier thermal regimes, as well as meltwater and sediment production (e.g., Griffith and Anderson, 1989).

Climatic conditions along the WAP range from subpolar to polar, but all of the study sites fall within the subpolar regime. Mean temperatures vary from ~0°C in the austral summer to -8 to -11°C in the winter (King et al., 2003), and seasonal sea ice forms within the fjords and on the shelf, although the fjords remain free of sea ice for most of the austral summer (Domack and Ishman, 1993). A 50-year temperature record from Faraday Station (65.2°S, 64.3°W), near Beascochea Bay (BSB, Figure 2.1b, lower right), indicates a general warming rate of 5.7±2.0°C per century, the most rapid in Antarctica (Vaughan et al., 2003), as well as a statistically significant increase in the number of precipitation days over the same time period (Turner et al., 2005). Approximately 70% of the Antarctic Peninsula surface area north of 70°S experiences occasional to frequent surface melting (Rau and Braun, 2002), and the fraction of annual accumulation experiencing melting has increased tenfold in the past ~600 years (Abram et al., 2013). Such melting generally favors sediment production by glacial erosion, as well as sediment transport and release to fjords where the glaciers terminate. The spine of the Antarctic Peninsula, with mountains that rise up to 3500 m above sea level, is heavily glaciated, and many of the glaciers terminate as massive tidewater glaciers.

Farther north, the South Shetland Islands experience a transitional climate between sub-polar and temperate, with winter temperatures between -3 and -5°C, and summer temperatures above freezing (Reynolds, 1981; King et al., 2003). Over the past four decades, this area has warmed 3.7±2.1°C per century, the second fastest warming documented for Antarctica (Vaughan et al., 2003). Approximately 170 mm of the total annual precipitation (~1200 mm) falls as rain during the summer months, and produces more meltwater than along the WAP (Yoon et al., 1998; Turner et al., 2002). Currently, the South Shetland Islands are covered in ice fields with a mean thickness of ~250 m that terminate both on land and in the sea (Rückamp and Blindow, 2011).

Along the coastline of southern Chile, strong westerly winds generate a large precipitation gradient. Precipitation peaks at ~7000 mm yr^{-1} in the core of the westerlies, near 50°S, and decreases northward to ~2500 mm yr^{-1} at 40°S, and southward to ~500 mm yr^{-1} at 55°S (Hulton et al., 2002). The northernmost study area reported herein, which is on the west side of the Southern Patagonia Icefield, Europa Fjord (50°S), experiences ~4000 mm $yr^{-1}$of precipitation and a mean annual temperature of 7°C (Hulton et al., 2002). The second site in South America, Marinelli Fjord in Tierra del Fuego (54°S), typically receives between 500 and 1000 mm yr^{-1} of precipitation, and annual temperatures average 5°C (Hulton et al., 2002; Boyd et al., 2008). All of the glaciers entering the fjords of western Chile are temperate (Anderson and Domack, 1991).

2.3 ^{210}Pb Geochronology

^{210}Pb geochronology has been used to calculate recent sediment accumulation rates in a wide range of marine sedimentary environments (e.g., Nittrouer et al., 1979; Harden et al., 1992; Dukat and Kuehl, 1995; Domack and McClennen, 1996; Jaeger et al., 1998; Sommerfield and Nittrouer, 1999; Degeest et al., 2008). Despite the considerable extent of coastlines in high latitudes and the amplified impacts of recent climate change in this region (Holland and Bitz, 2003; Vaughan et al., 2003), few measurements of modern sediment accumulation exist along glaciated margins relative to their fluvial counterparts. ^{210}Pb forms naturally as one of the last daughter isotopes in the ^{238}U decay series and enters the marine environment in surface runoff and atmospheric precipitation; the *in situ* decay of its parent, ^{226}Ra, directly supplies ^{210}Pb to seawater. ^{210}Pb rapidly and irreversibly adsorbs to fine-grained particles in suspension, and is typically scavenged from the water column within a year in coastal waters (Nittrouer et al., 1979 and references therein). Once deposited on the seabed, the adsorbed ^{210}Pb decays to its daughter ^{210}Bi with a half-life of 22.3 years until it reaches the activity supported by *in situ* decay of ^{226}Ra. The decay of excess ^{210}Pb, the activity of ^{210}Pb in excess of the supported level, can be used to study sediment accumulation over approximately a century.

The sediment accumulation rate is calculated from the slope of the regression line fit to the vertical semi-log profile of excess ^{210}Pb activity versus depth. A typical decay profile contains three distinct vertical zones: a surface layer, a region of logarithmic decrease, and a zone of supported activity. The upper portion of the profile often contains a surface layer (~10 cm thick) of uniform activity due to physical and biological particle mixing, above a zone of log-linear decrease (Figure 1 in Nittrouer et al., 1979). This decrease represents steady-state accumulation, assuming the activity of newly supplied sediment remains constant (Figure 2.2a)

(A comprehensive review of ^{210}Pb sediment-dating models are presented in Appleby, 2002). If the accumulation rate changes and stabilizes at a different rate, the log-linear profile shows two linear sections with a break in slope (Figure 2.2c; e.g., Bentley, 1996; Sommerfield and Nittrouer, 1999; Palinkas and Nittrouer, 2006). Where the substrate is physically quiescent and subsurface burrowers are uncommon, ^{210}Pb profiles can show steady-state accumulation (i.e., log-linear decay) extending from the sediment surface (e.g., DeMaster et al., 1985). The third distinct zone occurs below the region of linear decrease, and is characterized by nearly uniform ^{210}Pb activity supported by the decay of its effective parent, ^{226}Ra, in the seabed.

If accumulation rates have varied in time, the vertical profile of excess ^{210}Pb can still reveal temporal information about sediments reaching the seabed. If either the ^{210}Pb activity of the newly supplied sediment or the accumulation rate change on short time scales (<10 years), the profile will show fluctuating activity with no clear vertical pattern (Figure 2.2d; e.g., Dukat and Kuehl, 1995; Jaeger and Nittrouer, 1999a). Episodic sediment delivery events, such as submarine gravity flows, create distinct zones in ^{210}Pb profiles that typically consist of low excess activity due to the high concentration of particles that settle on the seabed and compete for limited ^{210}Pb (e.g., Mullenbach and Nittrouer, 2000). Low-activity regions can also reflect deposition of coarse-grained particles, as their surface area is relatively small and adsorbs less ^{210}Pb (Figure 2.2b; e.g., Nittrouer et al., 1979; Kuehl et al., 1989). The specific ^{210}Pb activity of particles depends on many oceanographic factors, including: 1) circulation patterns in the fjords and shelf, 2) the depth of water through which the particle settles, and 3) ^{210}Pb concentration of fjord waters.

2.4 Methods

Two cruises in 2005 and 2007 aboard the *RV/IB Nathaniel B. Palmer* provided the sediment-core and bathymetric data presented here. The first cruise, NBP0505, collected the five kasten cores used in this study from two fjords in southern Chile spanning 50°S to 54°S (Figures 2.1c, d). An additional sixteen kasten cores were collected from ten bays and fjords in the South Shetland Islands and along the WAP during the 2007 cruise, NBP0703 (Figure 2.1b). Prior work had shown that the distribution of sediments is highly variable in Antarctic Peninsula fjords and bays (Griffith and Anderson, 1989); thus, the initial survey collected multibeam maps and 3.5-kHz CHIRP seismic surveys to identify locations where sediments are ponded in glacier-proximal settings. Sediment coring was guided by results from these surveys. In several of the fjords, ice-distal cores were also collected to examine variations in sedimentation along a fjord axis.

Onboard the *RV/IB Palmer*, the 3-m-long kasten cores were photographed, described, and subsampled for further analysis. The top 25-50 cm were sampled in 1-cm increments for ^{210}Pb dating; the underlying sediments were sampled every 2 cm to an approximate depth of 1 m, followed by sampling every 5 cm to a depth of 2 m. If the core was longer than 2 m, samples were obtained every 10 cm in the lowermost section. The samples were placed in sterile bags and refrigerated until they were analyzed in the laboratory. Archive sections of each core were sent to the Antarctic Marine Geology Research Facility at Florida State University, where x-radiographs of the half-round subcores were obtained (note: images are shown as x-radiograph positives, where lighter colors indicate relatively fine-grained sediment).

Sediment accumulation rates were calculated by generating profiles of excess ^{210}Pb using a procedure similar to Nittrouer et al. (1979). Sediment samples were homogenized, dried at 70°

C, and crushed. The dry bulk density (indicated as “bulk density” hereafter) for each sample was calculated by comparing the wet and dry sediment weights, assuming a particle density of quartz (2.65 g cm^{-3}). A known activity of ^{209}Po was added to approximately 5 g of each sample. The sediment was then digested with solutions of both 15.8 N HNO_3 and 6 N HCl, and the Po isotopes were plated onto a silver planchet for ~20 h. Alpha spectroscopy was used to measure the activity of ^{209}Po and ^{210}Po, and the total ^{210}Pb activity in each sample was calculated based on measured values of ^{210}Po, the granddaughter isotope. Excess ^{210}Pb values were calculated by subtracting the supported activity at depth in the core from the total activity measured. A mean supported activity level of 0.9 ± 0.2 dpm g^{-1} was determined from the region of low, uniform activity below the zone of logarithmic decay. This value was observed in profiles from both the Chilean and WAP study sites that had steady-state accumulation, and was used to calculate excess activities for all cores.

Sediment accumulation rates (mm yr^{-1}) were determined using least-squares linear regression of the semi-log profile. Mass accumulation rates (g cm^{-2} yr^{-1}) were calculated using the mean bulk density from each core. For profiles with a distinct, visual change in slope within the log-linear region, linear regression was applied to each line segment, providing two accumulation rates. Profiles with r^2 values < 0.75 were considered non-steady state and classified as either vertically uniform or varying, depending on the pattern of ^{210}Pb activity with depth (see Table 2.1). For cores whose ^{210}Pb profiles suggested non-steady accumulation with depth, detailed grain-size distributions were generated on specific intervals using a Malvern Laser particle diffractor (McCave et al., 1986).

2.5 Results

For each core site, the sediment accumulation rate and other pertinent information are compiled in Table 2.1. Additional context for each core site follows.

Table 2.1. *Summary of Antarctic Peninsula to Chile Transect Cores*

Core	Location[a]	Latitude (°S)	Longitude (°W)	Core length (m)	Accumulation rate (mm yr^{-1})	Accumulation style[b]	Distance from ice front (km)
			Southern Chile				
KC28P	Europa Fjord (EF)	50.278	73.949	2.0	N/D[c]	varying	7.1
KC35P	Europa Fjord	50.282	73.923	2.0	11.4	SS	5.2
KC50P	Marinelli Fjord (MF)	54.390	69.591	1.2	23.6	SS	12.3
KC79P	Marinelli Fjord	54.350	69.585	1.1	N/D	varying	17.1
KC80P	Marinelli Fjord	54.361	69.577	2.0	N/D	varying	16.6
			South Shetland Islands				
KC14	Maxwell Bay (MB)	62.196	58.833	1.6	5.5, 2.0[d]	change in SS	3.4
KC21	Maxwell Bay	62.205	58.739	0.45	6.6, 2.8	change in SS	0.2
KC22	Maxwell Bay	62.214	58.777	2.17	5.2, 1.3	change in SS	1.9
KC23	Maxwell Bay	62.253	58.710	0.39	1.6, 1.4	SS, event	4.8
			Antarctic Peninsula				
KC10	Hope Bay (HB)	63.386	57.010	0.34	3.0	SS	3.5
KC65	Cierva Cove (CC)	64.157	60.863	0.48	N/D	vertically uniform	1.0
KC63	Brailmont Cove (BC)	64.290	60.982	1.2	N/D	vertically uniform	0.1
KC33	Lapeyrere Bay (LB)	64.373	63.289	2.9	2.2	SS	1.2
KC28	Lapeyrere Bay	64.402	63.252	2.9	3.2	SS	6.8
KC60	Charlotte Bay (CB)	64.632	61.519	0.36	2.8	SS	3.2
KC57	Andvord Bay (AB)	64.872	62.425	1.3	5.6	SS, event	0.8
KC29	Flandres Bay (FB)	65.066	63.103	1.9	2.8, 3.0	SS, event	5.7
KC41	Collins Bay (CLB)	65.346	63.056	2.7	N/D	vertically uniform	1.2
KC48	Beascochea Bay (BSB)	65.510	63.708	1.0	6.4	SS, event	0.9
KC45	Beascochea Bay	65.589	63.830	1.0	2.2	SS	2.0
KC44	Beascochea Bay	65.607	63.817	1.8	7.0	SS	0.7

[a] The location acronym in parentheses refers to core sites shown in Figure 2.1.
[b] Accumulation styles include: steady state (SS, Figure 2.2a); varying ^{210}Pb activity with depth; SS with an event layer (Figure 2.2b); change in SS rate (Figure 2.2c); and relatively uniform ^{210}Pb activity with depth (all excess or all supported, Figure 2.2d).
[c] Accumulation rates for non-steady core types cannot be determined (N/D).
[d] The first rate refers to the more recent sediments.

2.5.1 Western Antarctic Peninsula

The four southernmost samples in this study were collected from the Graham Coast: three cores from Beascochea Bay (BSB), KC44, 45, and 48, and core KC41, from Collins Bay (CB) (Figures 2.1b, 2.3a,b). Cores KC44 and KC45, collected in a deep trough just seaward of Cadman Glacier (Figure 2.3a), contain relatively uniform profiles of bulk density and steady ^{210}Pb accumulation at rates of 7.0 and 2.2 mm yr^{-1}, respectively (r^2=0.83, 0.96; Figures 2.3c,d).

KC48, in front of the Lever Glacier (Figure 2.3a), shows a steady-state accumulation profile of 6.4 mm yr^{-1}, overlain by ~40 cm of sediment with lower bulk density and relatively uniform, excess ^{210}Pb activity that decrease slightly in the uppermost 5 cm (Figure 2.3e). The entire length of KC41 contains generally uniform bulk density and varying excess ^{210}Pb activity of 0.6-1.4 dpm g^{-1}, nearly all of which falls within the 0.9 ± 0.2 dpm g^{-1} range of supported activity for this region (Figure 2.3f). X-radiographs of regions showing steady accumulation are characterized by relatively homogenous sediment with some dropstones and few, faint laminations (Figures 2.3g,h,j). In the upper section of KC48 with high, uniform ^{210}Pb activities, the x-radiograph reveals mm-scale laminations (Figure 2.3i), while x-rays of KC41 show relatively homogeneous sediment with few visible laminations (Figure 2.3k). Of the cores collected along the WAP, KC44 and KC48 were collected near the ice front for two of the largest WAP glaciers; they record the fastest sediment accumulation for this region (Table 2.1).

Slightly farther to the north, in Flandres Bay (FB; Figures 2.1b, 2.4a), core KC29 shows steady-state accumulation separated by a 10-cm-thick section characterized by much lower ^{210}Pb activity (Figure 2.4d). Below this low-activity layer, sediment accumulated at 3.0 mm yr^{-1}, and above the layer, modern sediment has accumulated at 2.8 mm yr^{-1} (r^2=0.90, 0.99; Figure 2.4d). The x-radiograph image and grain-size analyses of the particles in the low-activity region indicate this section is coarser (darker color in x-ray, mean size of 1.0 mm versus 0.01 mm) and is denser than the rest of the deposit. Likely, the coarse grain size (reduced surface area) accounts for both the decrease in ^{210}Pb activity and increases in density (Figures 2.2f, 2.2g, 2.3d). Along the Danco Coast, core KC57 from Andvord Bay (AB; Figure 2.4b) contains a region of uniform bulk density and steady-state ^{210}Pb accumulation at 5.6 mm yr^{-1} (r^2=0.97) overlain by a 60-cm-thick deposit containing varying bulk density and ^{210}Pb activity (Figure 2.4e). ^{210}Pb from core

KC60 in Charlotte Bay (CB; Figure 2.4c) shows bulk density increasing slightly with depth and steady sediment accumulation at a rate of 2.8 mm yr^{-1} (r^2=0.93) (Figures 2.1b, 2.4f). X-radiographs of steady-state ^{210}Pb regions reveal fine-grained deposits with scattered small dropstones and faint laminations (Figures 2.4g, i, j), whereas images from non-steady regions show coarser-grained (darker) intervals and more distinct layering (Figures 2.4g, h).

On Anvers Island, nearly 3-m-long cores were collected in each of the two arms of Lapeyrere Bay (LB; Figures 2.1b, 2.5a). KC33 and KC28 both show uniform bulk density with depth and steady-state ^{210}Pb accumulation; rates are 2.2 mm yr^{-1} (r^2=0.96) and 3.2 mm yr^{-1} (r^2=0.98), respectively (Figures 2.5b,c). X-radiographs from both cores show fine-grained sediment with small dropstones throughout (Figures 2.5d,e). Sediment accumulates faster at the more ice-distal site, and seismic profiles from the main fjord basin (where KC28 was collected) show the thickest sediments, reflecting greater input from Illiad Glacier, the largest glacier entering the basin (Figure 12 in Griffith and Anderson, 1989).

Proceeding north, one core was collected each in Cierva and Brailmont Coves off Hughes Bay (BC and CC; Figures 2.1b, 2.6a). Excess ^{210}Pb activity in core KC63 from Brailmont Cove is relatively uniform and low within 90 cm of the seabed (Figure 2.6c). KC65 from Cierva Cove contains uniform excess ^{210}Pb activity that extends from the surface to a depth of 36 cm (Figure 2.6b). In both cores, bulk density fluctuates with depth. The x-radiograph from KC65 shows very few laminations and some dropstones, while the image from KC63 shows mm-to-cm scale laminations throughout the core (Figures 2.6d, e, f). The northernmost core on the WAP, KC10, from the center of Hope Bay (HB; Figures 2.1b, 2.7a), contains sediment with bulk densities that slightly increase with depth, and steady ^{210}Pb accumulation at 3.0 mm yr^{-1} (r^2=0.95; Figure 2.7b). X-radiographs reveal homogenous sediment with no evidence for layering (Figures 2.7c, d).

2.5.2 South Shetland Islands

Four sediment cores were collected in three coves that fringe Maxwell Bay (MB) on King George Island (Figures 2.1b, 8a). ^{210}Pb profiles for three of these cores show a distinct change in the rate of accumulation, in all cases increasing by a factor of two to four in the last few decades (Figures 2.8b, c, d). The accumulation rate determined for KC14 in the inner bay increased from 2.0 to 5.5 mm yr^{-1} around 1980 (respective r^2=0.98; Figure 2.8b). In core KC21, from Marion Cove, the rate increased from 2.8 to 6.6 mm yr^{-1} around 1984 (r^2=0.99, 0.91; Figure 2.8c). Similarly for KC22, also collected in Marion Cove slightly farther from the current glacier terminus, the rate increased from 1.3 to 5.2 mm yr^{-1} around 1978 (r^2=1.0, 0.97; Figure 2.8d). X-radiographs from the region of change in each of the ^{210}Pb profiles do not indicate a similar change in the sediment composition or structure; all cores contain ice-rafted debris and no apparent layering (Figures 2.8f, g, h). KC23, near the mouth of Potter Cove, was the most seaward and ice-distal core collected in Maxwell Bay. Unlike the other cores, KC23 contains a ~8-cm-thick interval characterized by relatively uniform excess ^{210}Pb activity that punctuates otherwise steady accumulation of ~1.5 mm yr^{-1} (r^2=0.94, 0.91; Figure 2.8e), however a distinct change in the sediment composition or structure is not visible in the x-radiograph (Figure 2.8i). Bulk densities are relatively uniform in all cores, except in KC21, where they increase with depth. A statistical comparison shows no correlation between bulk density and ^{210}Pb activity.

2.5.3 Chilean Fjords

In Tierra del Fuego, three cores were collected in the outer basin of Marinelli Fjord (MF; Figure 2.1d). Closest to the glacier, at KC50P, sediment has accumulated steadily at 23.6 mm yr^{-1} (r^2=0.87; Figure 2.9a), while ^{210}Pb profiles from cores KC79P and KC80P, both in the distal, outer region of the fjord, indicate variable low ^{210}Pb activities (Figures 2.9b, c). The two northernmost cores were collected from the long, narrow, Europa Fjord (EF; Figure 2.1c), on the southwest side of the Southern Patagonia Icefield. The ^{210}Pb profile from KC28P, 7.1 km from the ice front, indicates varying and very low ^{210}Pb activities (Figure 2.9d), whereas KC35P, 5.2 km from the ice front, records steady-state accumulation at 11.4 mm yr^{-1} (r^2=0.83; Figure 2.9e). In all five cores, bulk density is uniform with depth around 1 g cm^{-3}, with the exception of the basal portion of KC80P, where the density is greater. Only the x-radiograph from KC79P indicates distinct cm-scale layering; x-radiographs of the other cores show homogenous sediment (Figures 2.9f-j).

2.6 Discussion

2.6.1 Interpretation of ^{210}Pb Profiles

Steady accumulation rates:

In 15 of the 21 cores presented here, profiles of excess ^{210}Pb indicate that sediments have been accumulating at a relatively constant rate over approximately the last century, suggesting that the frequency, magnitude, and source of sediment-delivery events have not changed appreciably in time (Figures 2.3c, 2.3d, 2.4f, 2.5b, 2.5c, 2.7b, 2.8b-d, 2.9a, 9e). X-radiographs of these cores all show deposits with little visible layering and a uniform scattering of ice-rafted debris, consistent with steady sediment accumulation at rates of a few mm yr^{-1} (Figures 2.3g, 2.3h, 2.3j, 2.4j, 2.5d, 2.5e, 2.7c, 2.7d, 2.8f-h). Previous studies have observed similar steady-state ^{210}Pb profiles in WAP fjords and in basins relatively distant from glaciers (e.g., Harden et al., 1992; Domack and McClennen, 1996). Such steady-state sediment accumulation at the stationary core sites throughout the last century is surprising in view of the extreme environmental changes that have occurred during this period. The increase in mean annual temperatures along the WAP measured over the last 50+ years exceeds the global average sixfold (Vaughan et al., 2003). This exceptional warming, together with the coincident increase in melt percentage to a level unprecedented during the last millennium (Abram et al., 2013), would likely accelerate glacial sliding, erosion, and sediment transport to fjords. But this expected increase in sediment accumulation at any site would tend to be offset by the substantial recent glacial retreat in this region: over 87% of the glaciers in the Peninsula have retreated (mean ~580 m, max ~5 km) in the past 50+ years (Cook et al., 2005; Pritchard and Vaughan, 2007). Because rates of accumulation generally decrease exponentially down fjord (e.g., Cowan et al., 1997 in Figure 10; Jaeger and Nittrouer, 1999a), and glacial retreat increases the distance between the ice front and any proglacial core site, accumulation rates would tend to decrease with time at any core site, thereby tending to offset the increase in sediment flux expected due to the warming climate.

Changes in accumulation rate:

In contrast with the steady-state profiles of excess ^{210}Pb collected from the WAP, profiles in the South Shetland Islands appear consistent with ongoing climatic changes in this region, which experiences a relatively warm and wet climate. Three of the four ^{210}Pb profiles show a break in slope (Figures 2.2b, 2.8b-d), reflecting a recent two-to-fourfold acceleration of accumulation for the three ice-proximal cores, which agrees well with independent analyses of other Maxwell Bay cores (Yoon et al., 2000, 2010; Monien et al., 2011; Majewski et al., 2012). Although the x-radiographs show no visible change in the sedimentary character, the timing of the accumulation-rate increase was ~25 years ago and coincides with the period during which glaciers north of 64°S retreated the fastest (Cook et al., 2005). The increase in accumulation rate preserved in the sedimentary record may reflect a sensitive transition in the glaciers of the South Shetland Islands from subpolar to temperate. The increase in nearby surface temperatures and in the frequency of precipitation events, measured since ~1969 and ~1956 respectively (Turner et al., 1997; Vaughan et al., 2003), could increase sediment accumulation rates by generating more vigorous periglacial weathering and mass wasting, as well as increased volumes of meltwater, which transport sediment to Maxwell Bay (DaSilva et al., 1997; Yoon et al., 1998). The trends observed in the ^{210}Pb profiles from Maxwell Bay suggest that if the region continues to warm, increased meltwater production and faster sediment accumulation could extend to the WAP.

Complex ^{210}Pb profiles:

In addition to steady accumulation described above, some of the ^{210}Pb profiles exhibit a variety of sediment accumulation patterns and reflect diverse glacimarine sedimentary processes. Vertically uniform profiles with significant excess ^{210}Pb typically indicate rapid, possibly instantaneous, sediment deposition. The high activities (such as KC65, Figure 2.6b) suggest 1) a relatively vigorous circulation of seawater renews the inventory of ^{210}Pb in the local water column, and/or 2) the sediments entered the fjord entrained in a buoyant surface plume from which they settled through deep water columns, scavenging ^{210}Pb. Vertically uniform profiles with low activities (KC41 and KC63, Figures 2.3f and 2.6c), however, could represent supported ^{210}Pb values (~0.9 dpm g^{-1}), and thus sediment sufficiently old (>100 years) for all excess ^{210}Pb to have decayed to negligible levels. Alternatively, these ^{210}Pb profiles could indicate the deposition of particles with negligible excess ^{210}Pb activity, which would occur if particles were delivered by gravity flows with mixtures of glacial meltwater and limited sea water (e.g., Dukat and Kuehl, 1995; Mullenbach and Nittrouer, 2000).

Four of the profiles characterized by steady-state accumulation are interrupted by ~10 to 60 cm-thick zones of relatively uniform excess ^{210}Pb activity; they represent one or many discrete, rapid depositional events (Figures 2.3e, 2.4d, 2.4e, 2.8e), which can result from diverse sedimentary processes. Rapid settling from a sediment-laden meltwater plume would create a deposit of uniform, high excess activity (potential examples: KC48 and KC23, Figures 2.3e and 2.8e), while the release of a large volume of coarse ice-rafted debris or a gravity flow would form sediment intervals of low activity (e.g., KC29, Figure 2.4d). X-radiographs from these deposits help determine the formative sedimentary processes; for example, the low-activity layer in KC29 corresponds to a region of concentrated coarse-grained material (Figures 2.2f, 2.2g, 2.4g). Confidently distinguishing between these possibilities, however, would require additional data, such as shorter-lived radioisotopes to measure processes occurring on event time scales (e.g., weeks to months) (e.g., Jaeger and Nittrouer, 1999a), and detailed evaluation of the individual cores is beyond the scope of this paper.

Biological factors:

As mentioned earlier, biological factors can alter the distribution of ^{210}Pb within the cores and impact the interpretation of sedimentary processes and accumulation rates from profiles of excess ^{210}Pb. Burrowing benthic organisms can mix the upper sediment, potentially creating a zone of uniform activity like those seen in a few of the cores, which otherwise show steady-state accumulation (Figure 2.5b). Regional measurements of bioturbation intensity along the WAP indicate that burrowing is confined to the upper 8 cm, and that local benthic organisms primarily utilize surface organic material year-round (McClintic et al., 2008). The steady-accumulation profiles presented here all show log-linear decay to at least 30 cm (e.g., Figures 2.3d, 2.5c), which would be very deep for biological community mixing and implies little or no vertical mixing (c.f. Nittrouer et al., 1984; Harden et al., 1992). In addition, x-radiographs do not show evidence of tubes or burrows.

In addition to biological mixing, the fraction of biologically produced sediment accumulating on the seabed is also of considerable interest, especially when using total sediment masses to develop terrigenous sediment budgets and infer glacial erosion rates (Koppes and Hallet, 2002, 2006, 2010; Cowan et al., 2010; Koppes, 2012). The coastal and shelf waters of the WAP support a productive biological ecosystem, in which sea-ice cover primarily controls productivity during the austral summer (e.g., Ducklow et al., 2007). The relative contribution of biogenic particles within the seabed generally increases with primary productivity and decreases as the accumulation rate of terrigenous sediment increases. Thus, the biogenic component generally increases southward, and with increasing distance from the ice front, due to the general decrease in rates of terrigenous sediment accumulation (e.g., Dunbar et al., 1985; Griffith and Anderson, 1989; Domack and Ishman, 1993). In the productive waters of the Ross Sea, biogenic silica accounts for 1-7% by weight of total sediment accumulation in most areas, with a maximum contribution of ~40% in the southwestern Ross Sea (Ledford-Hoffman et al., 1986). Along the WAP, biogenic silica accounts for <5% of total sediment particles in a polar fjord south of the study sites (Gilbert et al., 2003), ~12-14% in the outer portion of Andvord Bay (Domack and Ishman, 1993) and ~6% since the Little Ice Age in Maxwell Bay (Milliken et al., 2010). Offshore of Maxwell Bay, measurements from the Bransfield Strait indicate biogenic contribution of ~12% in deep basins (DeMaster et al., 1991). Thus, in the glacier-proximal study sites, biogenic silica is likely to be a minor (i.e., <10%) component of the sediments.

2.6.2 N-S Transect Trends

Along the 15° N-S transect, modern rates of sediment accumulation in temperate fjords of southern Chile substantially exceed those in the subpolar fjords of the South Shetland Islands and WAP (Table 2.1, Figure 2.10). In Chilean fjords, rates range from 11.4 to 23.6 mm yr^{-1} (n=2, mean=17.5 mm yr^{-1}), whereas along the WAP and South Shetland Islands, they range from 1.3 to 7.0 mm yr^{-1} (n=14, mean=4.2 mm yr^{-1}). Moreover, the WAP and South Shetland Islands accumulation rates are two to three orders of magnitude smaller than ice-proximal rates derived from seismic data in southern Chile, including Laguna San Rafael and Marinelli Fjord (Koppes, 2007; Koppes et al., 2009). It is likely that this contrast is related to the abundance of meltwater in the Chilean glacier systems. The higher annual temperatures and precipitation in southern Chile favor meltwater production, which is likely to increase the basal water pressure leading to faster sliding (Iken and Bindschadler, 1986; Anderson et al., 2004; Bartholomew et al., 2010). Additionally, high basal water pressures promote subglacial erosion by quarrying especially where they fluctuate frequently (Hallet, 1996; Iverson, 2012). Indeed, increases in sliding velocities (inferred from measured increases in the surface speed) have been correlated with increases in the production and transport of glacial sediment (e.g., Humphrey and Raymond, 1994; Anderson et al., 2004; Riihimaki et al., 2005).

For the relatively cool and dry climatic regime in the southern part of this study, sediment accumulation rates in the South Shetland Islands and along the WAP do not decrease with increasing latitude as was expected based upon previous studies (Harden et al., 1992; Domack and McClennen, 1996). The transitional climate of the South Shetland Islands, plus the well-documented occurrence of seasonal debris-laden meltwater emanating from the King George Island icecap (Griffith and Anderson, 1989; Domack and Ishman, 1993; Yoon et al., 1998), suggest that sediment accumulation rates should be intermediate between polar and temperate. The modern accumulation rates measured in Maxwell Bay, however, are just above the 4 mm yr^{-1} mean accumulation rate from the WAP, and agree well with previous measurements (e.g., Yoon et al., 2000, 2010; Majewski et al., 2012). These modest rates likely reflect the limited size and vigor of the glaciers and ice caps that cover the South Shetland Islands, compared to the ice masses along the WAP (Koppes and Hallet, 2010; Koppes, 2012).

Within the WAP fjords, the accumulation rates of 3-7 mm yr^{-1} measured in this study are within the range of values reported previously (Harden et al., 1992; Domack and McClennen, 1996). It is important to stress that none of the sites presented here represents a true polar setting, where basal meltwater would be negligible and glacial erosion rates would nearly vanish (Cuffey et al., 1999). The lack of a distinct N-S pattern within these subpolar sites suggests that the expected general decrease in sediment accumulation rates with temperature is confounded by site-specific factors; these likely include the meltwater production regime, distance to the ice front, fjord bathymetry, the glaciated basin area, and ice flux (Domack and McClennen, 1996; Koppes and Hallet, 2010; Koppes, 2012).

2.6.3 Comparison with ^{210}Pb Measurements from Other Glacimarine Settings

Many of the excess ^{210}Pb profiles from WAP and Chilean fjords, as well as those previously reported from other WAP fjords (Harden et al., 1992; Domack and McClennen, 1996) suggest sediment accumulation at a uniform rate over the past ~100 years. This is remarkable not only because the WAP has warmed exceptionally quickly and most glaciers have retreated significantly in the last century, but also because it contrasts with profiles of excess ^{210}Pb from ice-proximal, temperate fjord settings. Profiles collected from multiple fjords in Alaska typically exhibit non-steady-state behavior (Cowan et al., 1997; Jaeger and Nittrouer, 1999a), which for these glacier-proximal settings likely indicate the greater contribution of individual sediment-delivery events to fjord sediments in Alaska, as well as temporal changes in their frequency and magnitude. The low values of excess activity for these profiles suggest either that particles settle through the water column too quickly to scavenge ^{210}Pb, or that sediment is delivered near the bed as submarine gravity flows (Jaeger and Nittrouer, 1999a). Either scenario is consistent with the rapid deposition of sediment, which is known to occur in these Alaskan fjords at seasonal rates up to 9 cm d^{-1} and annual rates of at least 9 m yr^{-1} near the terminus (e.g., Molnia, 1983; Cowan and Powell, 1991). Where ^{210}Pb-derived rates can be calculated near temperate glaciers, they confirm rapid accumulation at least two orders of magnitude greater than ice-proximal accumulation in subpolar fjords (Figure 2.10). In such ice-proximal, temperate regions generally characterized by non-steady and rapid sediment accumulation, shorter-lived isotopes such as ^{234}Th are generally more useful in quantifying accumulation rates (e.g., Jaeger and Nittrouer, 1999a); however, ^{210}Pb geochronology provides a considerably useful means for interpreting sedimentary processes in these environments, as well as for determining accumulation rates in more ice-distal regions in temperate settings, such as the continental shelf off the southern coast of Alaska (Jaeger et al., 1998), and in subpolar glacimarine settings (e.g., Smith et al., 2002; Szczucinski et al., 2009).

Unlike the patterns observed in ^{210}Pb profiles from ice-proximal locations in temperate fjords, the steady accumulation profiles observed in most of the cores shown here resemble profiles collected in other subpolar fjords, as well as in temperate, ice-distal settings. For example, most ^{210}Pb measurements from subpolar fjords in East Greenland and Svalbard indicate steady sediment accumulation rates of 1 to 10 mm yr^{-1} (Figure 2.10) (Smith et al., 2002; Szczucinski et al., 2009; Andresen et al., 2011), which encompass the rates observed along the WAP and South Shetland Islands in this and previous studies (Harden et al., 1992; Domack and McClennen, 1996). In addition, the more ice-distal regions of the outer Alaskan fjords and the adjacent continental shelf experience uniform accumulation at rates of ~1-2 cm yr^{-1} (Figure 2.10) (Cowan et al., 1997; Jaeger et al., 1998). The similarity between sediment accumulation patterns and rates in the distal regions of temperate fjords and the proximal areas of subpolar fjords suggests that both settings receive glacially derived sediment continuously with infrequent "events" when averaged over typical sampling intervals of 5 cm, which correspond to periods of 50 to 5 years, respectively, for accumulation rates of 1 to 10 mm yr^{-1}. On temperate shelves fed with glacial sediments, accumulation tends to be rather steady because of the considerable distance to the sediment source, which reduces accumulation rates, attenuates event signals, and increases the averaging time for ^{210}Pb; in addition, the more temporally uniform accumulation reflects input from multiple glaciers and mixing due to post-depositional transport on the shelf. In ice-proximal subpolar settings accumulation also tends to be steady; this is presumed to be due to the long averaging time for ^{210}Pb concentrations that correspond to the slow accumulation, as well as the rare and spatially limited occurrence of large depositional events due to the relative dearth of meltwater.

From temperate to polar settings, ^{210}Pb-derived accumulation in ice-proximal settings (~5 km from modern ice front) slows by more than two orders of magnitude (Figure 2.10) (Harden et al., 1992; Domack and McClennen, 1996; Cowan and Powell, 1997; Smith et al., 2002; Szczucinski et al., 2009; Andresen et al., 2011). The general decrease in accumulation rate with distance from the glacial sediment source within individual temperate, subpolar and polar fjords is widely recognized in ^{210}Pb data (Cowan et al., 1997; Gilbert and Domack, 2003; Szczucinski et al., 2009; Andresen et al., 2011) and in data representing both longer and shorter timescales derived with ^{14}C dating and sediment traps, respectively (e.g., Figure 7 in Cowan and Powell, 1991; Figure 13 in Gilbert et al., 1998; Figure 10 in Jaeger and Nittrouer, 1999a; Figure 8b in Szczucinski and Zajaczkowski, 2012). However, the compiled data from various fjords, even when within the same climatic regime, do not reflect this well-documented pattern (Figure 2.10) (e.g.,Harden et al., 1992; Smith et al., 2002), presumably due to large inter-fjord differences in the factors that control sediment production rates (e.g., catchment size, lithology, joint density, geometry, ice flux); these are currently under study.

2.7 Conclusions

Herein, ^{210}Pb-derived rates of modern sediment accumulation are presented from 21 cores collected in 12 bays and fjords spanning from 50°S to 65°S. In 15 of these 21 cores, profiles of excess ^{210}Pb indicate relatively constant rates of sediment accumulation over approximately the past century, despite the recent rapid warming, increase in the frequency of surface melting events, and considerable glacier retreat in this region (e.g., Vaughan et al., 2003; Cook et al., 2005; Abram et al., 2013) . Accumulation rates increase markedly from fjords along the South Shetland Islands and WAP (~1-7 mm yr^{-1}) to Chilean fjords (~10-20 mm yr^{-1}), and this increase highlights the role of a warmer and wetter climate in southern Chile for accelerating glacial motion and the production and transfer of sediment. In contrast with sediment cores from the WAP that show steady accumulation, ^{210}Pb records from the South Shetland Islands show that sediment accumulation accelerated over the last few decades. Increasing air temperatures and precipitation events likely generated more vigorous periglacial weathering, mass wasting, and increased volumes of meltwater, which resulted in the delivery of more sediment-laden meltwater to fjords as the region shifted toward temperate conditions. With additional warming and meltwater production, it is expected fjord sediment accumulation rates to increase in the subpolar region of the Antarctic Peninsula, which would likely impact the pelagic and benthic communities (e.g., Dierssen et al., 2002).

The relatively large and temporally variable rates of sediment accumulation in the Chilean records resemble those in temperate Alaskan fjords; they all, presumably, reflect the role of meltwater in the sporadic delivery of sediment to ice-proximal fjord settings. The lower accumulation rates in the majority of subpolar fjords presented here are similar to rates in ice-distal settings of temperate fjords, because of the limited supply of terrigenous material in both settings and tendency for “events” to be smoothed when averaged over a typical 5-cm sampling interval. It is inferred that the sediments accumulate steadily in both settings for different reasons. In the ice-distal areas of temperate fjords, accumulation is relatively steady because inputs from multiple glaciers average out and attenuate the signal from single sedimentation events, and moreover, deposited sediments are mixed due to transport on the shelf. In contrast, subpolar-fjord accumulation is relatively steady because it is rarely interrupted by substantial delivery of sediment-laden meltwater from the subglacial hydraulic system, presumably because surface melt seldom reaches deep into the subpolar glaciers despite the recent increase in surface melt events. In conclusion, the steady nature of accumulation in subpolar fjords experiencing rapid warming likely reflects counteracting processes; a temporal increase in meltwater production accelerates the rate of sediment delivered to down-fjord sites, while terminus retreat increases the distance between the sediment source and down-fjord coring sites.

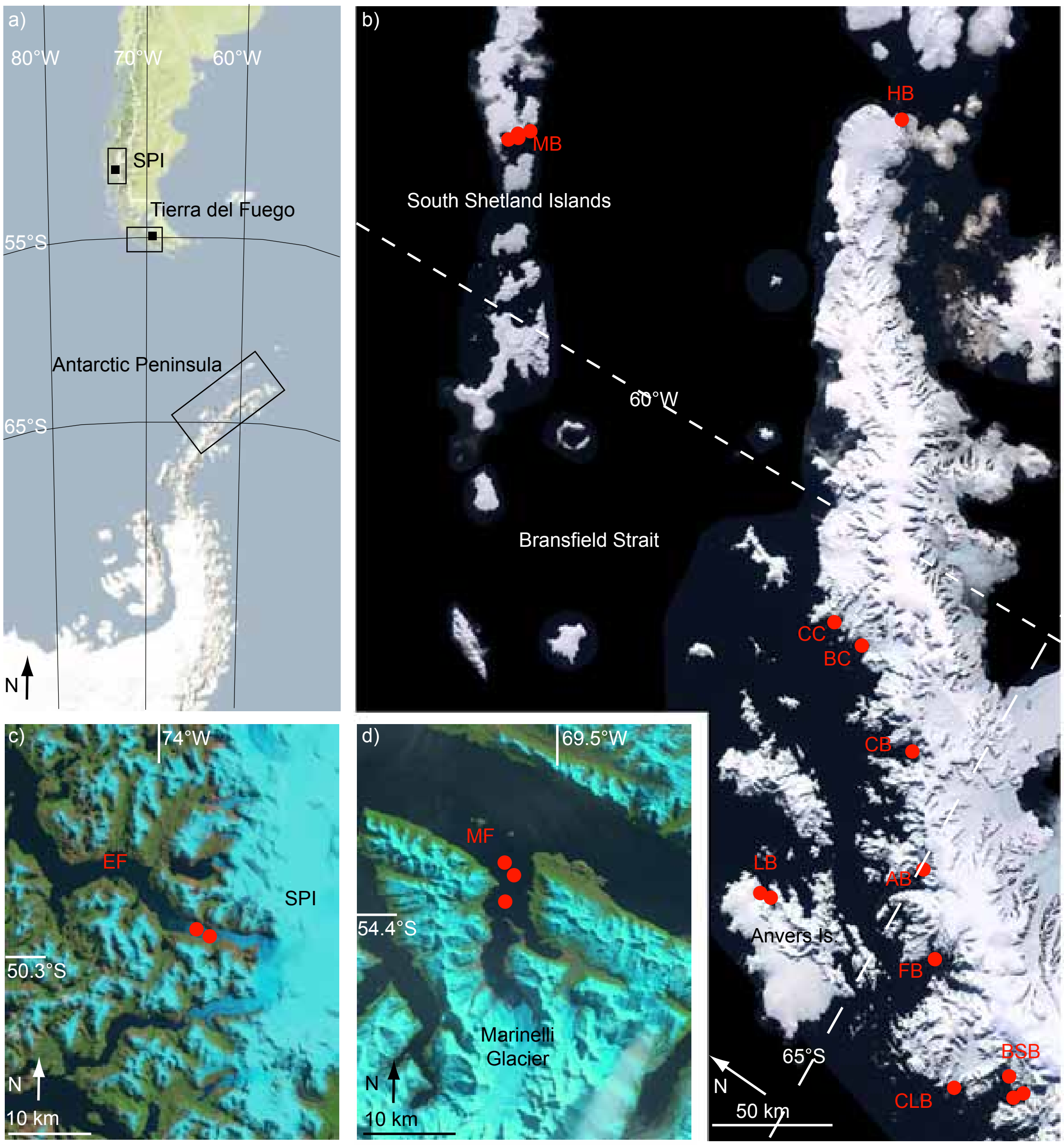

Figure 2.1 Antarctic Peninsula and Patagonia Core Sites
(a) Black boxes outline study areas, the southernmost of which is expanded in (b). Study sites within the black squares are expanded in (c) and (d). **(b)** Red circles represent core locations along the western Antarctic Peninsula, with site names abbreviated as in Table 2.1 (NSIDC image). **(c)** Red circles show core locations in Europa Fjord adjacent to the Southern Patagonia Icefield (SPI), and **(d)** in Marinelli Fjord, Tierra del Fuego (USGS landsat images).

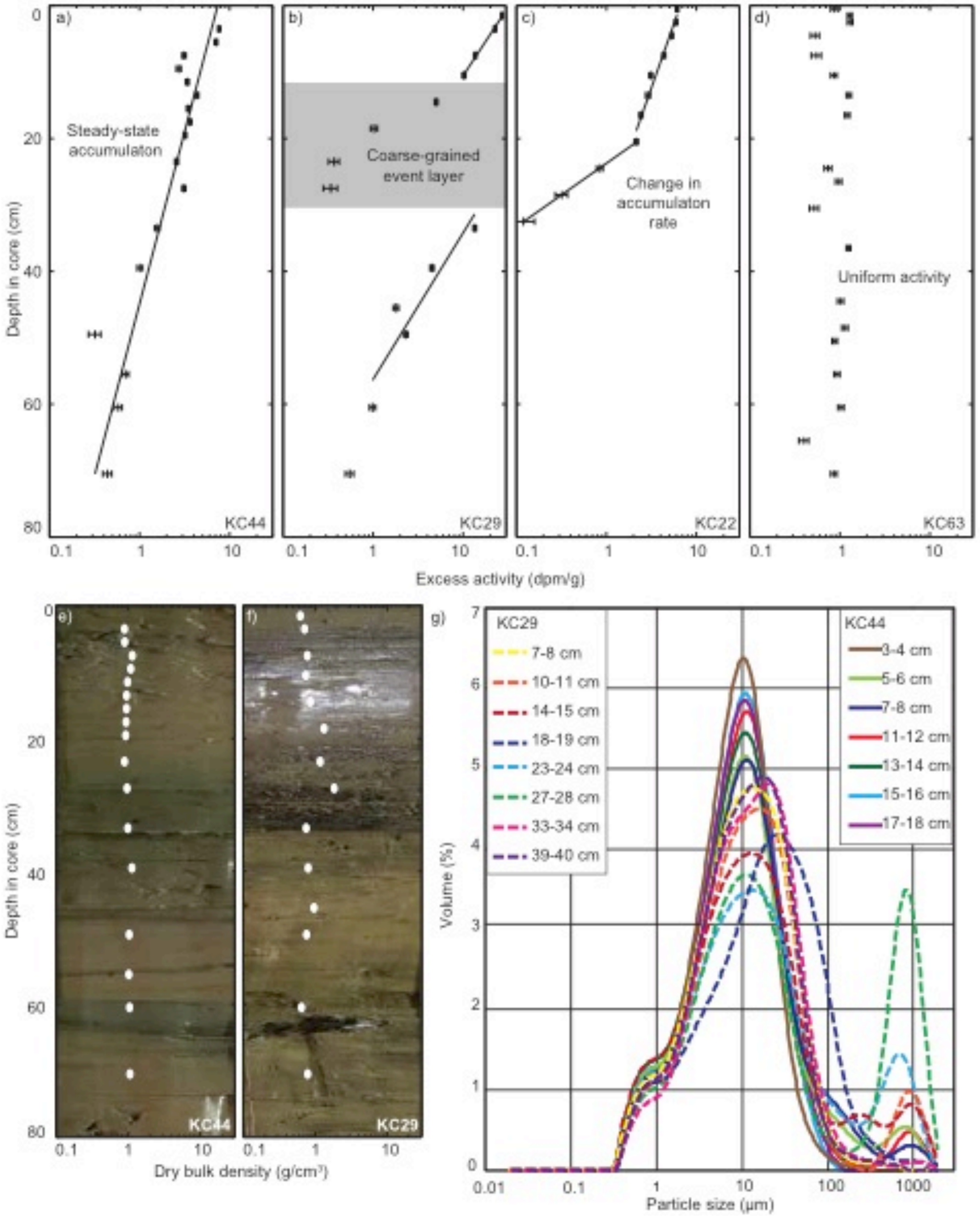

Figure 2.2 Representative Core Properties

Four types of ^{210}Pb profiles were observed in this study: **(a)** steady-state accumulation, **(b)** an event layer indicated by a region of lower ^{210}Pb activities in an otherwise steady-state profile, **(c)** a change in the rate of steady-state accumulation, and **(d)** complex accumulation or grain-size characteristics with slight variability in activity with depth in the core. **(e)** and **(f)** Representative core photographs and associated profiles of bulk density (white circles): one reflecting steady-state accumulation (KC44), and a second steady-state core with an event layer (KC29). Intervals with elevated bulk densities in KC29 are those with relatively coarse-grained sediments and bi-modal grain-size distributions, shown in **(g)**.

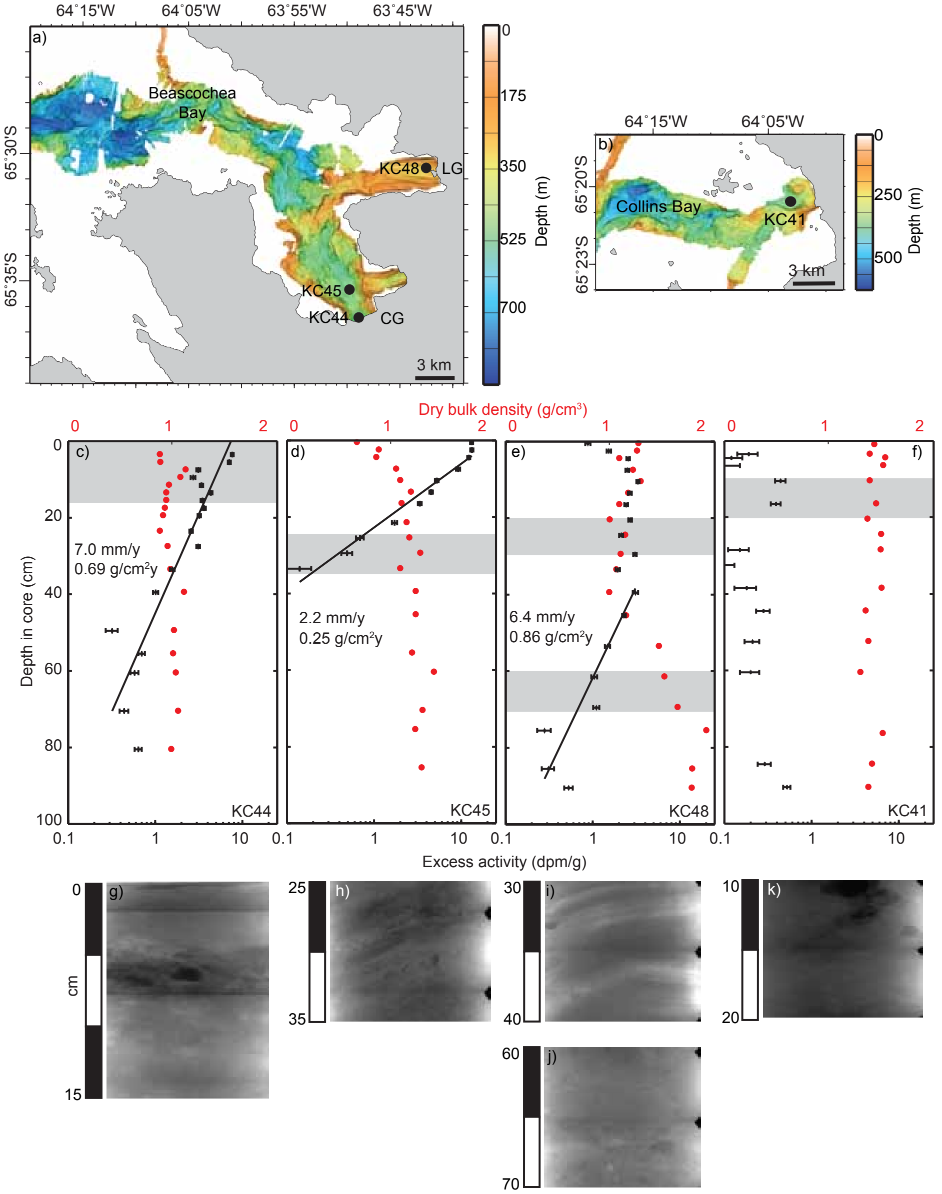

Figure 2.3. Beascochea Bay and Collins Bay Cores

(a,b) Bathymetry for Beascochea and Collins Bays, with locations of the four ice-proximal cores. LG and CG show locations of Lever Glacier and Cadman Glacier, respectively. Land and glacier-covered areas are shown in light gray; marine regions beyond the multibeam bathymetric data are colored white. **(c,d)** Cores KC45 and KC44 show steady-state ^{210}Pb accumulation (black symbols; lower abscissa), with relatively uniform bulk density profiles (red dots, upper abscissa). **(e)** KC48 records steady-state accumulation in front of Lever Glacier below a region of relatively uniform, high excess activities and lower bulk densities. **(f)** KC41 from Collins Bay shows uniform, low excess ^{210}Pb activities, corresponding to relatively uniform bulk densities. **(g-k)** Representative positive x-radiographs below each core image the gray-shaded areas in the above profiles (note artifacts of x-radiograph processing: black triangles along the right edge and corresponding dark horizontal lines).

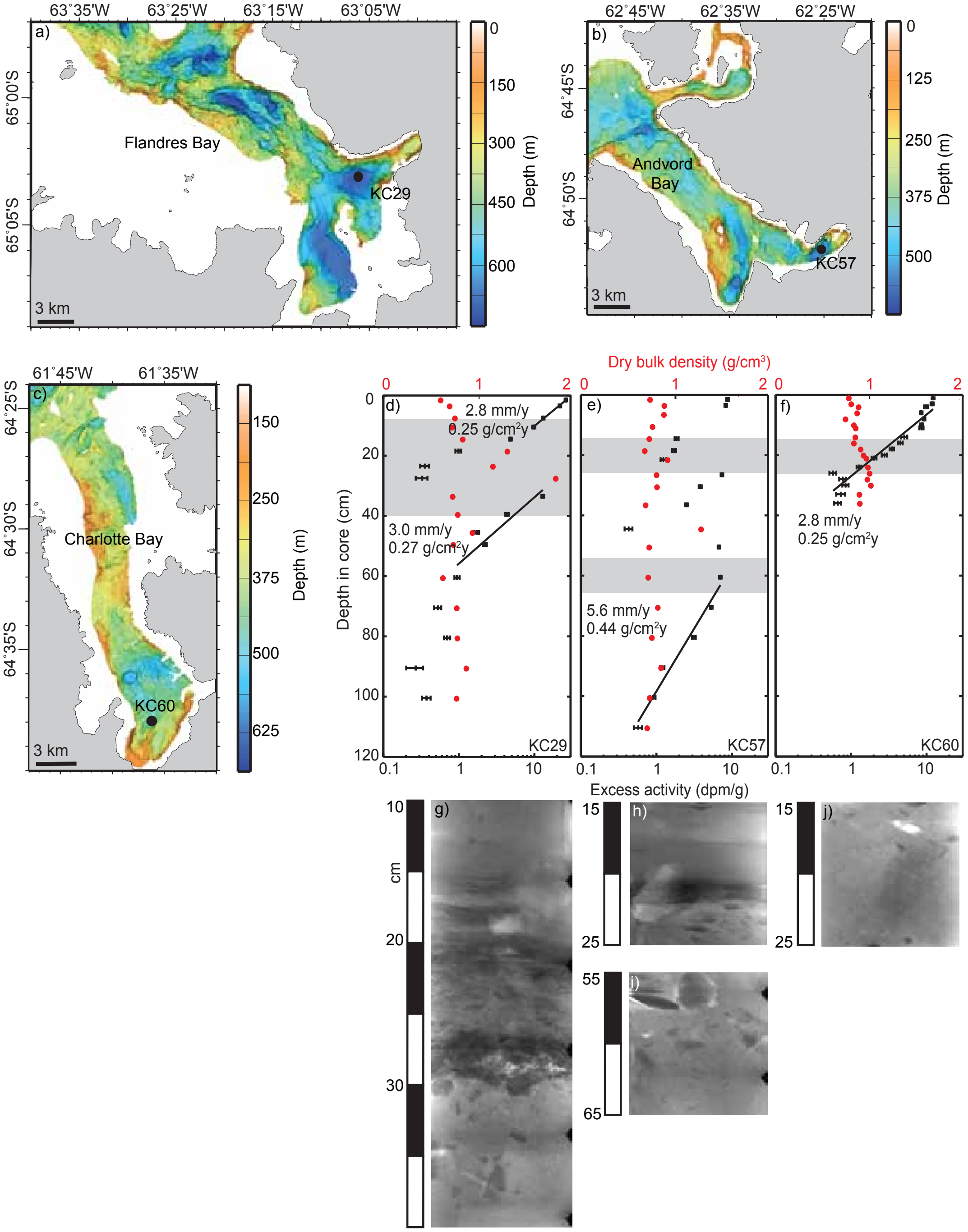

Figure 2.4. Flandres Bay, Andvord Bay, and Charlotte Bay Cores
(a,b,c) Land and glacier area (light gray), and multibeam bathymetry for Flandres, Andvord, and Charlotte Bays, with core locations indicated. Symbols are the same as for Figure 2.3. **(d)** A section of relatively low excess activity and higher bulk density interrupts otherwise steady accumulation in KC29, **(e)** steady-state sediment accumulation with uniform bulk density in KC57 was followed by accumulation with varying ^{210}Pb activity and density, and **(f)** relatively uniform bulk densities and steady-state accumulation of 2.8 mm yr^{-1} characterize KC60. **(g-j)** X-radiograph positives are shown for core sections shaded in gray, and reveal stratification and numerous dropstones.

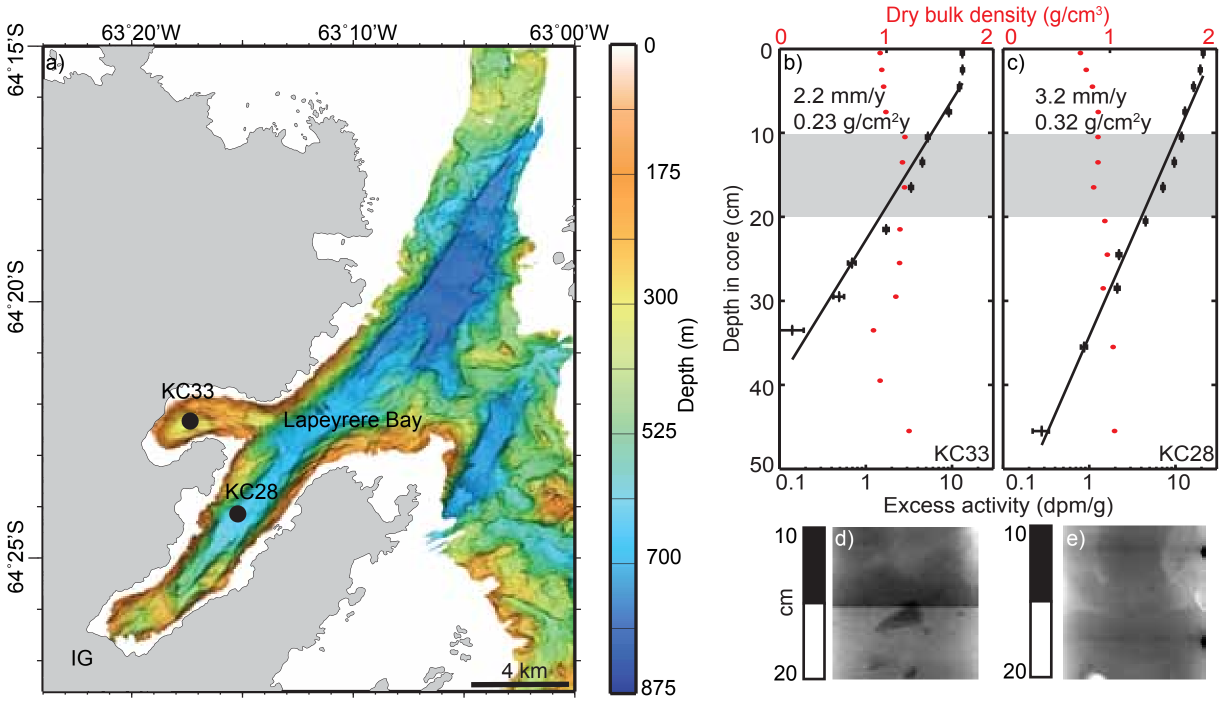

Figure 2.5. Lapeyrere Bay Cores
(a) Core locations from Lapeyrere Bay shown with multibeam bathymetry. IG indicates the location of Illiad Glacier. **(b,c)** Profiles of excess ^{210}Pb and bulk density indicate steady-state accumulation in KC33 and KC28. **(d,e)** X-radiograph positives highlight shaded intervals in KC33 and KC28. Dark triangles and horizontal lines are artifacts of x-radiograph processing. Colors and symbols are explained in Figure 2.3 caption.

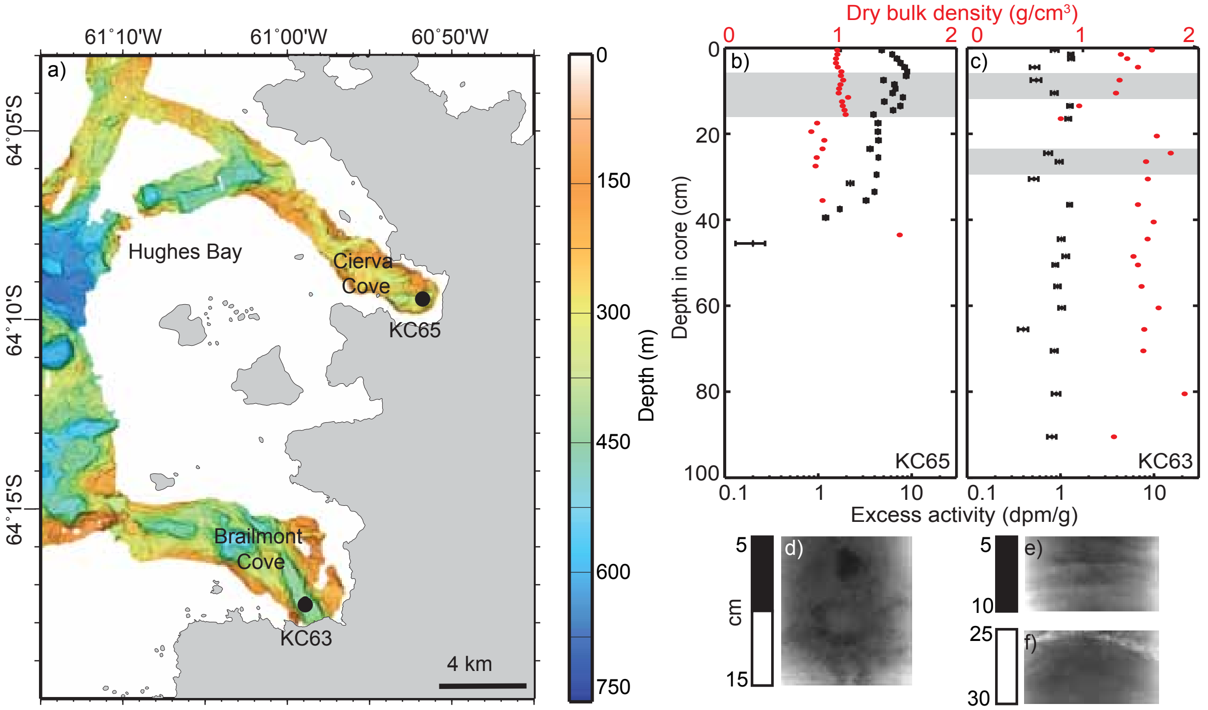

Figure 2.6. Cierva Cove and Brailmont Cove Cores
(a) Core locations in ice-proximal depocenters and multibeam bathymetry for Hughes Bay. Both the excess ^{210}Pb profiles for KC65 from Cierva Cove **(b)** and KC63 from Brailmont Cove **(c)** show relatively uniform high and low excess activities, respectively, extending the length of the cores. Bulk density profiles indicate fluctuations down core, consistent with those in ^{210}Pb activity. **(d-f)** X-radiograph positives corresponding to gray shaded areas show scattered dropstones in (d), and laminations in (e) and (f). Colors and symbols are explained in Figure 2.3 caption.

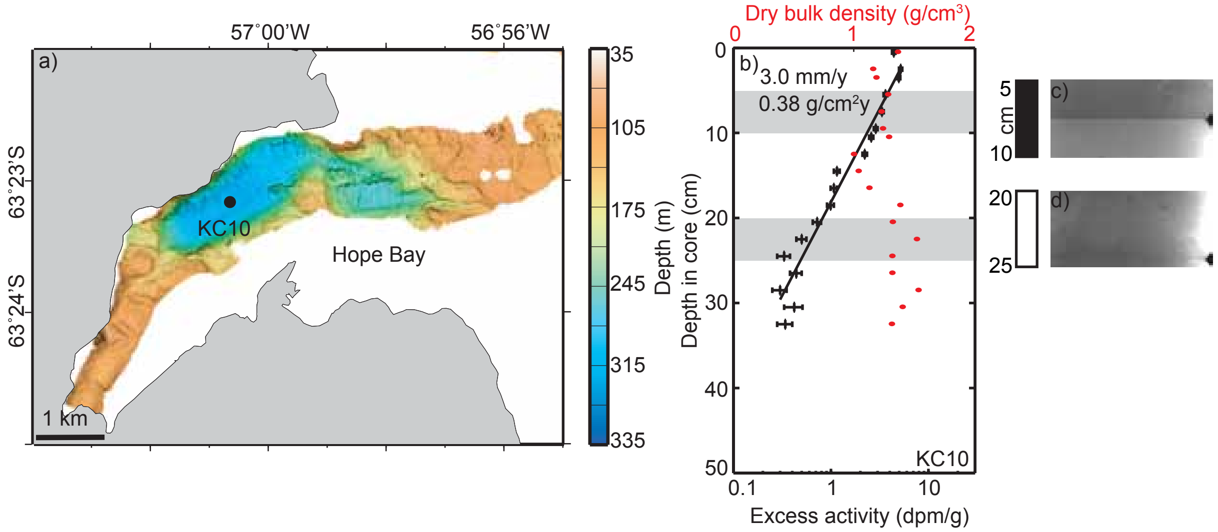

Figure 2.7. Hope Bay Core

(a) Multibeam bathymetry and core location for Hope Bay. The excess ^{210}Pb profile for core KC10 **(b)** indicates steady-state accumulation; bulk densities fluctuate from ~1-1.7 g cm^{-3}. **(c,d)** The x-radiograph images highlight the gray-shaded regions in (b). Dark triangles and horizontal lines are artifacts of x-radiograph processing. Colors and symbols are explained in Figure 2.3 caption.

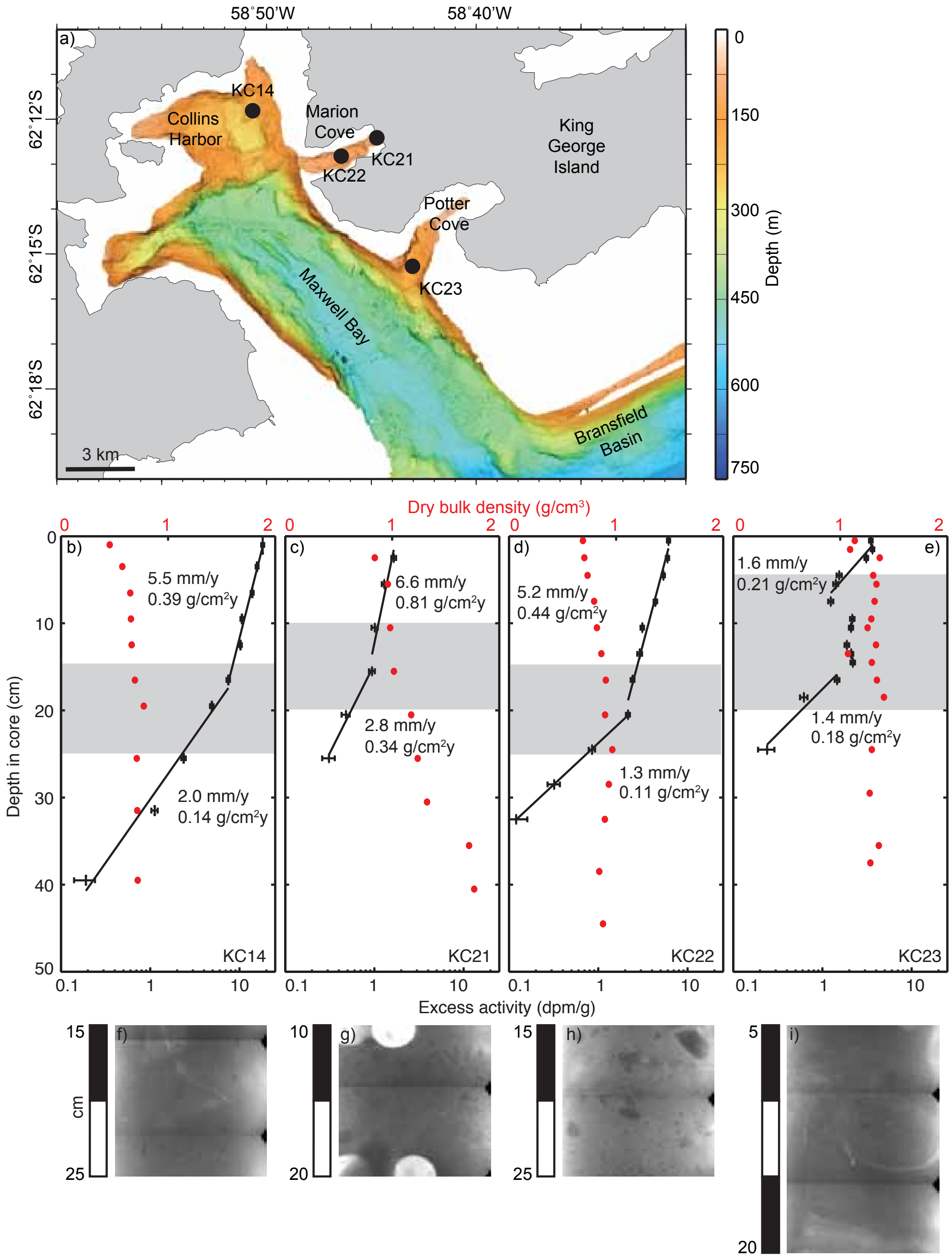

Figure 2.8. Maxwell Bay Cores
(a) Multibeam bathymetry and core locations near Maxwell Bay, South Shetland Islands. **(b,c,d)** ^{210}Pb profiles for the three ice-proximal cores; distinct break in slopes reflects abrupt increase in accumulation rate. **(e)** KC23, the most ice-distal, contains an event layer between the regions of steady-state accumulation. Bulk densities are relatively uniform in all cores except KC 21, where they increase with depth. **(f-i)** X-radiographs correspond to the areas shaded in (b-e), with numerous dropstones visible in (g) and (h). Dark horizontal lines extending from black triangles along the right edge of each image are artifacts of x-radiograph processing. White circles in (g) are empty spaces where samples were collected. Colors and symbols are explained in Figure 2.3 caption.

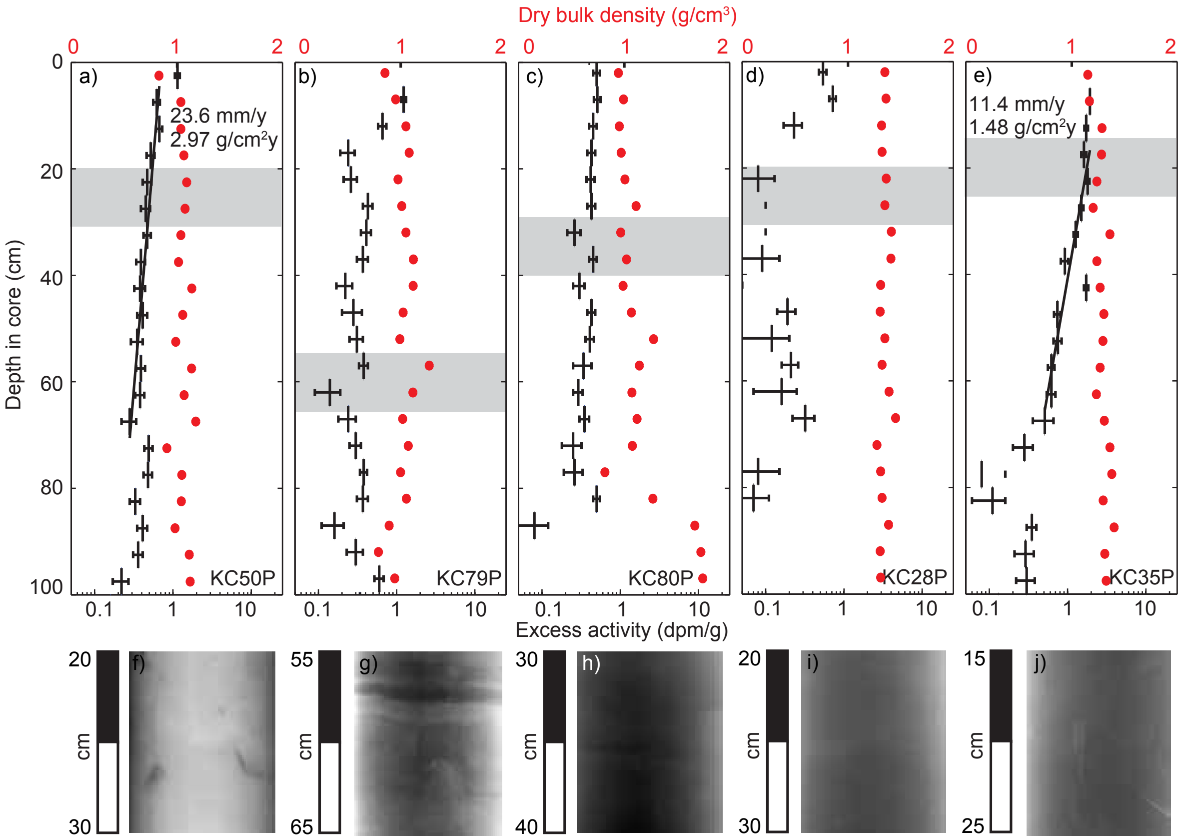

Figure 2.9. Chilean Cores

Five cores collected from southern Chile. Marinelli core KC50P **(a)** records the fastest steady accumulation in this study, 23.6 mm yr^{-1}. KC79P **(b)** and KC80P **(c)** from the outer Marinelli Fjord contain ^{210}Pb profiles with varying activity. KC28P **(d)** and KC35P **(e)** from Europa Fjord show varying, low activity and steady-state accumulation, respectively. The bulk density is relatively uniform and close to 1 g cm^{-3} for all cores except for the base of KC80P (e). **(f-j)** X-radiograph positives show the regions shaded in gray. Symbols are explained in Figure 2.3 caption.

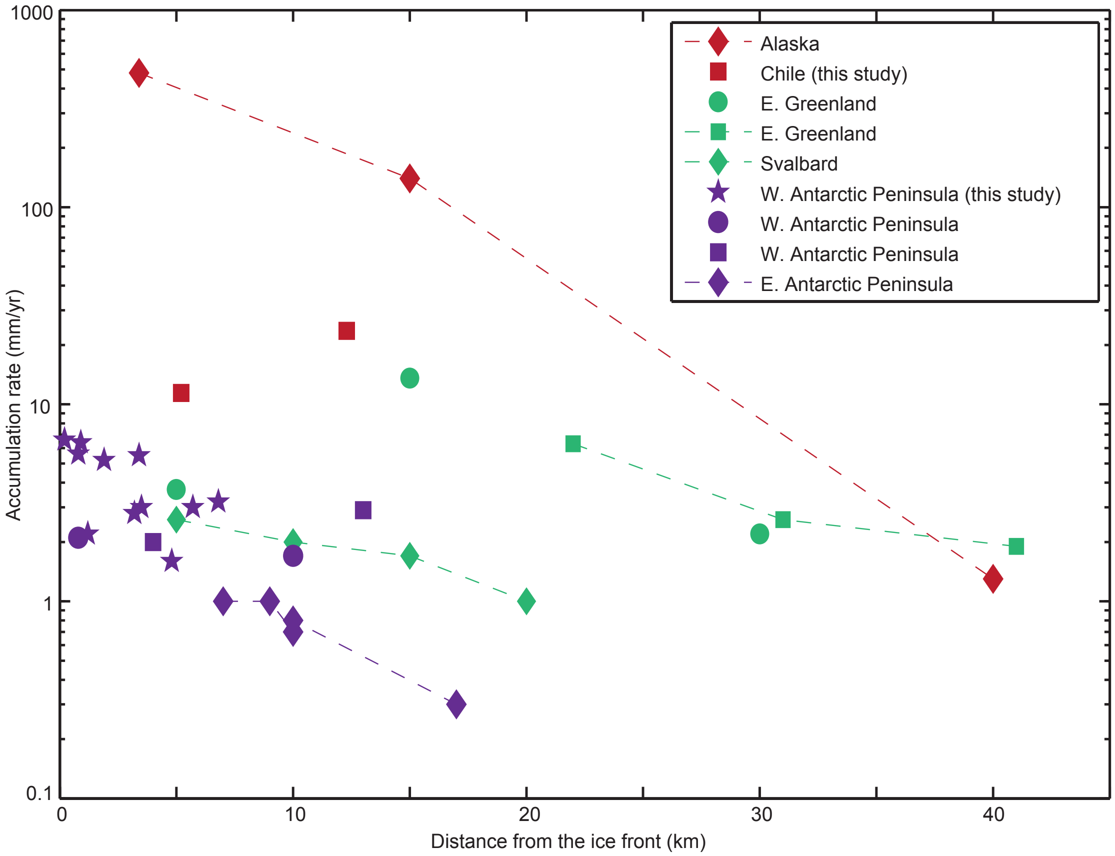

Figure 2.10. Worldwide ^{210}Pb Accumulation Rates
Compilation of published ^{210}Pb-derived accumulation rates for glacially influenced fjords. Red markers: temperate fjords in Alaska (Cowan et al., 1997) and Chile (this study); green markers: subpolar fjords in East Greenland (circles, Smith et al., 2002; squares, Andresen et al., 2011) and Svalbard (Szczucinski et al., 2009); and purple markers: cold subpolar to polar fjords in the Western Antarctic Peninsula (stars, this study; circles, Domack and McClennen, 1996; squares, Harden et al., 1992), and the Eastern Antarctic Peninsula (Gilbert and Domack, 2003). Lines connect measurements within individual fjords.

Chapter 3: Observations and modeling of fjord sedimentation during the 30-year retreat of Columbia Glacier, AK

3.1 Introduction

Over the past decades, marine-ending (*or tidewater*) glaciers around the world have lost mass at dramatic rates (e.g., Rignot and Kanagaratnam, 2006; Pritchard et al., 2009; Shepherd et al., 2012). This widespread accelerated loss of ice into the ocean is caused by more rapid surface melting, and especially by faster calving, submarine melting at the glacier terminus, and related processes that cause acceleration, thinning, and retreat (Luckman et al., 2006; Howat et al., 2007; van den Broeke et al., 2009). The difficulty in understanding processes occurring along this critical ice-ocean boundary has been identified as the major factor in limiting the accuracy of future sea-level rise predictions (Lemke et al., 2007; IPCC, 2013; Straneo et al., 2013). Roughly one third of current sea-level rise is caused by ice loss from mountain glaciers and ice caps (Lemke et al., 2007), and these glaciers are expected to dominate sea-level rise in coming century despite the much greater volume of the major ice sheets (Meier et al., 2007; Radić and Hock, 2011). Thus, the study of processes occurring along the critical ice-ocean boundary of tidewater glaciers has broad scientific and societal relevance.

One of the major factors controlling the rate of ice loss by calving and submarine melting is the water depth at the glacier terminus (e.g., Brown et al., 1982; Pelto and Warren, 1991; Jenkins, 2011; Motyka et al., 2013). This depth can decrease rapidly due to accumulation of sediment near the glacier terminus (Meier and Post, 1987; Alley, 1991). Sediment accumulation rates in fjords fed by temperate glaciers are known to be among the highest worldwide, reaching rates in excess of 10 m yr^{-1} at the ice front decreasing to ~1m yr^{-1} kilometers down the fjord (Cowan and Powell, 1991; Jaeger and Nittrouer, 1999a). These extreme rates of sediment accumulation and their variation in space and time merit close attention because they can affect glacier mass balance and stability by forming shoals that buttress the glacier, reduce buoyancy forces at the ice front, decrease the surface area available for submarine melting, and enable tidewater glaciers to advance into deep water (e.g., Meier and Post, 1987; Nick et al., 2007; Goff et al., 2012). This complex interaction has long been recognized, but has received little research attention. Moreover, the role of sedimentation is of special interest as, perhaps, the only known negative feedback that can slow or stop the demise of a marine-ending ice mass retreating in deepening waters (Alley et al., 2007; Schoof, 2007).

In addition to affecting glacial mass balance and stability, the sediments discharged by tidewater glaciers, which frequently accumulate in nearly closed fjord basins, form a valuable sediment record of glacier fluctuations, associated climatic changes, erosion and sediment-transfer events (e.g., Syvitski, 1989; Koppes and Hallet, 2002; Cowan et al., 2010; Willems et al., 2011). Accurately connecting fjord sediment deposits to their formative processes, such as changes in the glacial erosion rate or the climatic conditions, contributes to contemporary research focused on understanding how glacial erosion may link climatic and tectonic processes (e.g., Molnar and England, 1990; Berger et al., 2008). However, the potential for the subglacial storage of substantial volumes of sediments and their subsequent evacuation, highlighted in recent studies of Alaskan glaciers (e.g., Motyka et al., 2006; Cowan et al., 2010), complicates the interpretation of glacier erosion rates from fjord sediment deposits (e.g., Koppes and Hallet, 2002). Increasing our understanding of glacier archives from sediment deposits, as well as assessing the potential contribution of stored sediments to the preserved sediment record, is done best in settings for which the glacier behavior is known.

This study is focused on how the sediment flux of Columbia Glacier, near Valdez, Alaska, has varied during its well-documented 30-year retreat, and whether this variation is related to changes in glacier dynamics. This work leverages the extensive set of observations at Columbia Glacier that cover over three decades of dynamic retreat (USGS Professional Paper Series 1258, 1982-1989; Humphrey et al., 1993; Kamb et al., 1994; Meier et al., 1994; Krimmel, 2001; O'Neel et al., 2005; O'Neel et al., 2007; Pfeffer, 2007; Walter et al., 2010; Post et al., 2011; Rasmussen et al., 2011). Seismic surveys and bathymetric measurements in 2011 are considered in the context of the glaciological observations to (1) determine the volume and seismic architecture of sediment delivered by Columbia Glacier during its retreat; (2) develop a physically based numerical model to illuminate the formation of the sediment packages in Columbia Fjord as influenced by glacier retreat, sediment-flux history, and patterns of sediment deposition near the ice front that are affected by sediment-redistribution processes; and (3) interpret the modeled sediment-flux history in light of the documented glacier-dynamics history.

3.2 Columbia Glacier

Columbia Glacier is a temperate tidewater glacier in south-central Alaska (61.1°N, 147.1°W). It is presently 49 km long, covers an area of ~1000 km^2 and ranges in elevation from 0 to 3050 m above sea level (Figure 3.1a). The temperate climate of southern Alaska results in average annual rainfall and water equivalent snowfall of ~1.5 m yr^{-1} and ~1 m yr^{-1}, respectively, as measured at sea level in Valdez, AK, ~35 km east of the glacier (US National Weather Service). This relatively high precipitation sustains the extensive glaciers in the region, many of which extend to the sea. In the early 1980s, after a period of stability roughly two centuries long (Nick et al., 2007), Columbia Glacier entered a phase of rapid retreat (Meier et al., 1985). This sustained period of negative surface balance and thinning forced a dynamic instability, which resulted in accelerated surface lowering, retreat, and a permanent loss of contact with the stabilizing moraine shoal (Meier and Post, 1987; Pfeffer, 2007) (Figure 3.1b). The retreat accelerated until the mid 1990s, after which it slowed for two periods between 1994-1997 and 2000-2006 (Meier and Post, 1987; Pfeffer et al., 2000; O'Neel et al., 2005), and has accelerated again since September 2006 (Figure 3.1c). For the period 1996-2007, the average calving rate was about 8 km^3 yr^{-1}, which accounts for ~95% of the total glacier-wide mass loss (Rasmussen et al., 2011). Since 1957, the glacier has lost half of its volume and thickness (McNabb et al., 2012), the terminus has retreated 23 km at an average rate of ~0.7 km yr^{-1}, and within decades a deep fjord replaced a long ~1-km-thick glacier. In the next few decades, Columbia Glacier is expected to retreat another 14 km until the glacier bed rises above sea level. Present ice discharge from Columbia Glacier exceeds that of any other Alaskan glacier and accounts for ~6% of the sea-level rise contribution from Alaskan glaciers during the period 1962-2006 (Berthier et al., 2010). Because mass loss from all Alaskan glaciers accounts for 20% of global ice loss (Gardner et al., 2013), Columbia alone accounts for ~1% of global ice-mass loss.

Columbia Glacier has been surveyed in detail since 1976 by aerial photography at sub-annual intervals, and since 2004 with approximately daily time-lapse photography (Krimmel, 2001; O'Neel et al., 2005). This photographic record documents the entire retreat of Columbia Glacier and provides a history of the glacier terminus position, ice velocity, and rates of thinning (Figure 3.1b; Krimmel, 2001). Rasmussen et al. (2011) developed the time history of mass loss from Columbia Glacier, which was used by McNabb et al. (2012) to calculate ice thickness and bed topography over the entire glacier area. During its early retreat in 1987, two boreholes were drilled to the bed of Columbia Glacier to determine the properties of the glacier bed (Humphrey et al., 1993; Meier et al., 1994). These data, together with bathymetric measurements taken in 1997 (Krimmel, 2001), multibeam mapping in 2005 (Noll, 2005), and the bathymetric measurements in 2011, constrain the evolution of the fjord seabed as sediments accumulated in the fjord. While the retreat history of Columbia Glacier has been documented in detail, essentially nothing was known about the sediments it produces, except that a sediment shoal has long been inferred to play a central role in the stability of this glacier (e.g., Meier and Post, 1987; Nick et al., 2007).

3.3 Observational Methods and Analyses

3.3.1 Fjord Seabed and Sediment Datasets

In September 2011, during rare ice-free conditions, bathymetric and sedimentologic measurements were collected throughout the entire Columbia Fjord, including a previously uncharted area within 7 km of the 2011 glacier terminus (Figure 3.2). Seismic-reflection profiles of sediment basins were acquired using a 750 Hz bubble pulser, six kasten cores were collected in a transect extending to the ice front, and bathymetric measurements were obtained throughout the fjord. This dataset represents the first characterization of the sediments that have accumulated in Columbia Fjord since the onset of retreat around 1980.

The seismic-reflection profiles were single-channel data; they provided no information about sediment velocities that could be used to determine depths. Thus, the data were migrated and depth converted using a representative seismic speed of 1500 m s^{-1}. This represents an approximate speed of sound through brackish (~30 psu), cold (~6°C) water, as measured in Columbia Fjord (S Gay, pers. comm.; Fu-Xing et al., 2012), as well as through the upper, unconsolidated glacial marine sediments collected in the sediment cores. Any compaction in the sediments with depth would result the total sediment thickness being underestimated (Michalchuk et al., 2009; Milliken et al., 2009), as this reference speed is used for the entire sediment thickness. Depth-converted seismic profiles were analyzed using the open-source seismic interpretation software OpendTect 4.4.0.

From both the seismic images and the depth soundings, a large moraine complex (morainal shoal) was identified at the entrance to the fjord, where the water depth reaches a minimum of ~5-10 m and increases in both directions (A’ in Figures 3.2, 3.3). The moraine marks the advanced, stable position of the Columbia Glacier up to 1980. The fjord contains two distinct sediment basins, one that extends from the 1980 moraine to a sill midway down the fjord (Figure 3.3), and the second that extends from the sill to the modern terminus; they are referred to herein as the “outer basin” and “inner basin,” respectively (Figure 3.2).

3.3.2 Sediment Volume Calculations

For each seismic profile, the reflections corresponding to the top and bottom of the post-retreat sediment package were defined (Figure 3.3). The reflection marking the seabed-water interface was chosen as the most distinct reflection where the seismic facies changed from mostly transparent above to distinct, continuous, and parallel reflections below. The depth of this reflector was then compared to independently measured bathymetry to ensure consistency. The bottom of the sediment package was chosen as the most continuous and distinct reflection where the seismic facies changed from relatively high amplitude, parallel, and continuous above to a low-amplitude and discontinuous facies below. The choice of the bottom reflection is confirmed by the close agreement between the altitude of the former glacier bed from glacier borehole measurements (Meier et al., 1994) and the seismically chosen depth of the sediments at the same location (Figure 3.3).

In addition, a continuous reflector interpreted to be the 1997 seabed was inferred for the along-basin seismic line 11 based on water depth measurements made by A. Post and B. Hallet in 1997 (Figure 3.3) (Krimmel, 2001). This surface was interpolated throughout the outer basin and used to calculate the total volume of sediment deposited between the moraine and the sill from the start of retreat in 1980 until 1997, when the glacier had retreated across this basin.

To calculate the total sediment volume in the fjord, the location of the seabed and basin bottom reflectors were interpolated across the area of the sediment basins from the 1980 moraine to the modern terminus using both the inverse distance weighting and triangulation methods in OpendTect. The difference between the top and bottom surfaces provides the volume of sediment that accumulated in 30 years for each interpolation method, 3.3 x10^8 m^3 from inverse distance and 3.0 x10^8 m^3 from triangulation. The sediment volume was also estimated as 3.1 x10^8 m^3 simply based on the approximate mean basin width, sediment thicknesses, and sidewall slopes. The consistency of these estimates provides confidence in the estimation of the total sediment volume and helps assess the uncertainty. This volume likely underestimates the total sediment output of Columbia Glacier because they focus on the fine-grained, well laminated sediment in the basin, and do not fully account for coarser deposits that are seismically difficult to differentiate from the underlying, consolidated sediment or bedrock. Additionally, any sediment that was transported beyond the moraine is not accounted for.

From the calculated sediment volumes and the temporally constrained bathymetric evolution, the total estimated volume of fine-grained sediment in the recently deglaciated Columbia Fjord is $3.2 \pm 1.1 \times 10^8$ m^3. From these volumes, the corresponding sediment fluxes for the two relatively well constrained time periods, 1980-1997 and 1998-2011, averaged $3.0 \pm 1.0 \times 10^6$ m^3 yr^{-1} and $19 \pm 7 \times 10^6$ m^3 yr^{-1}, respectively.

3.3.3 Effective Erosion Rate

The basin-averaged bedrock erosion rate that would be required to sustain this flux of sediment to the fjord during the retreat can be determined, and is referred to as the effective erosion rate. The effective bedrock flux from the glacier, Q_{rock}, is calculated by accounting for the difference in density between glacimarine sediment and bedrock:

$$Q_{rock} = \rho_{sed} Q_{sed} / \rho_{rock} \quad (3.1).$$

The erosion rate, $\dot{E}$, averaged over the entire glaciated area, A, is then determined:

$$\dot{E} = Q_{rock} / A \quad (3.2).$$

For the 1000 km^2 catchment, an average bedrock density, ρ_{rock}, of 2700 kg m^{-3} is used. From the glacimarine sediment cores, the measured a dry bulk density, ρ_{sed}, is 1000 ± 200 kg m^{-3}. Because this density reflects only the unconsolidated surface sediments, for the erosion calculation an average dry bulk density of 1300 kg $m^{-3}$is used, which is representative of glacimarine sediment collected in many settings to a depth of tens of meters (e.g., Milliken et al., 2009). The effective erosion rate averages ~5.1 ± 1.8 mm yr^{-1} during the 30-year retreat.

3.4 Glacimarine Sedimentation Model

To explore the connection between sediment delivery, accumulation, and glacial retreat, I developed a numerical model of the 30-year record of sediment flux from Columbia Glacier that is consistent with the known rate of retreat, sediment distribution, and stratigraphic architecture. The model also allows the short-term, relatively instantaneous, sediment-deposition observations to be related to the ultimate glacimarine record preserved in fjords. *In situ* sediment-trap measurements and radioisotope decay profiles from Glacier Bay and Icy Bay, Alaska, show that in the short term, over periods of days and tens of days, sediment deposition decreases rapidly from 10's of m yr^{-1} within 500 m of the ice front to ~1 m yr^{-1} several kilometers away from the ice front (Cowan and Powell, 1991; Jaeger and Nittrouer, 1999a). Seismic profiles collected from these same temperate fjords typically image steep-sided walls free of sediment, fjord seabeds with remarkably little to no surface slope, and parallel internal seismic reflectors (Carlson, 1989; Cai et al., 1997; Koppes and Hallet, 2002; 2006; Cowan et al., 2010). The horizontal seabed geometry and parallel internal reflectors that are representative of these sediment basins suggest that high-concentration gravity-driven processes play a large role in sediment delivery and redistribution in temperate fjords (e.g., Syvitski, 1989). *In situ* measurements of these gravity-driven processes are difficult to obtain while active, but the few existing *in situ* measurements from river-fed fjords suggest turbidity currents occur regularly (e.g., Prior et al., 1987; Bornhold et al., 1994).

3.4.1 Model Development

The model addresses the evolution of sediment accumulation as a function of the time-varying position of the terminus and sediment input from the glacier. It is also used to develop a sediment-flux history compatible with the observed sediment thickness and internal architecture. The approach is guided by field studies of sedimentation (Cowan and Powell, 1991; Jaeger and Nittrouer, 1999a) and builds on the 1-D model developed by Koppes and Hallet (2002), wherein the sediment accumulation rate, $\dot{S}(x,t)$, decreases exponentially with distance down-fjord from the terminus, *x*:

$$\dot{S} = \dot{S}_0 e^{-x/\delta} \qquad (3.3).$$

$\dot{S}_0(t)$ characterizes the time varying accumulation rate at the ice front, and δ represents the falloff distance of the accumulation rate, which is the distance over which the rate drops 1/e of the value at the terminus. The total sediment accumulation at any location in the fjord, *S(x)*, is the time integral of the sediment accumulation rate:

$$S = \int_0^t \dot{S}_0 \, e^{-\dot{R}t/\delta} dt \qquad (3.4),$$

where the distance from the terminus, x, is the product of the retreat rate, $\dot{R}(t)$, and time, *t*.

Over long periods, if the rates of retreat and accumulation are both constant, the integral simplifies to

$$S = \frac{\delta \dot{S}_0}{\dot{R}} \qquad (3.5),$$

which shows that for steady retreat and sediment input, the resulting sediment thickness is uniform; as expected, it scales with the accumulation rate at the ice front and inversely with the retreat rate. Equation 3.5 expresses the intuitive result that if the sediment output from the glacier were constant in time, a faster retreat would distribute the same volume of sediment over a greater area, forming a thinner deposit. In reality, both $\dot{S}_0(t)$ and $\dot{R}(t)$ vary in time, so the sediment thickness in any location reflects the complex history of both the retreat rate and sediment accumulation rate. If the retreat rate is known, as in the case of Columbia Glacier, the time-variation of the sediment flux, represented by $\dot{S}_0(t)$, can be calculated from the observed sediment thickness, *S*.

In the model, both primary proglacial sedimentation and secondary reworking are represented explicitly, such that the change in seabed elevation reflects sediment derived directly from the glacier as well as subsequent downslope transport. The model begins with the simple conservation of mass in 2-D, where the change in basin elevation, $\frac{dz}{dt}$, equals the divergence in the flux of sediment, q, per unit width across the fjord at a given location:

$$\frac{\partial z}{\partial t} = -\frac{\partial q}{\partial x} \qquad (3.6).$$

The sediment delivery from the ice front is modeled as the sum of two exponential distributions that represent ice-proximal and distal sedimentation with short and long decay distances, respectively:

$$\frac{dz}{dt} = \dot{S}_{01}e^{-x/\delta_1} + \dot{S}_{02}e^{-x/\delta_2} \qquad (3.7).$$

Fast sediment accumulation that decreases rapidly from temperate glacier termini is well recognized from field measurements (e.g., Cowan and Powell, 1991; Jaeger and Nittrouer, 1999a). The falloff distances for each of the two exponential terms, δ_1 and δ_2, were approximated from *in situ* data collected by Cowan and Powell (1991) in Glacier Bay, AK. While these data can also be described by a power law decay, the sum of two exponential curves is used to permit examination of distinct roles of proximal and distal sedimentation processes in forming the sediment accumulation throughout the fjord. It is assumed that once sediment reaches the seabed, it tends to be redistributed downslope due to slumping, iceberg gouging, and other diffusional processes at a rate proportional to the seabed gradient,

$$q = -\kappa\frac{\partial z}{\partial x} \qquad (3.8),$$

where κ is an effective diffusivity of the sediments.

Combining Equations (3.6) and (3.8) yields the time-evolving sediment elevation after initial deposition due to both direct sediment delivery from the glacier and diffusive downslope transport,

$$\frac{dz}{dt} = \dot{S}_{01}e^{-x/\delta_1} + \dot{S}_{02}e^{-x/\delta_2} - \kappa\frac{d^2z}{dx^2} \qquad (3.9).$$

In essence, the gravitational redistribution of sediment throughout the fjord basin is modeled as diffusive transport, where the diffusivity, κ, represents broadly a “mobility factor” for fjord sediment. This simple approach enables the distribution of sediment in any fjord, and the stratigraphic architecture of sediment packages, to be modeled as functions of retreat, sediment-flux histories, and fjord geometry. For a system like Columbia Glacier, for which the basin geometry, sediment distribution, and ice retreat history are all well known, the model can be used to infer in considerable detail the time varying delivery of sediment by the glacier.

3.4.2 Model Applied to Columbia Glacier

The evolution of the sediment package in Columbia Fjord is modeled over a ~20-km-long transect along the fjord extending from the 2011 terminus position to the 1980 moraine (Figure 3.4). The retreat rate is calculated from the near-monthly terminus positions mapped from aerial photographs for 1980-2000 (Krimmel, 2001) and by time-lapse photography for 2000-2010 (T. Pfeffer, written comm., 2013) (Figures 3.1b, c).

The sediment flux, *Q(t)*, must account for the sediment accumulation over the entire fjord bottom from the ice front to the distance approaching ∞, as described by Equation 3.4, and evenly across a weighted mean width, $\widehat{W}$, consistent with seismic data that suggest uniform accumulation across the fjord bottom. Thus

$$Q(t) = \int_0^\infty \dot{S}(x,t)\widehat{W}(x)dx \qquad (3.10).$$

Integrating Equation 3.10 and using Equation 3.3 for $\dot{S}$ associated with the proximal and distal exponential terms yields the total flux from the glacier:

$$Q(t) = \dot{S}_{01}\delta_1\widehat{W}_1 + \dot{S}_{02}\delta_2\widehat{W}_2 \qquad (3.11).$$

The weighted widths, $\widehat{W}_1$ and $\widehat{W}_2$, represent the fjord width weighted by the thickness of sediment accumulating at that down-fjord distance. The widths are weighted with the sediment accumulation from the ice front to twice the distances δ_1 and δ_2 to represent ~90% of the total sediment delivered. This weighting captures important down-fjord variations in both the width and sediment-accumulation rate.

In addition, because the fjord widens upward, the width of the accumulation zone increases with time as the sediment deposit thickens. The increasing width is accounted for by assuming a parabolic shape corresponding to fjord cross sections that are both observed in the seismic data and generally representative of glacier valleys (e.g. Harbor, 1992). The rate at which the width increases as the basin fills for each along-fjord location is constrained by the measured sediment thickness and seafloor width. This enables the model to account for both spatial and temporal variations in the fjord width when calculating the modeled sediment flux.

The known sediment volume that accumulated during the two well defined time intervals (1980-1997 and 1998-2011) provides robust guidance for the modeled sediment-flux history, as it provides the first-order sediment-flux history (dashed lines in Figure 3.5a) on the basis of which the model can be optimized. Using the mean sediment flux for each of the two periods, described in section 3.3.2, together with a weighted width estimated from the known fjord geometry, the approximate rates of both proximal and distal sediment deposition are determined for each of the constrained periods.

To determine a detailed sediment-flux history that is broadly consistent with the observed internal seismic stratigraphy, sediment thickness distribution, total sediment volume, and retreat history of Columbia Glacier, the 30-year retreat is subdivided into ten discrete time intervals. For each interval, rates of sediment accumulation at the ice front are estimated such that the 30 years of accumulation, modified by diffusive gravitational reworking, approximates the observed sediment thickness. The sediment accumulation rate at the terminus for each time interval was estimated by applying a scaling factor to the mean sediment accumulation rate, which was calculated from the seismically determined sediment thickness. These scaling factors were chosen simply by trial-and-error such that the resulting sediment-flux history produces sediment deposits generally consistent with the observed sediment thickness distributions in 1997 and 2011. Judicious choices of scaling factors and model parameters resulted in a set of sediment-flux histories bracketing the optimal history resulting from this non-unique inverse problem.

3.4.3 Model Results

The optimal model output was chosen as the sediment-flux history that produces 1) a sediment distribution pattern minimizing the RMS difference between the modeled bathymetry and the actual bathymetry measured in both 1997 and 2011; and 2) a basin with internal architecture generally consistent with the sediments imaged in the seismic profiles (Figures 3.4a, b). The resulting sediment-flux history accounts for the measured sediment volume deposited between the start of retreat in 1980 and 1997, when the interim bathymetry is known, and also for the total volume deposited until 2011 (Figure 3.5a). The modeled sixfold increase in the sediment flux, from ~3 x10^{6} m^{3} yr^{-1} to ~20 x 10^{6} m^{3} yr^{-1}, that started in 1997 is consistent with the sediment record inferred independently of the model; the bathymetric records indicate that 70-80% of the sediment volume in the outer basin accumulated after 1997 (Figure 3.3).

Sedimentation falloff distances most consistent with published *in situ* sediment-trap measurements (Cowan and Powell, 1991) are of the order of 100 and 10,000 m for δ_1 and δ_2. The portion of the sediment flux associated with δ_1 accounts for the rapid sediment deposition near the ice front (up to 10's m yr^{-1}). In exploring the model parameter space, the sediment flux history is most sensitive to the accumulation rate at the ice front, $\dot{S}_{01}$ and $\dot{S}_{02}$, while the shape of the basin and the internal sedimentary stratigraphy depend most strongly on the sediment diffusivity. Varying the different parameters in Equation 3.11 produces a range of basin geometries and sediment-flux histories (e.g. Figures 3.6, 3.7); however, because the outputs are all constrained to produce the mean fluxes obtained from the seismic and bathymetric data, all model outputs show the sediment flux increasing non-uniformly with time.

While the modeled sediment flux history reproduces the sediment thickness distribution and internal stratigraphy of the outer and inner basins, it does not account for sediments on the major sill, or the perched deposits on the 1980 moraine (Figure 3.5b). The sediments on the sill are not well imaged in the seismic profiles (Figure 3.2), however, and there are no sediment samples from the area. As both the sill and perched deposits are situated in high points along the basin, and the other sediment deposits fill depressions with minimal surface slope, these "perched" deposits are interpreted as likely composed of coarser-grained sediment that would be considerably less mobile than the finer sediments filling most of the basin. By introducing an additional, low sediment diffusivity, the model could account for these less mobile deposits, but it would require an additional model parameter that is not well constrained. Moreover, using a low diffusivity for the entire fjord would not optimize the basins that are well imaged, further suggesting that these "perched" deposits are more resistant to the processes modeled by diffusion. Thus, a single, high sediment diffusivity is retained, and the volume of sediment contained in the perched moraine deposits is included in the RMS calculations, but the volume of the sill deposit is not.

3.4.4 Error Estimates

Errors in the sediment volumes and calculated sediment fluxes arise from several sources. The chosen seismic velocity of 1500 m s^{-1} is likely too low for the more consolidated sediments at the base of the deposits. The difference between the generic sound speed in water 1500 m s^{-1}, used above for both the water and sediments (chosen to best represent the speed in the shallow sediments), and 1550 m s^{-1}, the velocity found to match the seismic properties of ~100-m-long cores from the Antarctic Peninsula (Michalchuk et al., 2009; Milliken et al., 2009), is about 3%. Hence, by using the lower speed over the entire deposit, the sediment thickness, and thus the volume, are underestimated by a maximum of 3%. The error is most likely less, however, because the fjord narrows downward so the deeper parts of the sediment package account for a smaller percentage of the total volume. In addition, the volume of sediment calculated by the three methods of interpolating the seismic horizons representing the top and bottom of the sediment package varies by ~15%.

The seismic surveys did not cover the area closest to the ice (within approximately 1.5 km) of the west branch of Columbia Glacier because of icebergs blocking ship passage. Based on a measured annual retreat in 2011 of ~1.3 km (Figure 3.1c), the area not surveyed received sediment for ~1.15 years, and thus likely accumulated a sediment volume roughly equivalent to ~15% more than the total annual sediment volume accumulating close to the ice front. Using the modeled proximal sediment flux for 2011 (Figure 3.5a), the missing volume is estimated to be ~2.3 x 10^7 m^3, or ~7% of the total volume in Columbia Fjord. In seismic profiles from the inner basin, it is difficult to differentiate between coarse, poorly bedded material recently delivered by the glacier from consolidated older sediment at the base of the recent deposits; a ~3% uncertainty is therefore assigned to the sediment volume estimate in the inner basin.

Additional uncertainty in the sediment volume and fluxes results from assumptions regarding the source and sink of sediment in Columbia Fjord: that the fjord is a perfect sediment sink with all of the sediment delivered by the glacier being captured within the inner and outer basins, and that Columbia Glacier is by far the predominant source of sediments. An estimated ~10% increase in the volume is included to represent potential contributions from hillslopes and other secondary sources. This estimate is slightly lower than for similar studies (e.g., Koppes and

Hallet, 2006), however, the lack of evidence in the seismic profiles for material entering from the fjord sides together with the lack of significant rivers entering the fjord supports the lower value. The counteracting effect of these assumptions is stressed: sediment escaping the fjord would result in an underestimate of the glacier-supplied volume, while sediment entering from sources other than the glacier would result in an overestimate. Thus, a ± 35% uncertainty is applied in the sediment volume and flux calculations, and it is stressed that the results likely underestimate the total sediment delivered by Columbia Glacier during its retreat.

3.5 Discussion

3.5.1 Implications for the Evolution of Fjord Sediment Basins

New bathymetric and seismic data, when interpreted in the context of mid-retreat (1997 & 2004) bathymetry measurements (Krimmel, 2001; Noll, 2005) and the 1987 boreholes through nearly 1000 m of glacier ice (Meier et al., 1994), constrain the depositional evolution of the sediments that accumulated during the 30-year retreat of Columbia Glacier. Because the boreholes were drilled when the glacier occupied the fjord valley, the subglacial debris found at the base of the ice in the drill holes validates the assumption that the sediments above the prominent reflector accumulated during the retreat. The outer-basin borehole revealed ~7 cm of sand and gravel under the glacier, while the inner-basin borehole was underlain by ~60 cm of fine-grained sediment (Humphrey et al., 1993). That only decimeters of subglacial sediments were found at the base of these boreholes supports the interpretation that the tens of meters of sediments in the basins described herein were deposited since the most recent glacier retreat. While sediments in fjord basins are often interpreted as proglacial and not remnant from a previous glacial cycle (e.g., Powell, 1991; Hallet et al., 1996; Koppes and Hallet, 2002; 2006), studies in other Alaskan fjords show that glaciers can advance and retreat over unlithified sediments (e.g., Motyka et al., 2006; Cowan et al., 2010). Thus, the 1987 boreholes drilled through the former glacier give confidence about the interpretation of the former glacier bed in the seismic profiles and about constraining the sedimentary evolution of Columbia Fjord (Figure 3.3).

During Columbia Glacier's 30-year rapid retreat, the sediment flux from the glacier averaged 1.1 ± 0.4 $\times 10^7$ m^3 yr^{-1}, which is similar to that for other temperate Alaskan glaciers (e.g., Hunter et al., 1996a; Hallet et al., 1996; Seramur et al., 1997; Cowan et al., 2010). At the broadest temporal scale, the constraints on the sediment flux provided by the terminus positions and the bathymetric measurements suggest that the glacier delivered approximately six times more sediment to the fjord during the 1998-2011 period than in1980-1997. The flux increased after the glacier had retreated across the length of the outer basin (Figure 3.5a). Moreover, only ~1/4 of the outer basin deposit formed before the flux increase, as Columbia Glacier retreated across that basin (Figure 3.3). As discussed in section 3.5.3, the dramatic increase in flux is attributed to an increase in the sediment-transport capacity of the subglacial system. The filling of the outer basin long after the glacier had retreated across this area challenges the common assumption that sediment derived from a glacier only fills the most proximal basin (e.g., Cowan et al., 2010), and suggests that sediment is transported efficiently throughout the fjord, including over sills.

To determine whether the calculated sediment fluxes are physically reasonable, the overall water and sediment budgets of Columbia Glacier are compared. Modeled rates of ablation were 3.4 km^3 yr^{-1} and 4.0 km^3 yr^{-1} ice equivalent for 1982-1995 and 1996-2007, respectively (Rasmussen et al., 2011). If it is assumed that the source of water in the subglacial system is ablation plus the annual rainfall spread over the glacier surface area, the mean annual sediment fluxes for the two time periods suggests that the average annual suspended-sediment concentrations of the subglacial meltwater were ~1 g L^{-1} for early retreat and ~5 g L^{-1} from the later period. These concentrations are well within the range measured in proglacial streams from land-terminating glaciers (Pearce et al., 2003; Riihimaki et al., 2005; Swift et al., 2005), and thus suggests there is plenty of water to carry the sediment load in subglacial rivers (Hunter et al., 1996a).

Previous modeling approaches, while successful in producing realistic glacial sediment fluxes, do not address the internal stratigraphy and basin geometry of fjord sediments (e.g., Koppes and Hallet, 2002; Mugford and Dowdeswell, 2011). To deliver sediment to the outer basin after 1997 and to produce the horizontal seabed, the processes represented by diffusion and the two exponential terms (Equation 3.9) play key roles in modeling the transport and distribution of sediment throughout the fjord. The majority of sediment delivered to temperate fjords enters via subglacial rivers (e.g., Hunter et al., 1996a), and the dominant sediment-transport process throughout the fjord depends strongly on the concentration of sediment in the subglacial meltwater. For suspended-sediment concentrations in excess of ~30 g L^{-1}, the density of freshwater laden with sediment exceeds the density of the ambient fjord seawater measured in Columbia Fjord (Mulder and Syvitski, 1995; S. Gay, pers. comm.), and the resulting high-concentration gravity flows are capable of carrying sediment along the fjord seabed far from the source (e.g., Prior et al., 1987; Syvitaki et al., 1987; Willems et al., 2011). For lower concentrations, fresh, subglacial meltwater becomes buoyant, forms plumes, and travels along the surface, while sediment progressively flocculates and settles to the seabed (e.g., Hill et al., 1998; Curran et al., 2004).

Modeling the sediment delivery from the glacier using a single exponential term can account for sediment deposition either close to or far from the ice. Two terms are useful, however, to represent both proximal (modeled using a short falloff distance, δ_1), and distal deposition. The latter accounts for the volume of sediment delivered to the outer basin after 1997, and suggests that efficient transport mechanisms deliver glacial sediment many kilometers from the terminus. These mechanisms likely include sediment entrainment in buoyant meltwater plumes (e.g., Powell and Molnia, 1989; Syvitski, 1989; Cowan and Powell, 1991; Hunter et al., 1996a), or transport along the fjord seabed as gravity-driven flows (e.g., Prior et al., 1987; Syvitski et al., 1987; Mulder and Syvitski, 1995); the model does not distinguish between mechanisms but combines them.

In addition to primary deposition, the processes represented by diffusive redistribution of sediment are critical to form the low slope and approximately parallel layered internal stratigraphy of the observed Columbia Glacier sediment basins. Similar sediment patterns are observed in other temperate fjords (e.g., Koppes and Hallet, 2002; Cowan et al., 2010). These features cannot be accounted for without considerable diffusive redistribution, represented by high diffusivities (κ values) (Figure 3.6). The processes represented by the diffusive model parameter include broadly the gravitational reworking of fjord sediments due to the combination of processes that include slumping on diverse scales, iceberg gouging, waves generated from calving icebergs, tidal currents, *et cetera* (Powell, 1981; Syvitski et al., 1987). Gravity flows, including hyperpycnal flows, are the major process associated with highly mobile sediment, a flat seabed, and approximately horizontal, parallel internal layering (e.g., Syvitski, 1989).

3.5.2 Implications for Glacial Erosion and the Subglacial Storage of Sediment

Temporal variations in the modeled sediment-flux history suggest two end-member interpretations (Figure 3.8). The erosion extreme is that all of the sediment delivered to the fjord is newly eroded bedrock. The sediment remobilization extreme is that all of the sediment delivered is being evacuated from subglacial basins or more widely distributed sediment under the glacier. For the erosion extreme, the basin-averaged erosion rate over the 30-year retreat is 5.1 ± 1.8 mm yr^{-1}. Temporal variations in the erosion rate scale with the sediment flux and range from ~2-15 mm yr^{-1}. These rates are comparable with other nearby glaciated areas (Hallet et al., 1996), and the average is essentially identical to the regional Holocene average (Sheaf et al., 2003). They are, however, lower than those reported in Koppes and Hallet (2002, 2006), at least partly, because here the fjord sediment is converted to its rock equivalent using the dry bulk density measured in glacimarine sediments worldwide (~1300 kg m^{-3}), and not the wet bulk density (~1700-2000 kg m^{-3}) as used previously. The incorrect use of the wet bulk density in these and related publications resulted in a ~40% over estimate of erosion rates (e.g. Hallet et al., 1996).

The mean erosion rate of ~5 mm yr^{-1} necessary to sustain the sediment flux during the entire period of retreat has interesting implications for the behavior and stability of Columbia Glacier during periods of advance. In their model of tidewater glacier advance, Nick et al. (2007) found that in order for Columbia Glacier to advance into water deeper than 250-300 m under favorable climate conditions, sediment production sufficient to build a morainal shoal was required. They determined that a sediment-production rate equivalent to basin-wide erosion of ~4 mm yr^{-1} was necessary for Columbia Glacier to advance at a realistic rate of ~30 m yr^{-1}, consistent with the most recent advance reconstructed from buried trees. The close agreement between the calculated effective erosion rate for Columbia Glacier during its 30-year retreat and the estimated erosion rate necessary for the glacier to advance over many hundreds of years suggests that the long-term erosion rate for this glacier is ~4-5 mm yr^{-1}.

If the majority of sediment delivered to Columbia Fjord during the period of retreat were derived from subglacial basins, then the outer fjord basin, inner fjord basin, and the remaining subglacial basin would all have been major potential sources of sediment (Figure 3.9). For the outer basin, the close match between the depth of the glacier borehole in the outer basin (386 m.b.s.l.) and the interpreted sediment base (Figure 3.3), together with the thin (< 1m) subglacial sediment layer found at the base of the borehole, suggest that the outer basin did not supply significant stored sediment during the retreat (Humphrey et al., 1993; Meier et al., 1994). For the inner fjord basin, the up-glacier borehole was drilled to a depth of ~520 m, which is slightly deeper than the interpreted sediment base of 500 ± 10 m (Humphrey et al., 1993; Meier et al., 1994). If a ~10-m-thick layer of sediment were evacuated from this entire inner basin, which covers an area of ~2.5 km^2, the equivalent volume would supply ~2 years of the mean annual sediment load. For the existing subglacial basin to provide the majority of the sediment flux, the average annual load would correspond to roughly a 2.5-m-thick sediment layer over the estimated 4 km^2 basin area (McNabb et al., 2012). The potential contribution from the existing subglacial basin is difficult to quantify, as there are no existing estimates of the basal debris thickness. Recent observations from Taku Glacier, Alaska, however, highlight that soft sediment is evacuated so rapidly that it can lower the ice-sediment interface at rates exceeding 4 m yr^{-1} (Motyka et al., 2006). These observations, together with the presence of subglacial basins below Columbia Glacier, suggest the likelihood that sediment is stored and evacuated from subglacial basins beneath Columbia Glacier.

Sediment is likely to be stored subglacially due to the presence of deep subglacial basins. During periods of retreat, however, this sediment would be quickly evacuated when considering the centennial-to-millennial time scale of advances. The average sediment flux delivered by Columbia Glacier would result in the complete filling of the remaining subglacial basin in ~2 decades. Similar deep basins would quickly aggrade due to the influx of sediment from the subglacial hydraulic system. Because existing subglacial basins would fill with sediment in only a few decades, the long-term sediment flux must be supplied by sediment produced by new bedrock erosion. Indeed, the study by Nick et al., (2007) addressing the advance of Columbia Glacier, gives credibility to the calculated long-term erosion rate (~5 mm yr^{-1}) being effective over time scales of centuries or more throughout cycles of glacier advance and retreat.

3.5.3 Implications for the Relationship Between Sediment Flux and Glacier Behavior

I now examine the model-derived sediment flux-history and assess the potential for subglacial sediment storage using the extensive glaciological data for Columbia Glacier, including ice velocity, ice flux, glacier geometry, ice thickness and retreat history. A close relationship between the ice velocity (ice flux per cross sectional area) and the sediment flux for any glacier is generally expected due to the control of the glacier sliding speed on the rate of erosion by both quarrying and abrasion (Hallet, 1979; Iverson, 1991).

During the early period of retreat between 1980 and 1995, the retreat rate and ice flux both steadily increased, while the sediment flux remained at a relatively constant, low value until approximately 1997, coincident with the maximum ice flux (Figure 3.8). The sediment flux increased sixfold when the retreating terminus had exposed the entire outer basin and the sill separating it from the adjacent basin upglacier (Figures 3.3, 3.5a). As the terminus pulled away from the sill into deeper water, the retreat accelerated (Figure 3.8). A second abrupt increase in sediment flux between 2007 and 2011 coincides with an increase in retreat rate and ice flux (Figure 3.8). Because the sediment flux remains quite low despite the large increase in ice flux before 1997, the sediment flux is clearly not directly reflecting the generation of sediment by bedrock erosion, as it would most likely accelerate with the sliding in the latter case.

I hypothesize that the distinct changes in sediment flux reflect an increase in the sediment transport by the subglacial fluvial system resulting in faster evacuation of water and sediment from under Columbia Glacier. To test this hypothesis, I assess the time-varying sediment flux from Columbia Glacier in light of the sediment transport capacity of the subglacial hydraulic system based on the evolving geometry of the glacier surface and bed. The flow of water under thick ice is driven by the hydraulic potential gradient, $\nabla\phi$, at the glacier bed (Rothlisberger, 1972; Shreve, 1972). The hydraulic potential depends on the ice surface elevation, z_s, the bed elevation, z_b, gravitational acceleration, g, and the densities of ice and water, ρ_i and ρ_w, respectively, such that:

$$\nabla\Phi = \rho_i g \nabla z_s + (\rho_w - \rho_i) g \nabla z_b \tag{3.12}$$

(Cuffey and Paterson, 2010). When the slope of the glacier bed and the ice surface are comparable, the ice surface slope exerts the dominant control on subglacial water flow (Shreve, 1972). However, when a reverse slope of the glacier bed (dipping upglacier) exceeds that of the equipotential surfaces within the glacier, equivalent to a bed slope of ~11 times the ice surface slope, subglacial water and sediment transport vanish. In addition, there is a thermodynamic control on subglacial water flow. Because water traveling along the base of a glacier is at the pressure melting point, the decrease in pressure as the water travels uphill along a reverse sloping bed can cause the supercooled water to refreeze at the base of the glacier if the heat dissipated in the water flow is insufficient to warm the water to the pressure melting point as it ascends along the bed (Rothlisberger, 1972). Refreezing is expected, if the bed ascends more steeply than 20-70% of the surface slope (Alley et al., 2003). When this condition is met, subglacial sediment transport and bedrock erosion are expected to vanish (Hooke, 1991; Alley et al., 2003).

Based on a series of ice-thickness profiles collected throughout the retreat (S. O'Neel, pers. comm.), and the known bed slope for the water-covered area from the seismic profiles and beneath the ice as calculated by McNabb et al. (2012), I calculate the hydraulic potential gradient and refreezing potential as a function of time over areas of reverse bed slopes to determine their probable effects on water and sediment transport in subglacial rivers during the retreat.

Steeply reverse-sloping beds occur at the down-glacier end of both the inner basin of the fjord and the only major subglacial basin remaining, just upglacier of the 2013 terminus (Figure 3.9 at downglacier distances of ~56 km and 48 km, respectively) (Rignot et al., 2013). From 1957 until sometime before 2001, the glacier surface slope over the distal portion of the subglacial basin was too shallow to permit stored sediment to escape in the subglacial fluvial system (near 48 km, Figure 3.10). In addition, the steep reverse slopes in both basins are sufficient to have caused basal water to refreeze throughout the retreat. Without evacuation, sediment transported in the subglacial system would rapidly accumulate in the subglacial basin until the sediment shoal was sufficient to decrease the bed slope and allow stored sediment to escape (Alley et al., 2003). For the major remaining subglacial basin with a length of 3500 m, a depth of ~60 m, and an approximate width of 500 m, based on estimates from McNabb et al. (2012), sediment accumulating at the mean annual rate of 1.1×10^7 m^3 over a period of ~15-20 years would sufficiently reduce the slope of the bed below the hydraulic threshold to permit the evacuation of the stored sediment.

Based on changes in both the ice-surface and glacier-bed slopes during the period of retreat, the dramatic increase in the sediment flux between 1997 and 2001 (Figure 3.8) is thus attributed to an increase in the sediment-transport capacity of the subglacial system. The sediment-transport capacity could increase by a decrease the reverse bed slope due to subglacial sediment accumulation, as well as a steepening the glacier surface slope, which occurs as the terminus approaches a given location (Figure 3.9), sufficient to evacuate stored sediment (Figure 3.10). The analysis suggests that both of these processes occur in the subglacial basin during the recent period of retreat.

The sediment-flux history, when analyzed in context of the existing glaciological observations, suggests the importance of the subglacial hydraulic potential and basal refreezing on the delivery of sediment to the fjord. Similarly, the subglacial hydraulic system appeared to control episodic discharges of sediment from the Bering Glacier, Alaska, during surges (Headley et al., 2013), and to limit the bedload of Matanuska Glacier, Alaska, ~50 km northwest of Columbia Glacier (Pearce et al., 2003). Because neither ice flux nor retreat rate simply controls the sediment flux of Columbia Glacier, as was expected based on the results of Koppes and Hallet (2002, 2006), the preserved sediment record in the fjord is not a simple archive of changes in climate, erosion rate, or glacier dynamics. Rather, changes in subglacial hydrology can dominate the sediment record on a short time scale (year to decades). The tendency for the ice-surface slope to steepen over a given area during terminus retreat can cause stored sediments to be rapidly flushed from a subglacial basin. This effect renders the interpretation of the glacimarine sediment record challenging especially for short time scales. In addition, subglacial hydraulics are arguably the least understood component of any glacier system (e.g., Cuffey and

Paterson, 2010). Despite these complications, refinement of the modeling approach developed here provides the potential for unraveling complex glacial histories.

3.6 Conclusions

In this study, the sediment accumulation created by Columbia Glacier during its 30-year retreat (1980-2011) was analyzed. Seismic profiles collected throughout the fjord indicate that a minimum of $3.2 \pm 1.1 \times 10^8$ m^3 of sediment accumulated in the newly created fjord since 1980 at an average rate of $3.0 \pm 1.0 \times 10^6$ and $19 \pm 7 \times 10^6$ $m^3\,yr^{-1}$ for 1980-1997 and 1998-2011, respectively. A numerical model of the glacier's sediment-flux history was developed to help understand the seismically imaged sediment-thickness distribution and the internal architecture of the sediments in the major basins in the context of the known glacier retreat. In addition to being consistent with the total sediment volume and geometry of the fjord, the modeled sediment-flux history is constrained by borehole depths through the glacier in 1987 and bathymetric measurements in 1997 and 2011.

The modeled sediment-flux history produces a sediment distribution and architecture consistent with observations, and suggests that the flux increased sixfold between 1997 and 2000. Sediment must be transported many kilometers from the ice in order to form the outer basin deposits, and sediments must be highly mobile (as represented by a high sediment diffusivity in the model) to account for the horizontal bathymetry and approximately parallel internal stratigraphy. These results suggest that fjord sediments are likely transported and/or redistributed efficiently by sediment gravity-driven processes at the seabed.

A basin-averaged erosion rate of 5.1 ± 1.8 mm yr^{-1} is necessary to sustain the observed mean sediment flux over the period of retreat. This effective erosion rate during the period of retreat is surprisingly similar to the sediment-production rate necessary to enable Columbia Glacier to advance into its deep fjord on a time scale of centuries to millennia, as calculated by Nick et al. (2007). The similarity between the two completely independent estimates based on entirely different approaches and data representing different time spans suggests that they are producing a realistic value for the long-term erosion rate by Columbia Glacier.

In combination with temporal variations in sediment delivery calculated, the unique set of glaciological observations collected during the retreat of Columbia Glacier allows for the assessment of the role of subglacial sediment storage. By examining the modeled sediment-flux history in light of the concurrent ice flux, retreat rate, and glacier geometry, it was determined that the sediment flux is not simply controlled by ice dynamics, as commonly suggested for other glaciers. The analysis of the subglacial hydrologic system suggests that a steep reverse-sloping section of the bed under Columbia Glacier could impede and even stop the subglacial transport of water and sediment during much of the retreat. The dramatic increase in the sediment flux around ~1998 is attributed to an increase in the ability of the subglacial hydraulic system to transport stored sediment, due in part to the progressive steepening of the glacier surface during the retreat. The control of the glacier surface and bed geometries on the output of sediment, rather than ice dynamics, highlights the many factors that affect glacial sediment fluxes and that are ultimately reflected in the glacimarine stratigraphic record.

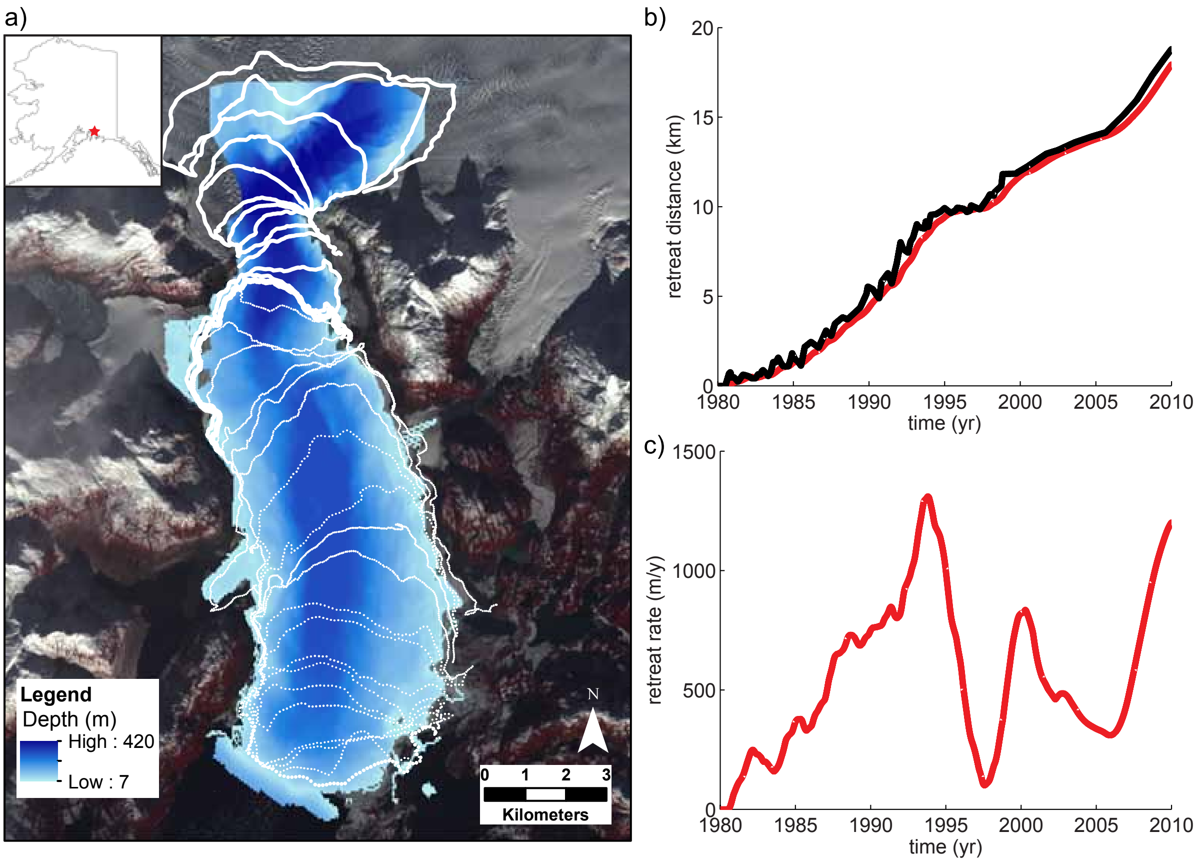

Figure 3.1. Columbia Glacier Retreat
(a) Inset shows the location of Columbia Fjord in northeast Prince William Sound, AK. Bathymetry of Columbia Fjord, collected by NOAA (Noll, 2005) and this study, is shown in graded blue. Columbia Glacier terminus positions are indicated by the white dotted line. The southernmost line represents the stable terminus position of Columbia Glacier, measured in 1954, and subsequent lines show annual terminus positions during the retreat from 1980 to 2011. **(b)** Retreat position of Columbia Glacier. The black line shows inter-annual variability, and the red line is the smoothed position used to calculate the retreat rate, shown in **(c)**.

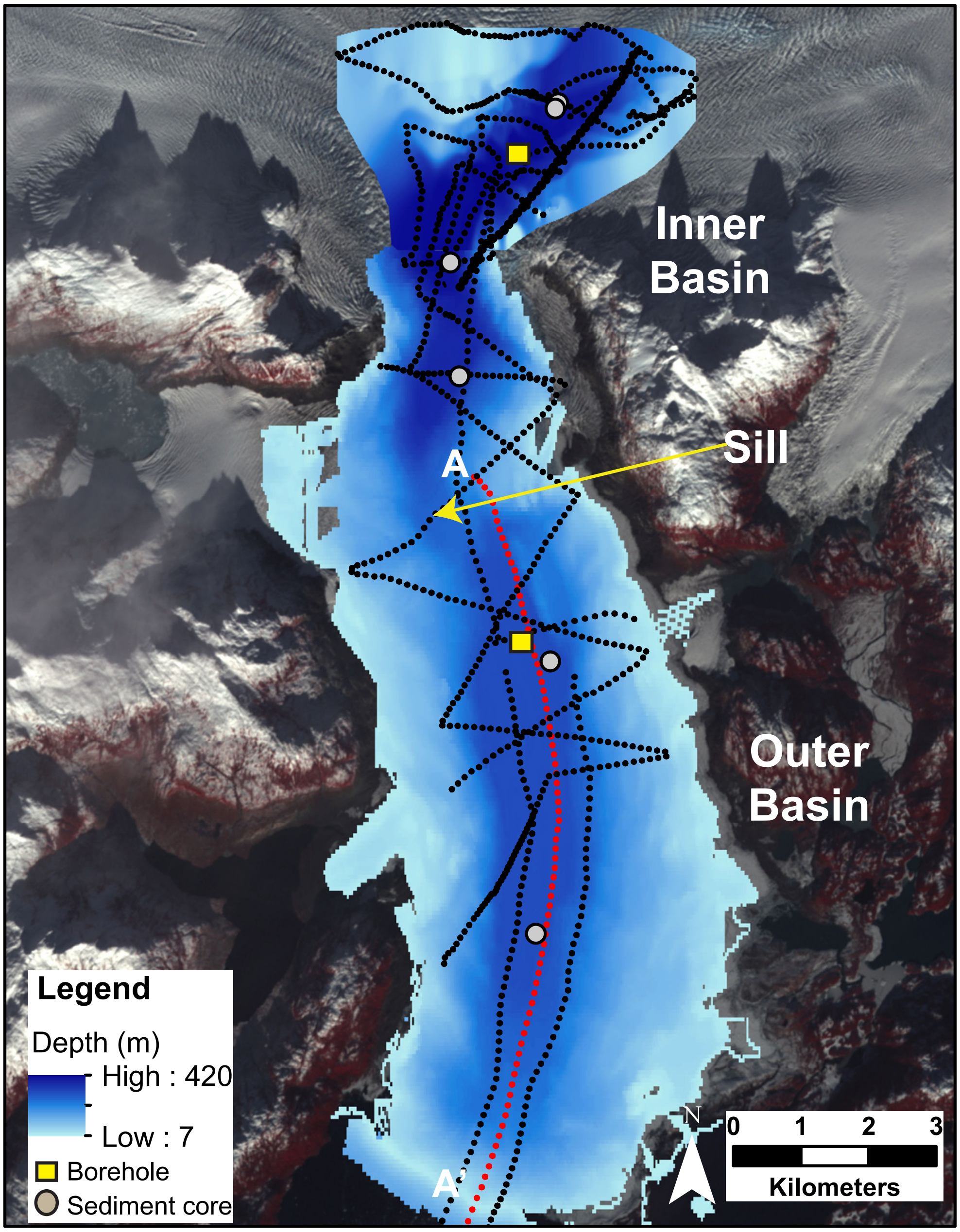

Figure 3.2. Location of Samples in Columbia Fjord
Black dotted lines indicate the locations of seismic profiles, and the red dotted line between A and A' highlights the seismic line shown in Figure 3.3. Yellow squares represent the locations of boreholes drilled through the glacier before its retreat in 1987 (Meier et al., 1994). Gray circles show sediment core locations.

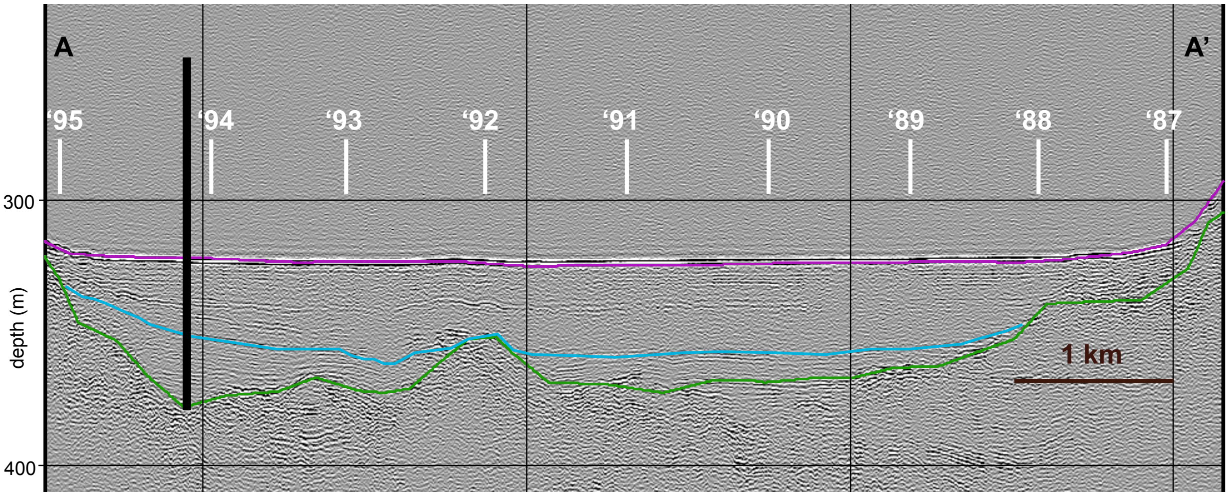

Figure 3.3. Along-Fjord Seismic Line

Seismic line from the sill separating the basins (A) to the moraine (A’) (see Figure 3.2 for location). White vertical lines show the terminus position in the year indicated. The black line represents the position and depth of the outer borehole drilled in 1987 (location in Figure 3.2; Meier et al., 1994). The green line indicates the chosen base of the post-retreat sediment deposit in the fjord, and the purple line delineates the sediment-water interface. The blue line is the interpreted seabed depth in 1997 based on bathymetric measurements.

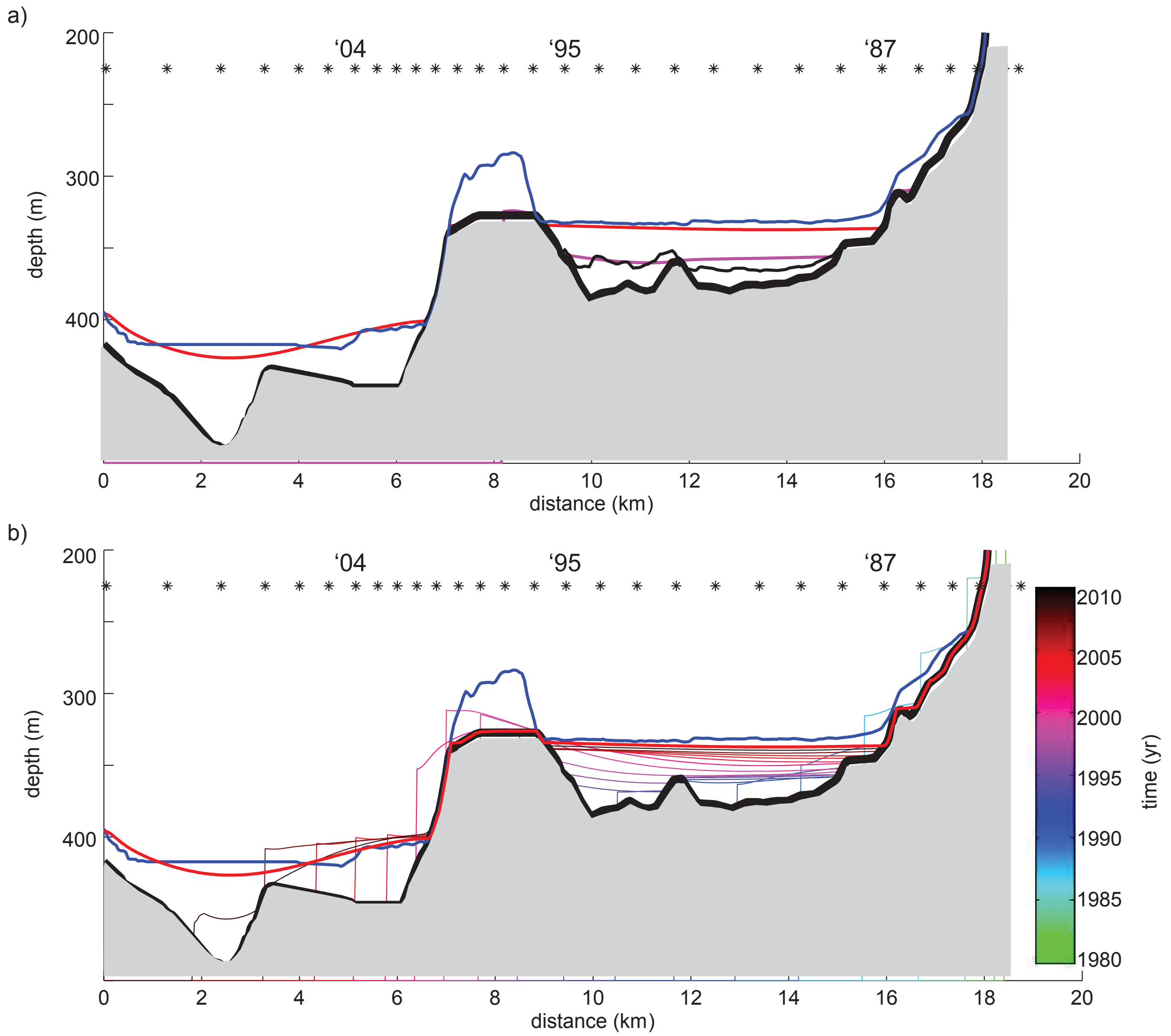

Figure 3.4. Modeled Sediment Basins

Model output of the sediment package created during the retreat of Columbia Glacier. In both **(a)** and **(b)**, gray shaded area is material underlying the sediment basin, the thick black line represents the interpreted base of the sediment package, and the blue line is the measured fjord depth. The basal surface is interpolated from crossing seismic lines between 5 and 8 km. Glacier retreat is from right to left, and the stars mark annual terminus positions from 1980 to 2010, with specific years shown. The "outer basin" is referred to as the area between the moraine (18 km) and the sill (8 km), and the "inner basin" is the area from the modern glacier terminus (0 km) to the sill. In **(a)**, the fine black line represents the interpreted seabed in 1997 (shown in Figure 3.3), the pink line represents the modeled seabed elevation in 1997, and the red line represents the modeled modern seabed elevation. In **(b)**, colored lines represent modeled seabed elevation in years shown in the legend. The thick red line is the final modeled seabed in 2010, same as shown in a). Lines above the thick red line (e.g., around 8 km) are areas where the sediment was redistributed.

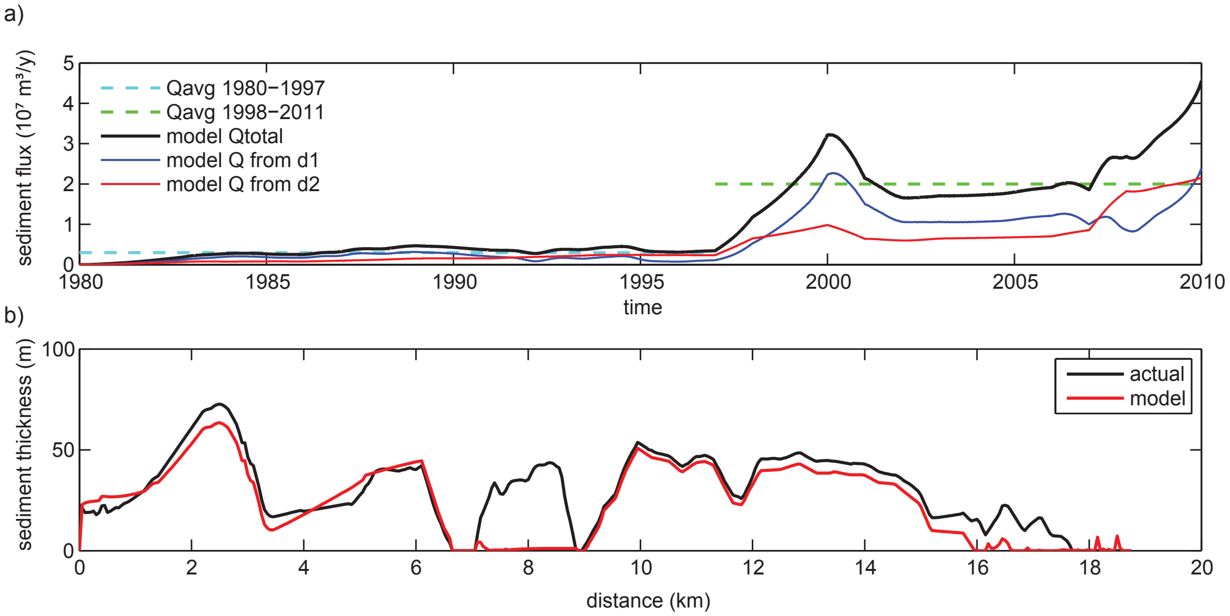

Figure 3.5. Modeled Sediment-Flux History and Distribution
(a) Sediment flux history. Green and teal dashed lines show the average flux for 1980-1997 and 1998-2010 estimated from the calculated seismic volumes. The thick black line shows the total modeled sediment flux through time, and the blue and red lines indicate the component attributed to proximal and distal accumulation (Equation 3.5), respectively. **(b)** Sediment thickness distribution, where the black like is the actual thickness measured from seismic profiles, and the red line is the final modeled sediment thickness distribution. The deposits on the sill (~8 km), and on the moraine (16-18 km) are not represented by the model; see section 3.4.3 for explanation.

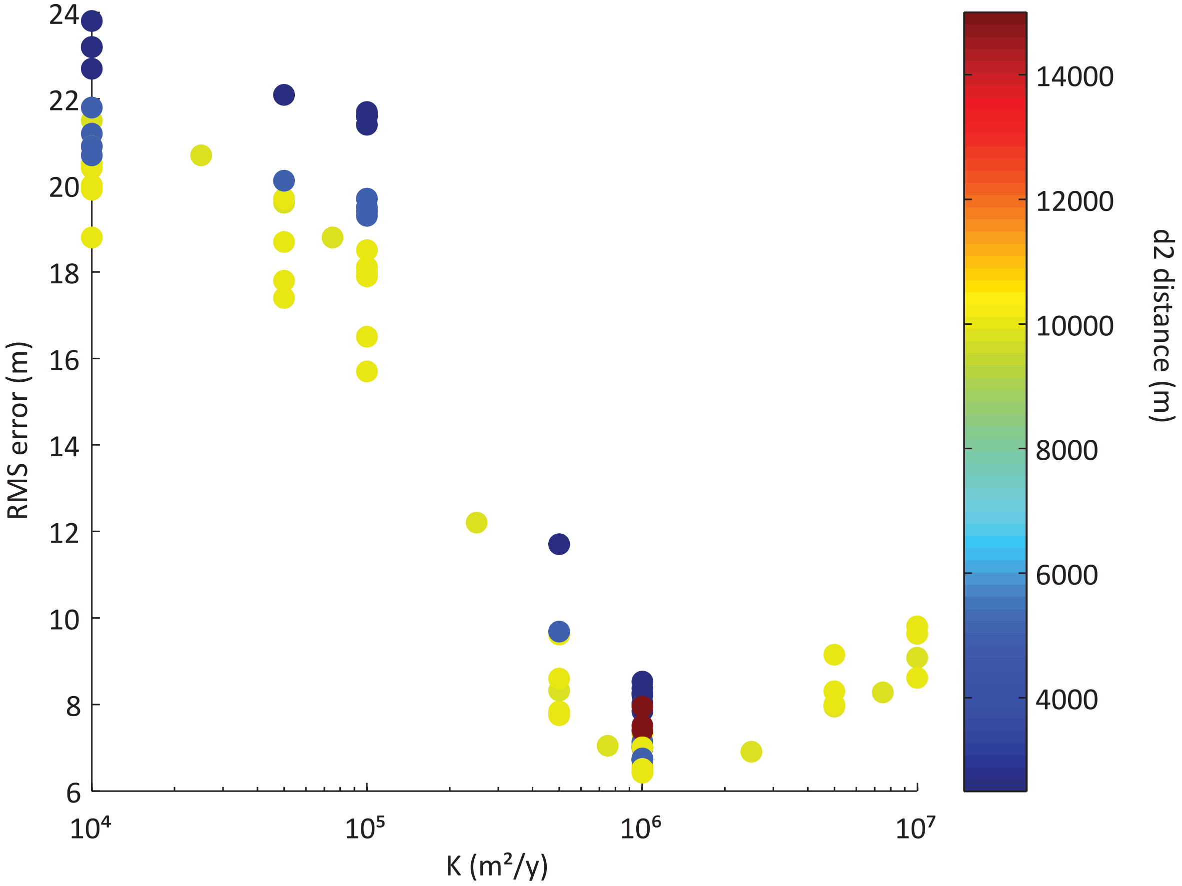

Figure 3.6. Model Sensitivity Tests
The relationship between the RMS error (measured as the distance between the modeled bathymetry and the actual bathymetry) and the diffusivity constant, κ. Colors indicate the value of the long decay distance, δ_2, where δ_1 is always 100 m. A diffusivity constant of $\kappa = 1\text{x}10^6$ m^2 y^{-1} was chosen, as it minimizes the RMS between the model and the actual fjord bathymetry.

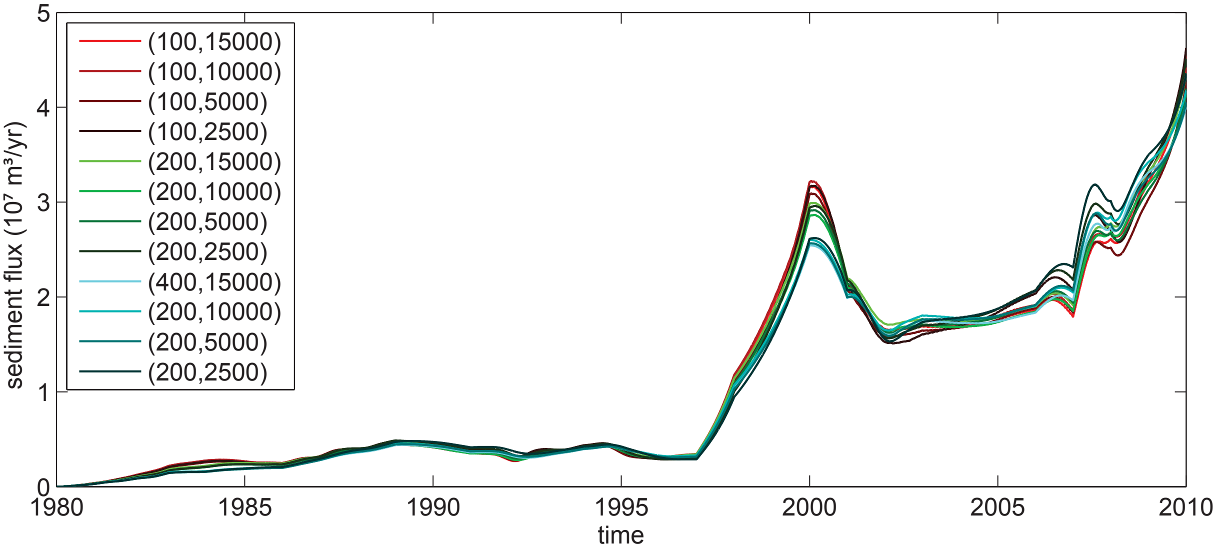

Figure 3.7. Variations in the Model Output
Sediment flux history showing the model sensitivity to the chosen exponential decay distances, δ_1 and δ_2. The parenthetical values in the legend indicate the δ_1 and δ_2 distances (in m) to produce the corresponding sediment flux history. κ is held constant at a value of 1×10^6 m^2 y^{-1}.

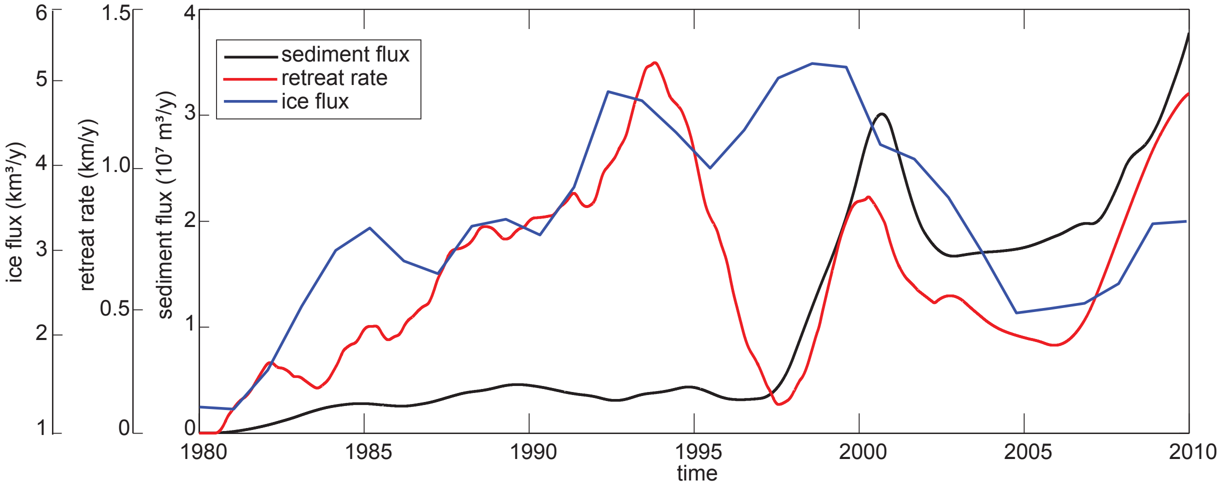

Figure 3.8. Sediment-Flux History Compared to Columbia Glacier Behavior
Temporal variations in the modeled sediment flux (black), the retreat rate (red), and the interpolated ice flux (blue) (from O’Neel et al., 2013). The ice flux is used as a proxy for ice speed, assuming a constant cross-sectional area.

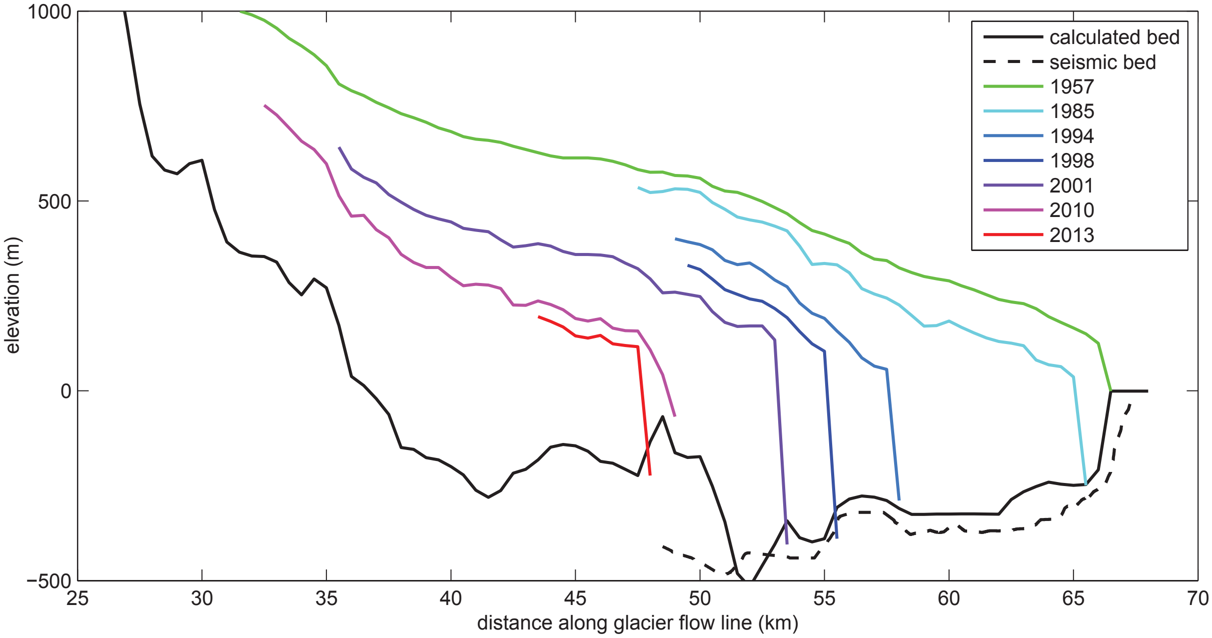

Figure 3.9. Columbia Glacier Surface Profiles
Along-glacier profiles for specific periods during the retreat (from O'Neel et al., 2013). The solid black line represents the calculated glacier topography from McNabb et al. (2011), and the dashed black line is the base of the sediment package from the seismic profiles collected in this study. Differences in the black lines are due to sedimentation between ~55 and 67 km, and lateral variations in the basal depth around ~50 km. Note the steep reverse-sloping beds at ~48 km and ~55 km.

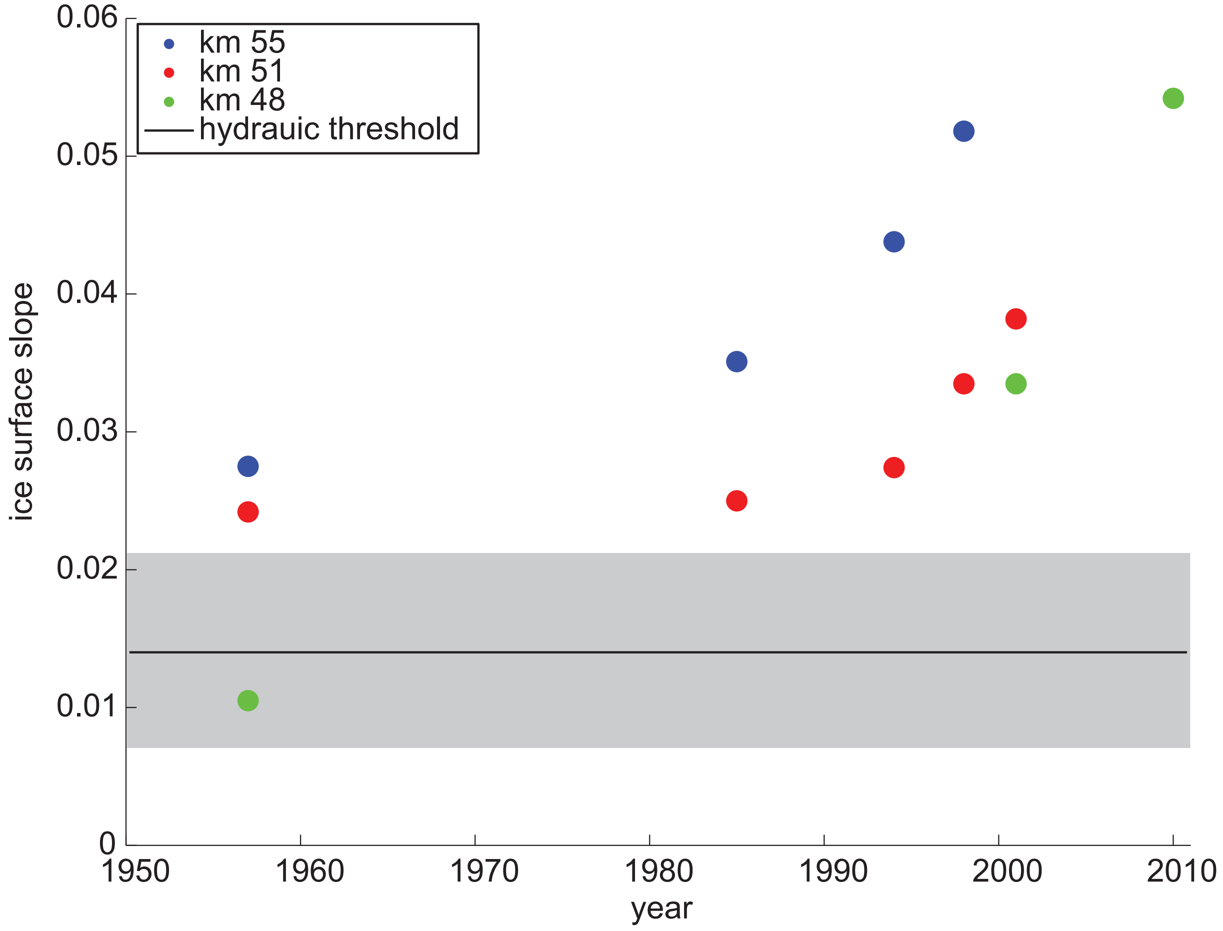

Figure 3.10. Columbia Glacier Ice-Surface Slope Evolution
Temporal trends of the ice surface slope at three locations near the 2010 terminus (see Figure 3.9 for locations). The "km 48" trend is over the portion of the subglacial basin with a steep reverse slope, which acts as a threshold for sediment evacuation from this basin. The surface slopes are calculated over an along-glacier distance of 1-2 km depending on the available data. The horizontal black line represents the hydraulic threshold, below which the glacier bed is too steep for water and sediment to be evacuated. The line corresponds to the negative of the reverse slope of the subglacial basin lip divided by 11 (see Section 3.5.3). The gray box represents 50 % uncertainty on the threshold.

Chapter 4: Fjord sediment dynamics during the rapid retreat of tidewater glaciers: case studies from Alaska and Patagonia

4.1 Introduction

Marine-ending glaciers and ice sheets around the world are thinning and retreating at dramatic rates, due in part to the presence of warm ocean water along the submerged icefronts (Holland et al., 2008; Jacobs et al., 2011; Joughin et al., 2012), and this mass loss is contributing directly to sea-level rise (Rignot et al., 2011; Shepherd et al., 2012; Gardner et al., 2013). The stability of marine-ending glaciers and ice sheets depends strongly on the geometry and characteristics of the glacier bed (e.g., Schoof, 2007); retreat from a relatively shallow sill into a deep subglacial basin causes a positive feedback for ice loss and the potential collapse of ice sheets (e.g., Joughin et al., 2014). While future sea-level-rise predictions depend on understanding the complex behavior along the ice-ocean interface (Straneo et al., 2013), the paucity of observations along this challenging margin limits the accuracy of current sea-level projections (Lemke et al., 2007). The water depth at the terminus controls the rate of mass loss by calving and submarine melting, and the dynamics of tidewater glaciers depend sensitively on the sediment shoals they produce (Meier and Post, 1987; Alley, 1991; Powell, 1991; Nick et al., 2007). Because the depth can change quickly where proglacial sediments accumulate rapidly, the accumulation of sediments near the termini of tidewater glacier merit close attention. In addition, examining the linkage between glacier behavior and ice-proximal sediment deposits illuminates the fidelity with which glacial deposits record changing glacial climatic conditions, and helps improve interpretations from glacimarine sedimentary archives (Cowan et al., 1997; Anderson et al., 2002; Andresen et al., 2011).

Modern fjords of marine-ending (or tidewater) glaciers provide ideal natural laboratories for process-based studies of the sediment deposits generated by these fast retreating glaciers. In temperate glaciers, meltwater transports the bulk of glacially derived sediment to fjords, where the sediment tends to accumulate (Powell and Molnia, 1989; Cowan and Powell, 1991; Hunter et al., 1996a; Cowan et al., 2010). The rapid erosion and large discharge of sediment-rich meltwater characteristic of temperate tidewater glaciers results in extremely high sediment fluxes and accumulation rates (Hallet et al., 1996; Koppes and Montgomery, 2009), which reach tens of meters per year near the glacier (e.g. Molnia, 1979; Cowan and Powell, 1991). The large volume of sediment accumulating in fjords results in seabed signatures that preserve a high-resolution history of glacier behavior and sediment delivery on time scales of days to decades (e.g., Cowan et al., 2010; Koppes et al., 2010; Willems et al., 2011; Boldt et al., 2013). For glaciers where the retreat history is known and the proglacial sediment package has been defined, the sediment-flux history can be reconstructed to shed light on the glacial characteristics that impact the sediment record preserved in proglacial fjords (e.g., Koppes and Hallet 2002; 2006; Koppes et al., 2010).

Sediments from temperate glaciers typically comprise interlaminated sands, muds, and ice-rafted debris, reflecting the formative sediment-transport processes over a range of timescales (tidal, diurnal, seasonal, calving frequency) (Mackiewicz et al., 1984; Cowan et al., 1999; 1997; Jaeger and Nittrouer, 1999a; 1999b; Willems et al., 2011). If the sediment-laden meltwater exiting the glacier is denser than ambient seawater (equivalent to a suspended-sediment concentration greater than ~30-40 g L^{-1}), when the meltwater enters the fjord it will move seaward as a hyperpycnal gravity flow (Mulder et al., 2003). Otherwise, the meltwater rises buoyantly as a turbulent plume that mixes with ambient seawater, and entrained sediment settles from suspension (Syvitski, 1989; Cowan and Powell, 1991; Hunter et al., 1996a; Curran et al., 2004; Mugford and Dowdeswell, 2011). Based on continuous seismic reflectors and the geometry of fjord sediment deposits, gravity flows are commonly suggested as one of the primary ways in which sediment is transferred through fjords (e.g., Syvitski et al., 1987; Cowan and Powell, 1991; Powell, 1991; Cowan et al., 2010), but there are few *in situ* observations to document these flows (Prior et al., 1987; Bornhold et al., 1994). Moreover, a better understanding of proglacial sediment-transport processes has the potential to elucidate the timing and vigor of the subglacial hydrologic system, which remains among the most poorly understood aspects of glaciology (Cuffey and Paterson, 2010).

This research compares observations and modeling results that shed light on the sediment output of two temperate tidewater glaciers that have experienced dramatic retreat in the past few decades. I focus on quantifying sediment-accumulation rates and defining temporal changes in sediment delivery. I previously developed a model relating the known glacial retreat history to the observed distribution and internal stratigraphy of fjord sediments for Columbia Glacier, AK, a tidewater glacier with a rich observational history (see Chapter 3). Here, the same model is applied to develop the sediment-flux history from Jorge Montt Glacier, one of the most rapidly retreating and thinning glaciers draining the relatively poorly studied Patagonian Ice Sheets of South America (Rignot et al., 2003; Rivera et al., 2012b; Willis et al., 2012). The complementary seismic, sediment-core, and retreat-history datasets for both glaciers enable the detailed examination of: 1) overall rates of sediment delivery and corresponding erosion; 2) temporal variations in the sediment flux during rapid retreat, and the associated glaciological conditions; and 3) the sediment-transport mechanisms likely responsible for the basin geometry and stratigraphy. Based on the comparison, I am also able to determine whether the sediment-glacier-fjord system at Columbia Glacier is representative of similar systems in different settings, and whether the model developed for Columbia Glacier sedimentation can be applied more generally. After descriptions of study sites and methods, observations and model results are presented and compared with the general goal to understand fjord sediment dynamics and the formation of fjord sediment deposits.

4.2 Study Sites

4.2.1 Columbia Glacier and Fjord

Columbia Glacier is a temperate tidewater glacier in south-central Alaska (61.1°N, 147.1°W) that covers an area of ~1000 km^2 (extending from 0 to 3050 m above sea level; masl) (Figure 4.1a). The closest US National Weather Service Office in Valdez, AK, at sea level and ~35 km east of the glacier, receives ~2 m of precipitation annually. In the early 1980s, after a period of stability more than a century long, the glacier entered a phase of rapid retreat and a permanent loss of contact with the stabilizing moraine shoal (Pfeffer, 2007). The retreat accelerated until the mid 1990's, slowed for two periods between 1994-1997 and 2000-2006 (Meier and Post, 1987; Pfeffer et al., 2000; O'Neel et al., 2005), and accelerated again after 2006. Since 1957, the glacier has lost half of its volume and thickness (McNabb et al., 2012). The terminus has retreated 23 km at an average rate of ~0.7 km yr^{-1}, exposing a deep fjord. The retreat of Columbia Glacier has been documented in detail through aerial photography (Krimmel, 2001), daily time-lapse photography (O'Neel et al., 2005), and a reconstructed history of mass loss (Rasmussen et al., 2011). In addition, two boreholes drilled through the former glacier (Meier et al., 1994; Humphrey et al., 1993), multiple bathymetric measurements (Krimmel, 2001; Noll, 2005), and the recent numerical reconstruction of glacier bed topography (McNabb et al., 2012) enable the close study of the fjord sediment basin evolution during the retreat.

4.2.2 Jorge Montt Glacier and Fjord

Jorge Montt (48.3°S, 73.5°W) is one of many large tidewater glaciers draining the Southern Patagonian Icefield of South America (Figure 1b). The glacier covers ~500 km^2 and extends from sea level to 1600 masl. A meteorological station deployed ~9 km from the glacier terminus between March 2011 to November 2013 recorded a mean daily precipitation of 6.5 mm, or ~2.5 m yr^{-1}. The glacier has been mapped by aerial photos and satellite images since 1945, and using time-lapse photography since 2010 (Rivera et al., 2012a and 2012b). Throughout the past century Jorge Montt Glacier has retreated 19.5 km, among the greatest retreat of any Patagonian glacier, and now terminates into the deep fjord previously occupied by the glacier (Rignot et al., 2003; Rivera et al., 2012b). During the retreat near the terminus, the glacier thinned ~18 m yr^{-1} (Rignot et al., 2003), and accelerated since 1983 from ~0.7 m d^{-1} (Enomoto and Abe, 1983) to 13.4 m d^{-1} in 2011 (Rivera et al., 2012a). Its total volume decreased 1.8 km^3 yr^{-1} (Willis et al., 2012). In 2011, the calving flux of Jorge Montt was 2.4 km^3 yr^{-1}, the highest recorded for a Patagonian glacier (Rivera et al., 2012a).

4.3 Observational Methods and Analyses

4.3.1 Field Methods

The data presented herein were collected during three primary field campaigns: in September 2011 in Columbia Fjord, and in February 2010 and March 2013 in Jorge Montt Fjord. During unusually iceberg-free conditions in Columbia Fjord, six ~2-m-long kasten cores were collected in a longitudinal transect (Figure 4.2a). Seismic-reflection profiles were also collected using a 750-Hz bubble pulser system, and bathymetric measurements throughout the fjord (Figure 4.2a). During the initial field campaign in Jorge Montt Fjord, the first data in the fjord were collected: seismic profiles with the same bubble pulser system, bathymetric measurements and CTD profiles. On a subsequent trip to Jorge Montt Fjord in 2013, 7 kasten cores were collected in a transect from the glacier terminus to a shoal interpreted as the Little Ice Age moraine (Figure 4.2b). CTD profiles in Jorge Montt Fjord were collected during these and other field campaigns between Feb 2010 and Mar 2013 (Moffat et al., in prep).

The ~2-m-long cores from both fjords were photographed, described, and subsampled onboard. A 2-cm-thick slab along the entire core length was sampled with 30-cm-long plexiglass trays for x-radiography, and the remainder of each core was sectioned in 2-cm increments along the length of the core and stored in bags.

From both the seismic images and depth soundings, submarine morainal shoals are identified at the entrance to both fjords. For Columbia Fjord, the shoal corresponds to the advanced position of the glacier until 1980 (Figure 4.1a), and for Jorge Montt Fjord, the shoal corresponds to the position of the stable terminus from 1945-1990 (Figure 4.1b). These shoals are referred to as the “1980 moraine” and the “1990 moraine”, respectively. Two basins containing sediments are identified between the glacier and the 1980 moraine in Columbia Fjord; they are referred to herein as the “outer basin” and “inner basin” (Figure 4.2a). Jorge Montt Fjord contains one basin between the modern terminus and the 1990 moraine, referred to as the “main basin,” and an additional basin exists between this moraine and the interpreted Little Ice Age moraine that I refer to as the “shallow basin” (Figure 4.2b).

4.3.2 Laboratory Analyses

Water-column suspended-sediment concentrations in Jorge Montt Fjord were determined with bottle samples and measurements from an optical backscatter sensor connected to the CTD. The bottle samples were filtered through a 0.45-μm mixed-cellulose-ester membrane. The backscatter sensor was calibrated by comparing sediment concentrations to the voltage reading in co-located samples; concentration increases linearly with voltage (n=16, r^2=0.90).

Sediment cores were examined for detailed sedimentary structures using a portable x-ray and digital imaging system. The x-ray negatives display core sections with a relatively high bulk density (i.e., sand) in light gray, and with a lower bulk density (i.e., silt and clay) in darker gray. A portion of the bagged core samples was wet sieved at 63 μm to separate sand and mud fractions, and the detailed particle-size distribution for the mud fraction was determined using a Sedigraph 5100 (Coakley and Syvitski, 1991).

To determine rates of sediment accretion, the samples were analyzed for the activity of naturally occurring radioisotopes ^{234}Th (half life 24.1 days) and ^{210}Pb (half life 22.3 years). The activity of ^{234}Th in the sediment samples was counted using a low-energy germanium detector and integrating the area of the 92.4 keV peak. ^{210}Pb activities were determined by adding a known quantity of ^{209}Po to each sample to use as yield determinant. The relative activities of this ^{209}Po and naturally occurring ^{210}Po, which is in secular equilibrium with ^{210}Pb, were counted using alpha spectroscopy. For a detailed description of the ^{210}Pb analysis procedure, see Nittrouer et al. (1979). The down-core decrease of each radioisotope was used to calculate the rate of seabed accretion on a time scale of 4-5 half lives.

The seismic-reflection profiles were bandpass filtered (260-750 Hz), deconvolved, migrated using an f-k algorithm, and then depth converted (Yilmaz, 2001). The data were single channel; hence no seismic velocity information is directly available from the data. For the migration and depth conversion, therefore, a simple estimate of seismic velocity, 1500 m s^{-1}, was used for the water column and upper glacimarine sediments, increasing to 1800 m s^{-1} at a travel time of 1 s. The slower velocity represents an approximate speed of sound through brackish

(~30 psu), cold (~6°C) water, as measured in Columbia Fjord and Jorge Montt Fjord, as well as through the upper, unconsolidated glacimarine sediments collected in the sediment cores. The increased velocity accounts for compaction in the lower sediments. Processed seismic profiles were analyzed using the open-source seismic interpretation software OpendTect 4.4.0.

4.4 Observational Results and Interpretations

4.4.1 Water Column Properties

Water-column hydrograph profiles collected during summer conditions in the inner portion of Jorge Montt Fjord showed a 10-m-thick freshwater layer at surface (~2 psu), underlain by 30 psu water ~6-8°C. There was very little suspended sediment in the freshwater layer. During the summer, the suspended-sediment concentration increased in the 50 m below the surface layer to a maximum of ~40 mg L^{-1} (Figure 4. 3). The sediment concentration ranged from 10 to 50 mg L^{-1} throughout water below the surface layer, and concentrations commonly peaked near the seabed. Significantly less sediment was in suspension in the shallow basin, beyond the 1990 moraine. During austral-winter conditions, the few water-column profiles collected from the main fjord basin showed low suspended-sediment concentrations, and no visible surface freshwater layer (Figure 4.3). Negligible suspended sediment was detected in casts from beyond the 1990 moraine during austral winter conditions.

4.4.2 Sediment Core Properties

Table 4.1. *Summary of Cores from Columbia and Jorge Montt Fjords*

Core	Latitude	Longitude	Water depth (m)	Core length (m)	^{234}Th deposition rate (cm d^{-1})	Distance from ice front (km)
			Columbia Fjord			
CG 1	61.139 °N	147.048 °W	394	0.26	N/M[a]	1.2
CG 2	61.065 °N	147.050 °W	320	1.70	0.4	9.2
CG 3	61.139 °N	147.049 °W	387	0.50	N/M[a]	1.2
CG 4	61.118 °N	147.078 °W	413	1.06	N/D[b]	3.0
CG 5	61.103 °N	147.075 °W	382	1.70	0.4	5.0
CG 6	61.029 °N	147.054 °W	322	1.66	0.4	13.3
			Jorge Montt Fjord			
JM 1	48.228 °S	73.502 °W	106	1.0	N/D[b]	14.0
JM 2	48.255 °S	73.436 °W	302	1.64	0.2	8.3
JM 3	48.301 °S	73.456 °W	308	1.20	N/M[a]	3.1
JM 4	48.287 °S	73.452 °W	362	2.50	0.3	4.6
JM 5	48.300 °S	73.456 °W	333	1.65	0.2	2.8
JM 6	48.270 °S	73.442 °W	360	1.65	0.2	6.7
JM 7	48.203 °S	73.502 °W	108	1.32	N/D[b]	16.0

[a] N/M: Activity of ^{234}Th was not measured.

[b] N/D: A deposition rate could not be determined from the ^{234}Th activity profile (see Figure 4.6).

In Columbia Fjord, the two ice-proximal cores (cores 1 and 3) were collected ~1.2 km from the ice front and were the shortest (26 and 50 cm, respectively) due to difficulty in penetrating the coarse sediment near the ice front. In these cores 1, the sediment is 50-80% sand, 10-30% silt, and ~10-15% clay by weight (Figure 4.4). The two cores from the center of the inner basin (cores 4 and 5, 3.0 and 5.0 km from the ice front, respectively) are ~1% sand, ~34% silt and ~65% clay, by weight (Figure 4.4). Cores 2 and 6, from the outer basin, 9.2 and 13.3 km away from the ice, are more cohesive than the inner basin cores and have similar grain-size distributions (~35% silt, 65% clay).

X-radiographs were obtained for the three most ice-distal cores (5, 2, and 6). Samples were not collected for x-ray analysis from core 4 due to the high water content (~70% porosity). The x-radiographs reveal laminated sediment (mm to cm scale), with discrete coarse-grained intervals likely from ice rafted debris (Figure 4.5). The x-radiograph from inner-basin core 5 also reveals several upward-fining units, ~5 cm thick, with a distinct relatively coarse base above an apparent erosional surface (e.g., 150 cm depth in CGF core 5; Figure 4.5).

In Jorge Montt Fjord, cores 5, 3, 4, 6, and 2 were collected in the main basin, respectively 2.8, 3.1, 4.6, 6.7, and 8.3 km from the terminus. Cores 1 and 7 were collected ~14 and 16 km from the terminus, within the shallow basin beyond the 1990 moraine (Figure 4.2b). All seven cores contain fine-grained, light gray glacimarine sediment with porosities of ~60% to a depth of 1 m. In core 5, closest to the ice, 0-14% of the sediment mass is composed of sand in discrete intervals, and the fine-grained fraction (<63 μm) is composed of approximately equal amounts by weight of silt and clay (Figure 4.4). The core farthest from the ice front within the main basin, core 2, contains almost no coarse grains (> 63 μm), ~33% silt, and ~66% clay, by weight (Figure 4.4). X-radiographs from all seven cores show laminations (scale of mm to cm) in the cores from both the main and shallow basins, with little evidence of coarse layers, ice-rafted debris, or bioturbation (Figure 4.5).

4.4.3 Sediment Accumulation Rates

A common technique for determining seasonal to decadal sediment-accumulation rates, and for interpreting sediment-transport mechanisms, is to measure the down-core decrease in activity of naturally occurring radioisotopes in the fjord sediments (Turekian and Cochran, 1978). Dissolved ^{234}Th and ^{210}Pb in seawater adsorbs to fine-grained particles suspended in the water, and once deposited, the adsorbed isotopes record sediment accumulation rates in the seabed over a few months (^{234}Th) and many decades (^{210}Pb) (Nittrouer et al., 1979; Aller et al., 1980; McKee et al., 1983; Jaeger and Nittrouer, 1999a). Sparse measurements of scavenging time for ^{234}Th and ^{210}Pb in nearshore coastal environments suggest that glacimarine particles settle sufficiently slowly to scavenge dissolved ^{234}Th (Aller and Cochran, 1976; McKee et al., 1986), but too quickly to adsorb significant ^{210}Pb (Jaeger and Nittrouer, 1999). Profiles of ^{210}Pb and ^{234}Th activities in cores from both fjords therefore provide a direct comparison of sediment accumulation rates between study sites.

From Columbia Fjord, activities of ^{234}Th and ^{210}Pb were measured within the four fine-grained, ~1.7-m-long cores farthest from the ice. Excess ^{234}Th is measured in the surface sediments of the three distal cores. The excess ^{234}Th decays within the upper ~40 cm in each core (Figure 4.6b). In core 4, located in the inner basin, no excess thorium was detected within the upper 100 cm. In the other cores, the excess ^{234}Th indicates deposition of ~40 cm in both the inner and outer basins within the preceding ~100 days (i.e., ~4 half lives; since June 2011). Profiles of total ^{210}Pb from the four long cores all show a uniform activity of 1.1 ± 0.2 dpm g^{-1} to the maximum depth analyzed (80-100 cm; Figure 4.6a).

From Jorge Montt Fjord, the four cores analyzed from the main basin also contained excess ^{234}Th in the surface sediment (Figure 4.6d). In cores 5, 6, and 2, excess ^{234}Th extends to ~20 cm, and in core 4 the excess ^{234}Th extends to ~30 cm. The two cores collected beyond the 1990 moraine (in the shallow basin) contained no excess ^{234}Th within the upper 60 cm. Total ^{210}Pb activities from the inner basin cores are all 1.0 ± 0.2 dpm g^{-1}, and the activity is approximately uniform to the maximum depth analyzed (100-150 cm; Figure 4.6c). The two cores in the shallow basin (cores 1 and 7) contain ^{210}Pb activities of 1.6 dpm g^{-1} that decrease to ~1 dpm g^{-1} in the upper 20 cm (Figures 4.2a, 4.6c).

Sediment deposition rates were determined by dividing the maximum depth of excess ^{234}Th in Columbia Fjord cores 5, 6 and 2, and Jorge Montt Fjord cores 5, 4, 6 and 2 (Figure 4.6b, d) by the 100-day-limit of the isotope. The ^{234}Th profiles from both Columbia Fjord and Jorge

Montt Fjord suggest deposition rates averaging ~0.4 and ~0.2-0.3 cm d^{-1}, respectively, at locations ~3-10 km from the termini during the preceding melt period of ~6 months.

Profiles of ^{210}Pb from cores collected in Jorge Montt Fjord and Columbia Fjord all show an approximately uniform activity of 1 dpm g^{-1} to core depths of ~100 cm (Figure 4 6a, c), which is consistent with rapid deposition. These profiles suggest a minimum accumulation rate of ~5 cm yr^{-1}, as the meter-long cores must have formed well within the 22.3-year half life. The low, uniform activity closely resembles profiles of ^{210}Pb from other temperate glacial fjords (e.g., Cowan et al., 1997; Jaeger et al., 1998; Jaeger and Nittrouer, 1999a; Boldt et al., 2013). The deposition rates suggested from the ^{234}Th profiles together with the 22.3-year half life of ^{210}Pb are consistent with a constant ^{210}Pb activity over 100 cm. Even for the lowest calculated deposition rate of 2 cm d^{-1} over a period of six months, a 1-m-long core represents just over two years of accumulation, during which time ^{210}Pb decays negligibly.

The low ^{210}Pb activities measured in the cores suggest either the sediment did not settle through the water column and therefore did not adsorb appreciable ^{210}Pb (e.g., Mullenbach and Nittrouer, 2000), or that the sediment settled too quickly to adsorb much excess ^{210}Pb in the water column (e.g., Jaeger and Nittrouer, 1999a). *In situ* measurements of the particle settling velocity near tidewater glacier termini indicate that flocculated particles settle to the seabed at rates of ~0.001 m s^{-1} (Hill et al., 1998; Curran et al., 2004), or roughly 2-4 days in Columbia and Jorge Montt Fjords. Sparse measurements of scavenging time for ^{234}Th and ^{210}Pb in nearshore coastal environments suggest that glacimarine particles settle sufficiently slowly to scavenge dissolved ^{234}Th (Aller and Cochran, 1976; McKee et al., 1986), but too quickly to adsorb significant ^{210}Pb (Jaeger and Nittrouer, 1999a). Because accumulation rates cannot be interpreted from the ^{210}Pb profiles, I rely on the clear, short-term deposition rates suggested by the ^{234}Th profiles.

4.4.4 Sediment Volume Calculations

In the seismic profiles in both fjords, reflections corresponding to the top and bottom of the sediment package deposited after glacier retreat were identified (Figure 4.7a, b). At the seabed-water interface, there was a distinct reflection in each profile separating the transparent water column above from a seismic facies characterized by high amplitude, continuous, and parallel reflections below. Independent bathymetric measurements confirmed the depth of the chosen water-bottom reflector. The surface separating the underlying bedrock or consolidated sediment from the recently deposited sediment was chosen by identifying onlapping reflectors and a distinct change to a slightly higher amplitude and discontinuous seismic facies, which are associated with the underlying strata. Because of the 3-D variations in fjord geometry, the 2-D seismic profiles often showed overlapping reflections at the sides of the fjord due to sideswipe; I consistently picked the reflector that did not overlap the side of the fjord when this occurred.

The seismic profiles collected throughout Columbia Fjord reveal two sediment basins separated by a sill and surrounded by relatively steep fjord walls. The mean depths to the top of the outer and inner sediment basins are ~320 m and 425 m, respectively (Figure 4.2a). A nearly horizontal seabed and parallel, continuous internal reflectors characterize the sediment basins in Columbia Fjord (shown in detail in Chapter 3).

In Jorge Montt Fjord, seismic profiles and bathymetry define a single sediment basin in the center of Jorge Montt Fjord and steep valley walls on both sides. The 365-m-depth to the top of the sediments is relatively uniform along the central 3.5 km of the 10-km-long basin; it decreases to ~300 m north and south over a distance of ~1.5 to 2 km, suggesting an average surface slope along the top of the sediment basin of ~3-4%. The seismic profiles reveal discontinuous, low amplitude seismic facies overlain by continuous, high-amplitude parallel reflectors within the basin sediments (Figure 4.7). While a second sediment basin exists between the 1990 and Little Ice Age morainal shoals, the analysis presented herein focuses on the sediment basin formed during the recent retreat.

Sediment volumes were determined for both fjords by interpolating the seafloor and basal surfaces throughout the sediment basins, from the most recent pre-retreat position at the moraine to the modern ice front. Mean annual sediment fluxes were calculated by dividing the total volume by the retreat period. I apply a 25% uncertainty to the calculated sediment volumes to account for the interpolation of the basin edges between the seismic profiles and for potentially inaccurate depth conversion because of the lack of velocity information from the single-channel seismic profiles. Basin features, total sediment volumes, and the corresponding mean annual sediment fluxes are presented in Table 4.2.

Table 4.2. *Comparison of Columbia and Jorge Montt Fjords*

	Columbia Fjord	**Jorge Montt Fjord**
Glaciated basin size	1000 km^2	500 km^2
Onset of rapid retreat	1980	1990
Sediment basin size	8 km x 1.2 km[a] 5 km x 0.6 km[b]	10 km x 0.4 km
Annual precipitation at sea level	~2 m	~2.5 m
Total post-retreat sediment volume	$3.2 \pm 0.8 \times 10^8\ \text{m}^3$	$8.0 \pm 2.0 \times 10^7\ \text{m}^3$
Mean annual sediment flux	$1.1 \pm 0.3 \times 10^7\ \text{m}^3\ \text{yr}^{-1}$	$4.0 \pm 1.0 \times 10^6\ \text{m}^3\ \text{yr}^{-1}$
Glaciated-basin-averaged erosion rate	$5.3 \pm 1.3\ \text{mm yr}^{-1}$	$4.0 \pm 1.0\ \text{mm yr}^{-1}$

[a,b] outer and inner basins, respectively (Figure 4.2a)

4.4.5 Glaciated-Basin-Averaged Erosion Rates

To compare the sediment fluxes from the glaciers entering the two fjords, the sediment flux, Q_{sed}, is normalized to the respective glaciated-basin areas, A. I account for the different densities of the bedrock, ρ_{rock}, which is assumed to be 2700 kg m^{-3} (a typical density for the sedimentary rocks around Columbia Glacier and for granite around Jorge Montt Glacier), and of glacimarine sediment, ρ_{sed}, for which a representative value of the dry bulk density for glacimarine sediment of 1300 kg m^{-3} is used. The equivalent bedrock flux, Q_{rock}, is then determined by:

$$Q_{rock} = \rho_{sed} Q_{sed} / \rho_{rock} \qquad (4.1).$$

This normalization provides a glaciated-basin-averaged erosion rate, or the rate of sediment production per area of glaciated basin necessary to sustain the measured sediment flux during the study period, such that,

$$\dot{E} = Q_{rock} / A \qquad (4.2).$$

Columbia and Jorge Montt Glaciers have been producing sediment at an estimated average rate of 5.3 ± 1.3 mm yr^{-1} and 4.0 ± 1.0 mm yr^{-1}, respectively. Despite probable differences in the underlying geographic, geologic, and tectonic settings, the glaciated-basin-averaged erosion rates for the two glaciers were approximately the same during the recent decades of rapid retreat.

4.5 Modeled Sediment-Flux Histories

In order to determine the temporal variation in sediment output from the glaciers and to study the evolution of the post-retreat sediment package in each fjord, I developed a numerical model to relate the fjord sediment distribution and seismic stratigraphy in the context of the known glacier retreat history. I first applied the model to Columbia Glacier, a system for which extensive glaciological measurements exist during the period of retreat (e.g., Meier and Post, 1987; Meier et al., 1994; Pfeffer et al., 2000; Krimmel, 2001; O'Neel et al., 2005;). At Columbia Glacier, the modeled sediment-flux history is compared to the known glaciological parameters, which highlights that the glacier and bed geometries controlled the storage and rapid release of sediment stored subglacially (Chapter 3). Here, the same model is applied to determine the sediment-flux history for Jorge Montt Glacier, a glacier with similar retreat behavior and climate conditions but without the detailed observational history and glaciological data that exist for Columbia Glacier.

The model includes both primary proglacial sediment delivery from the glacier as well as secondary reworking in the fjord basins. The essence of the model is represented by Equation 4.3 for the rate of change in seabed elevation, $\frac{dz}{dt}$. The first two terms on the right-hand side represent proximal and distal sediment accumulation, with rapid accumulation near the ice front decreasing quickly with distance from the ice, and the slower and more uniform sedimentation far (>1 km) from the ice (Cowan and Powell, 1991; Jaeger and Nittrouer, 1999a). The third term represents the diffusive redistribution of particles once they reach the seabed due to various gravity-driven processes (including sediment sloughing off valley walls, slope failures of oversteepened sediments, and gouging of the seabed by icebergs):

$$\frac{dz}{dt} = \dot{S}_{01} e^{-x/\delta_1} + \dot{S}_{02} e^{-x/\delta_2} + \kappa \frac{d^2 z}{dx^2} \qquad (4.3).$$

$\dot{S}_0(t)$ characterizes the time varying sediment-accumulation rate at the ice front; x is the distance from the ice front to a position in the fjord; δ represents the falloff distance of the sediment-accumulation rate (the distance over which the rate drops 1/e of the value at the terminus); and κ, the seabed diffusivity, which represents the effective mobility of sediments. $\dot{S}_{01}$ and $\dot{S}_{02}$ are the sediment-accumulation rates associated with each decay distance, δ_1 and δ_2, respectively. Equation 4.3 thus reflects the direct input of sediment from the glacier as well as diffusive downslope transport and redistribution.

The model, when applied to Jorge Montt Glacier, produces the post-retreat sediment packages and flux history shown in Figures 4.8 and 4.9. A 35% uncertainty is applied to the modeled sediment fluxes. 25% is due to uncertainty in the sediment-volume calculations (Section 4.4.4), and the additional 10% is due to the lack of measurements within ~2 km of the ice front, the assumption that all sediment is captured within fjord basins, and the assumption that Columbia Glacier and Jorge Montt Glacier are the only sources of sediment (see Chapter 3).

4.6 Discussion

4.6.1 Observational and Modeled Sediment Dynamics

From the seismic and sediment-core observations, I can respectively determine the total volume of sediment delivered by the glaciers during retreat and measure sediment accumulation on sub-seasonal time scales. In both fjords, profiles of excess ^{234}Th provide sediment-deposition rates for the ~100 days prior to sampling. As both coring campaigns took place toward the end of the melt season, it is likely that much of the annual sediment delivery was during this melt period. Winter water-column properties in Jorge Montt Fjord suggest little glacial meltwater present in the fjord (Moffat et al., in prep), and studies in other temperate fjords also report little suspended sediment during winter months (Mackiewicz et al., 1984; Cowan and Powell, 1991). These observations lead to the commonly held notion that the subglacial system is relatively inactive during the winter months (e.g., Fountain and Walder, 1998). Thus, assuming the glacier actively delivers sediment to the fjord at the measured rate of 04 cm d^{-1} from mid spring through mid fall, the outer basin of Columbia Fjord received approximately 75 cm of sediment in 2011. The negligible and varying activities in cores 4 and 5 from Columbia Glacier indicate that more than ~1 m of sediment accumulated in the inner basin in 2011 (Figure 4.6b). In Jorge Montt

Fjord, approximately 35 cm of sediment accumulated in 2013 over most of the basin area, and 55 cm accumulated at the location of core 4. Based on these rates, the laminations a few mm thick visible in the many of the x-radiographs would likely have formed on a diurnal time scale, suggesting a dominant modulation by daily variation in meltwater (Figure 4.5).

Over longer time scales, the spatially averaged vertical accumulation rate can be independently estimated as the ratio of the mean annual volume of sediment delivered by the glacier during the decadal period of retreat to the surface area over which it accumulated. For the inner basin of Columbia Fjord, the annual load would create a ~5-m-thick deposit, and estimates from inner-basin ^{234}Th profiles also suggest rapid accumulation likely greater than 1 m yr^{-1}. In the outer basin of Columbia Fjord, the expected accumulation of ~85 cm agrees well with the ~75 cm estimate from ^{234}Th. For Jorge Montt Fjord, the mean annual sediment volume averaged for 1990-2010 of ~4 x 10^{6} m^{3} would create a ~1-m-thick layer over the ~4 km^{2} sediment basin surface area in a given year (Table 4.2). However, the short-term deposition rate calculated from ^{234}Th only accounts for ~40% of the total expected accumulation. Differences in the estimated deposit thickness and the annual ^{234}Th-derived deposition rate in Jorge Montt Fjord suggest the sediment volume delivered in 2013 was considerably less than during most of the retreat period. Because the short-lived radioisotope records do not preserve a record of temporal changes in the accumulation rate, discrepancies in estimates of sediment accumulation on different time scales imply complexity in the sediment-flux history of a glacier.

To quantitatively explore such temporal variations in sediment dynamics over the period of retreat, the glacimarine sedimentation model allows for the comparison between the short-time-scale sediment-core observations and the decadal-time-scale sediment-volume calculations. For Columbia Fjord, the model parameters and the resulting sediment-flux history are tightly constrained by detailed observations made throughout the retreat, which include the terminus position through time, the glacier surface and bed geometries, as well as the fjord bathymetry (Chapter 3). Previously, I determined the glacial and sediment-transport processes that were important in forming the sediment shoal in Columbia Fjord. By applying the model to Jorge Montt Fjord, I can determine whether the processes are also important to sediment-basin formation here. I expect the same processes to be dominant because of the similarities in the basin geometries, seismic architecture, glaciated-basin-averaged erosion rates, and glacier retreat patterns (Table 4.2; Figures 4.1, 4.7).

For Jorge Montt Fjord, the model is applied to evaluate the time-varying sediment-flux history, which can then be interpreted in light of relevant glacier behavior. The modeled history creates realistic sediment basin characteristics and accounts for the known glacier-retreat history. Here, the maximum sediment flux occurs during the early years of retreat, when the glacier was retreating most rapidly, ~1 km yr^{-1} (Figure 4.10b). The few available measurements indicate an increase in the ice velocity from ~0.7 m d^{-1} before the onset of retreat (Enomoto and Abe, 1983) to ~5.6 m d^{-1} during the period of fastest retreat (M. Pritchard, pers. comm.). However, while the sediment flux and retreat rates both decreased after the period of rapid retreat (1993-1995), the measured glacier surface velocity peaked at ~13 m d^{-1} in 2011 (Rivera et al., 2012a). The similar pattern between the sediment flux and retreat rates on a time scale of several years for Jorge Montt is similar to that observed at Columbia Glacier after ~1998 (Figure 4.10a), as well as at other retreating tidewater glaciers in Alaska and Patagonia (Koppes and Hallet, 2002, 2006; Koppes et al., 2009). However, the occurrence of the largest sediment flux during a period of relatively slow ice motion suggests that processes other than glacier dynamics control the sediment flux.

A close relationship between ice velocity and sediment flux is expected due to the control of the glacier sliding speed on the rate of erosion by both quarrying and abrasion (Hallet, 1979; Iverson, 1991), but processes other than bedrock erosion can influence or control the sediment flux. By comparing the modeled sediment flux to changes in the glacier surface and bed slope at Columbia Glacier, I determined that the sediment flux is largely controlled by subglacial sediment storage, at least during the early retreat. The steep reverse-sloping bed at the downstream side of a subglacial basin likely impeded the transport and evacuation of sediments under the glacier by subglacial rivers. This likely continued until the ice slope steepened sufficiently as the glacier retreated to allow efficient evacuation of the sediment trapped subglacially (Chapter 3). The glacier-specific geometries and the potential for trapping large volumes of sediment subglacially over decades, as shown for Columbia Fjord, may also account for the low sediment flux from the Jorge Montt Glacier during the latter part of the retreat, when the velocity was relatively high (Figure 4.10). Velocity profiles along the lower 30 km of Jorge Montt Glacier reveal a threefold increase in speed over an area ~16 km from the terminus, which, by continuity of ice mass, suggests that the ice is flowing more quickly over a much deeper bed (E. Rignot, pers. comm.). These velocity profiles suggest the presence of a substantial glacial overdeepening with the potential to trap sediment.

4.6.2 Physical Implications of Model Parameters

Confidence in the model results for Columbia Glacier enables the relative importance of the physical processes represented by the model components to the formation of the observed sediment distribution and stratigraphy in both fjords to be considered. For Columbia Fjord, both proximal and distal sediment accumulation, represented by the exponential terms associated with δ_1 and δ_2, respectively, are essential to account for the observed sediment deposit. Proximal accumulation is necessary to fill the inner basin at rates >5 m yr^{-1}, and distal accumulation is necessary to deliver 75% of the sediment volume to the outer basin after the glacier retreated over the sill separating the two sediment basins (Chapter 3). Distal sedimentation is also required for creating continuous, parallel seismic reflectors along the length of the outer basin, many kilometers from the ice front. The similar, basin-continuous seismic reflectors present in Jorge Montt Fjord are reproduced in the model only when sufficient sediment is transported far from the ice, confirming the importance of distal sedimentation to basin formation in this fjord.

In addition, the model results from Columbia Glacier highlight the importance of diffusive sediment redistribution and transport for creating the flat seabed characteristic of the sediment basins and the near-horizontal, parallel seismic reflectors. Model results from Jorge Montt Fjord, however, suggest diffusive processes affect the deposited sediments differently than in Columbia Fjord. When the evolution of the sediment basin in Jorge Montt Fjord is modeled with the same diffusive transport parameter as for Columbia ($\kappa=10^6$ m^2 yr^{-1}), the shape of the basin center is replicated, but the slightly sloping deposits on either side are not (Figure 4.8a). Using a lower diffusivity ($\kappa=10^5$ m^2 yr^{-1}) reproduces the average 2° surface slope throughout the Jorge Montt Fjord basin, but does not capture the horizontal bathymetry observed in the center of the basin (Figure 4.8b); the basin shape in Jorge Montt Fjord seems to reflect a combination of these two diffusion parameters.

The model results from Jorge Montt Fjord likely highlight the differential behavior of coarse- and fine-grained sediments delivered to the fjord. Fine-grained sediments can be transported far from the glacial source (Figure 4.4). Once deposited, they remain highly mobile and susceptible to diffusive redistribution. In comparison, the coarser particles tend to accumulate near the ice and quickly stabilize. A close examination of the seismic profiles across the center of the sediment basin in Jorge Montt Fjord reveals a vertical facies change that is interpreted to mark a transition from particles delivered by bedload to those delivered from suspension. The seismic profiles reveal flat, parallel, high-amplitude, and continuous reflectors overlaying more chaotic and discontinuous reflectors (Figure 4.7). This change in the seismic facies suggests a change in sediment character. No samples were collected from the underlying chaotic seismic facies, but all of the cores from the surface sediments more than ~2 km from the ice front indicate silt and clay down to at least 1.5 m below the seabed (Figure 4.4). Thus, to account for the different behavior of coarse and fine sediment, the best model representation of Jorge Montt Fjord is a combination of highly mobile fine-grained sediments and less mobile coarser particles (Figure 4.8a, b). This interpretation suggests the two exponential accumulation terms, with falloff distances δ_1 and δ_2, likely represent the delivery of bedload and suspended load, respectively, and supports the use of two distinct exponentials, rather than one power law, in modeling glacial sediment output (Cowan and Powell, 1991).

The insight into proximal and distal sediment transport from Jorge Montt Fjord helps shed lights on why the use of high diffusivity values that simulated the flat basins in Columbia Fjord did not account for the deposits on the moraine or the sill separating the sediment basins (Chapter 3). These deposits are likely composed of coarser-grained material than the sediment sampled in the cores from the basins (e.g., Powell, 1981; Cowan and Powell, 1991; Jaeger et al., 1998; Salcedo-Castro et al., 2013), and thus are not preserved under highly diffusive model conditions (Chapter 3). This differential behavior of coarse and fine sediment within the fjord sediment basins is consistent with sandy grain-size distributions located <2 km from the ice, and the very fine sediment collected in cores >2 km from the terminus (Figure 4.4). Thus, correctly interpreting fjord sediment records requires understanding spatial variations in deposition patterns and temporal variations in sediment flux; the glacial sedimentation model provides a quantitative tool for developing this understanding.

4.6.3 Interpreting Fjord Sediment-Transport Mechanisms

I now relate the model parameters to the sediment-core and seismic properties and interpret the processes likely forming the sediment deposits in both Columbia and Jorge Montt Fjords. Proximal sedimentation involves the rapid deposition of coarse-grained particles near the glacier terminus largely delivered to the fjord by subglacial rivers (e.g., Powell, 1981). Processes associated with distal sedimentation include: particles settling to the seabed from a buoyant, seaward-moving freshwater plume; ice-rafting of glacial debris; and sediment gravity-driven flows traveling along the seabed (e.g., Powell, 1981; Syvitski, 1989; Mugford and Dowdeswell, 2011). Gravity-driven flows on many spatial scales result in highly mobile reworking, a nearly horizontal seabed, and approximately horizontal, parallel internal layering (e.g., Syvitski, 1989). In temperate glacial settings, subglacial rivers deliver the majority of sediment and meltwater to fjords (e.g., Cowan and Powell, 1991; Hunter et al., 1996a). The sediment concentration of the subglacial meltwater controls the dominant processes by which the sediment will be transported throughout the fjord. If the density of the sediment-laden meltwater plume exceeds that of the ambient seawater (equivalent to a suspended-sediment concentration of ~30 g L^{-1} for the average salinity of both fjords), a hyperpycnal plume will form and travel as a gravity flow along the seabed, driven by its excess density (Mulder et al., 2003).

The suspended-sediment concentration of the subglacial water, averaged broadly over time and space, can be approximated for both fjords as the ratio of the meltwater flux, which is constrained by the amount of precipitation averaged over the area of each glacier, to the sediment flux. Assuming that the flux of water in the subglacial system is primarily from rainfall and snowmelt with negligible contribution due to change in glacier volume, based on the temporally averaged precipitation and mean sediment fluxes for the two fjords, the average suspended-sediment concentration of the subglacial meltwater is ~3 g L^{-1} for Jorge Montt Fjord and ~5 g L^{-1} for Columbia Fjord (Table 4.2). This concentration range is consistent with sediment concentrations measured in proglacial streams from land-terminating glaciers under quiescent conditions (e.g., Pearce et al., 2003; Riihimaki et al., 2005; Swift et al., 2005). Following large precipitation events or during subglacial lake outburst floods, however, concentrations commonly increase at least a four-to-fivefold and can exceed 20 g L^{-1} (Mackiewicz et al., 1984; Cowan et al., 1988; Merrand and Hallet, 1996; Denner et al., 1999; Motyka et al., 2013).

Under quiescent conditions, the subglacial meltwater entering the fjord is less dense than the ambient seawater, hence a rising turbulent plume is expected from which particles settle as the plume expands down the fjord (e.g., Mugford and Dowdeswell, 2011; Salcedo-Castro et al., 2013). In temperate glacial fjords, particles suspended in the water column settle toward the seabed at a rate of ~0.001 m s^{-1} (Hill et al., 1998; Curran et al., 2004). In Jorge Montt Fjord, estuarine circulation occurs within uppermost 50 m of the water column, while deeper water does not actively circulate out of the fjord (Moffat, 2014). Thus, settling particles would travel vertically though the water layers moving into and out of the fjord before a parcel of buoyant meltwater traveled horizontally at ~0.1 m s^{-1} along the ~10 km length of Jorge Montt Fjord (Moffat, 2014). This comparison indicates that most suspended sediment will be trapped in the main basin of the fjord, which is consistent with the observations of very little suspended sediment present in the water column beyond the main basin (Figure 4.3). Additionally, the integrated sediment mass in the main-basin water column during summer conditions is consistent with ^{234}Th deposition rates of a few mm d^{-1}. Importantly, sediment settling from suspension would create a sediment drape of uniform thickness over the underlying seabed (e.g., Syvitski, 1989), which is a stratigraphic style quite different from the essentially horizontal seabed and internal architecture characterizing the fjord sediment basins.

The discrepancy between the likely sediment-delivery mechanism under average, quiescent conditions (i.e., settling from suspension) and the sediment-basin architecture characterized by horizontal, parallel internal layers suggests the importance of sediment delivery by hyperpycnal flows emanating from the glacier primarily during discharge events and/or post-depositional redistribution processes. The key role of diffusive sediment redistribution in modeling the evolution of Columbia and Jorge Montt Fjord sediment basins indicates that gravity-driven processes are necessary to form and maintain the basin geometry and stratigraphy observed in these temperate tidewater glacial fjords (e.g., Carlson, 1989; Cai et al., 1997; Koppes and Hallet, 2006; Cowan et al., 2010). The potential for hyperpycnal flows is greatest when large volumes of water occur at the bed of the glacier and sufficiently increase the sediment-transport capacity of the subglacial system, such as following large precipitation events (e.g., Denner et al., 1999; Motyka et al., 2013). Without direct measurements of subglacial discharge from either of the study glaciers, occasional releases of large volumes of subglacial water are inferred from abrupt, significant decreases in ice velocity over large areas of the glacier. Rapid decreases in ice velocity, as measured throughout the year at Columbia Glacier over areas of several square kilometers (O’Neel, 2013; I. Joughin, pers. comm.), are likely caused by the release of large volumes of freshwater (with sediment) to the fjord.

Seismic evidence of deposits inferred to form from basin-wide gravity flows from other temperate fjords (e.g., Cowan et al., 1997; Willems et al., 2011) suggests that gravity-driven sediment transport occurs along fjord seabeds under certain conditions (Prior et al., 1987;

Bornhold et al., 1994). This evidence supports the expectation that large subglacial meltwater events deliver sediment with concentrations exceeding the ~30 g L^{-1} threshold. Additional evidence from the sediments in the inner basin of Columbia Fjord is consistent with formation by concentrated-sediment gravity flows. Core 4, which is closest to the terminus, is the only site from either fjord that does not contain excess ^{234}Th to a depth of ~1 m (Figure 4.6b). This suggests the particles did not settle through the water column and rather were transported near the seabed (e.g., Mullenbach and Nittrouer, 2000). The sediment in this core lacked sufficient cohesion to sample for x-radiography; however, x-radiographs from core 5, also in the inner basin of Columbia Fjord, contain a distinct sandy layer that appears to have an erosional base, such as might be expected for a gravity flow (CGF core 5, ~150 cm, Figure 4.5) (Mulder et al., 2003). The level surface of the inner basin, combined with the most rapid accumulation rates measured (~5 m yr^{-1}), support the interpretation that direct hyperpycnal gravity flows are active in this basin. Conclusive evidence of the specific processes suggested by the seabed signatures and the high sediment mobility represented in the relatively realistic models requires *in situ* documentation of water velocity and suspended-sediment concentrations, which is very difficult to obtain near the actively calving termini of tidewater glaciers or along the soft sediment beds of their proglacial fjords. With adequate, comprehensive instrumentation, however, the termini of temperate tidewater glaciers are good candidates for documenting *in situ* hyperpycnal flows.

4.6.4 Implications for Glacier Stability

Modeling results and sedimentary evidence from both Columbia and Jorge Montt Fjords indicate that sediment accumulates rapidly in these basins, and that the fjord seabed is a dynamic component of the integrated ice-ocean-seabed system. The rapid sediment accumulation near the glacier termini likely reduces the vigor of fjord circulation due to shoaling, insulates the submarine ice face from the warm fjord water (e.g., Rignot et al., 2010; Straneo et al., 2010), and buttresses the glacier. These effects collectively provide one of the only known negative feedbacks to slow or stop the shrinkage of tidewater glaciers retreating into deeper water (Alley et al., 2007). The recognition that the retreat of many outlet glaciers into deep submarine basins will likely cause their disintegration in Antarctica (Joughin et al., 2014; Rignot et al., 2014) stresses the importance for a greater understanding of glacier-bed geometries. The significant difference between the bed over which the glacier retreated (as measured in seismic profiles) and the fjord seabed (as measured in bathymetric soundings) is shown herein as the changes of tens of meters in fjord water depth over a period of 1-2 decades (Figures 4.4, 4.8). The former glacier bed imaged in seismic profiles is comparable to calculated glacier beds from models (McNabb et al., 2012; Rignot et al., 2014), and is consistent with boreholes through Columbia Glacier (Meier et al., 1994). It is quite different, however, from the fjord seabed, which affects modern circulation and melting patterns (e.g., Sutherland et al., 2013). Thus, future endeavors to measure fjord oceanographic properties (e.g., those proposed in Schjøth et al., 2012; Straneo et al., 2013) should focus on collecting both seismic profiles and fjord bathymetry, as these data together shed light on past and current conditions that can affect glacier stability.

4.7 Conclusions

Herein, the first observations of the sediments formed during the retreat of Jorge Montt Glacier, which drains from the Southern Patagonia Icefield, are presented. Since the start of rapid retreat in 1990, I estimate that $8.0 \pm 2.0 \times 10^7$ m^3 of sediment has accumulated at an average rate of 4.0×10^6 m^3 yr^{-1}. Seismic, sediment-core, and retreat-history datasets from Jorge Montt Glacier are compared to those for Columbia Glacier, where considerable existing data documenting glacial and bathymetric conditions are leveraged. When converted to basin-averaged erosion rates required to sustain the sediment fluxes, the glacier-basin averaged erosion rates for Columbia Glacier and Jorge Montt Glacier are approximately the same, ~4-5 mm yr^{-1} during their rapid retreats. The similar rates are surprising in view of the significant geographic and tectonic differences, and likely differences in bedrock resistance to erosion. Sediment-accumulation rates from ^{234}Th profiles indicate deposition of 0.2-0.4 cm d^{-1} of fine-grained sediment kilometers away from the ice front in both fjords. This corresponds to 40-75 cm yr^{-1}, assuming the glacier delivers sediment over the six-month melt period. Due to the rapid accumulation rates documented by the ^{234}Th and seismic records, ^{210}Pb profiles are not long enough to provide an independent assessment of accumulation rates, but they provide bounding lower values that are consistent with estimates from ^{234}Th.

Seismic profiles from Jorge Montt Fjord and model results from both fjords suggest distinct for coarse- and fine-grained material in fjord sediment basins. This difference supports the use of two distinct decay terms when modeling glacimarine sedimentation. The accumulation term with a long falloff distance is consistent with the transport of fine-grained particles kilometers from the ice front. Seismic profiles and model results from both fjords highlight the key role of diffusive gravity-driven processes for both sediment delivery and dispersal for creating the observed sediment deposits, which seem representative of deposits formed by temperate tidewater glaciers around the world. Sedimentary evidence from the inner basin of Columbia Fjord suggests that hyperpycnal flows occur during major precipitation events and are most likely to originate where subglacial rivers enter the fjord at the base of the glacier terminus.

The model results for Jorge Montt suggest that the flux of sediment to the fjord was greatest during the early retreat period, when the retreat was fastest. This is in contrast to

Columbia Glacier, where the sediment flux remained low during the early years of rapid retreat. In both systems, however, the sediment flux does not parallel changes in the ice velocity, and is thus not related simply to an increase in sediment production by erosion due to faster sliding. For Columbia Glacier, temporal changes in the glacier surface and bed slopes indicate that the release of sediment stored subglacially is able to cause rapid changes in the sediment flux. The presence of a deep basin beneath Jorge Montt Glacier, and thus the likelihood of subglacial sediment storage, could account for similar changes in the sediment flux from Jorge Montt Glacier during its retreat.

Overall, the modeled sediment-flux histories from both glaciers suggest that temporal variations during retreat reflect changes in glacier-specific surface and bed geometries that control subglacial sediment storage. The tendency for the glacier surface slope over a subglacial basin to increase as the terminus retreats represents an important mechanism accounting for the evacuation of subglacial sediments and the high flux of sediment to fjords during rapid retreat. That temporal variations in the sediment flux can be dominated by subglacial sediment storage and release, and not ice dynamics or climate, suggests that the connections between climate, glacier properties, and the glacimarine sediment deposits are complex and require careful consideration.

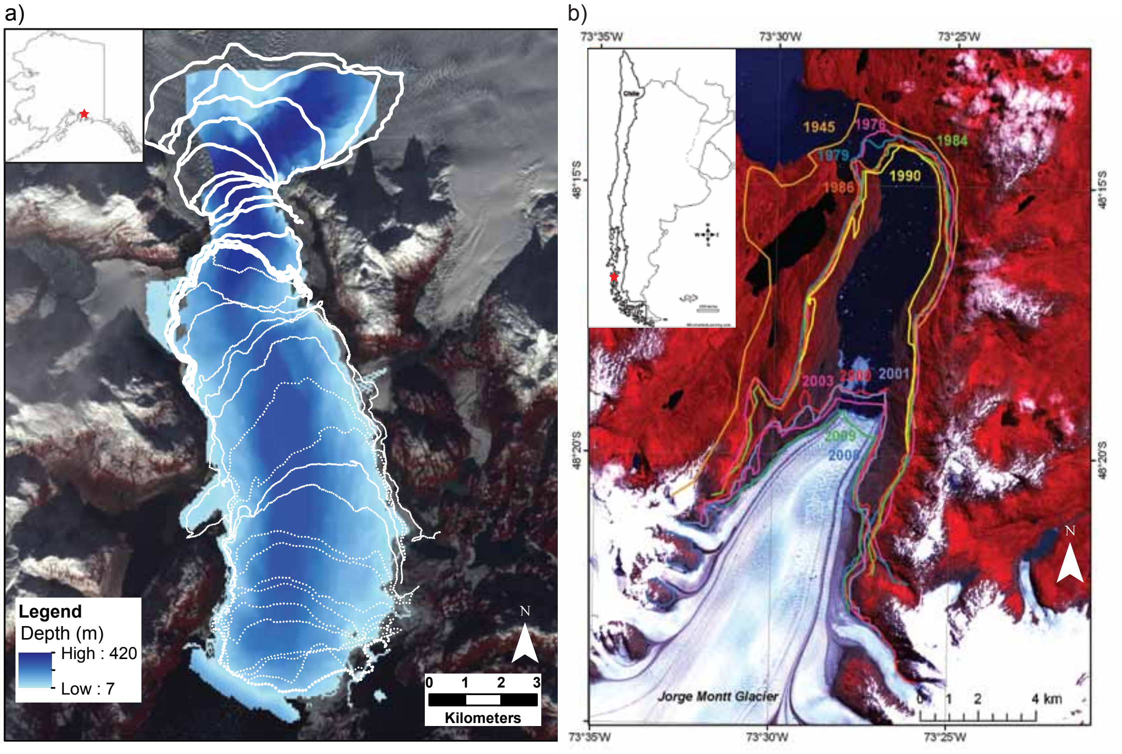

Figure 4.1. Columbia and Jorge Montt Glacier Terminus Positions
(a) Annual position of the glacier terminus from 1980 (bottom) to 2011 (top), in white lines, and the bathymetry for Columbia Fjord in blue. Inset: location of Columbia Glacier in Prince William Sound, AK. **(b)**. Terminus positions for Jorge Montt Glacier are shown in the years indicated (modified from Rivera et al., 2012b). Inset: location of Jorge Montt Glacier in Chile draining from the northern edge of the Southern Patagonia Icefield.

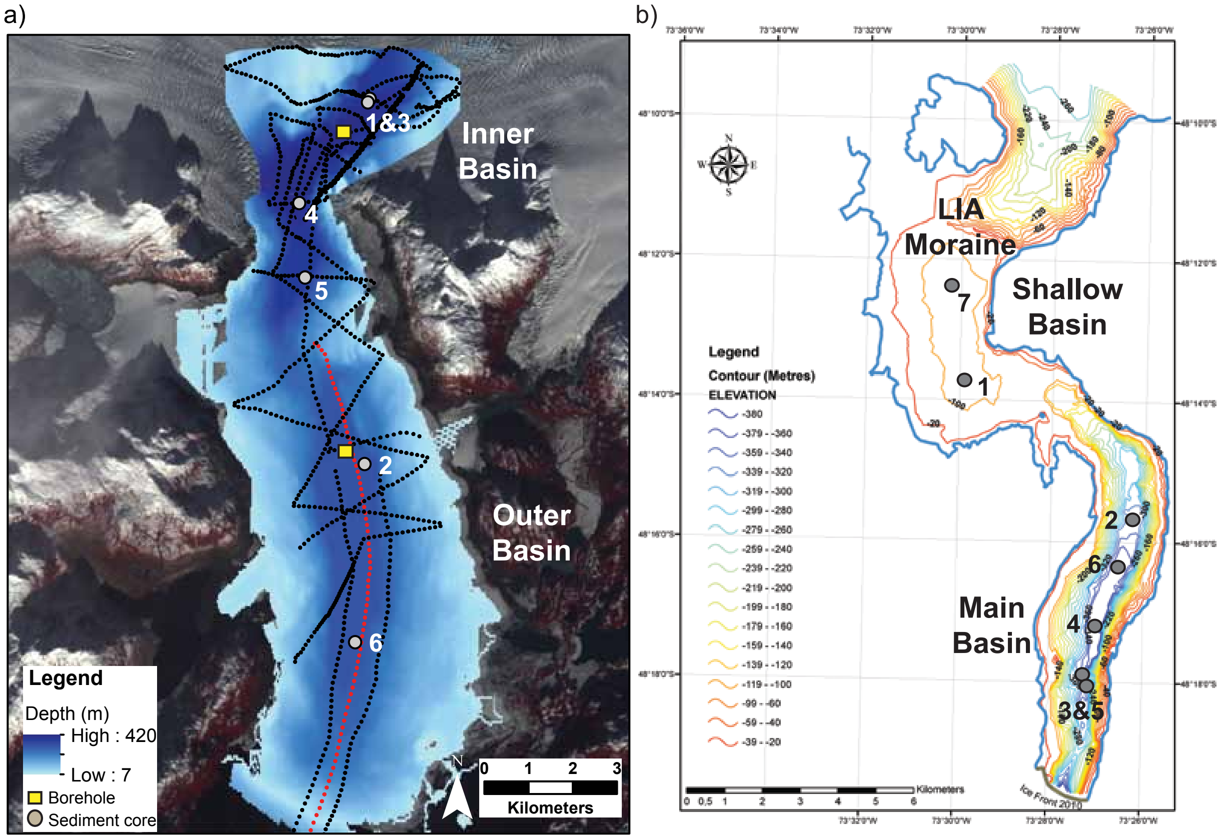

Figure 4.2. Fjord Bathymetry and Sample Locations
(a) Bathymetry and sample locations in Columbia Fjord. The black and red lines are locations of seismic profiles, yellow squares indicate boreholes drilled through the ~1000-m-thick glacier in 1987 (Meier et al., 1994), and the gray circles are locations of sediment cores. Cores 2 and 6 are in the outer basin, and cores 1, 3, 4, and 5 are in the inner basin. **(b)** Bathymetry for the main and shallow basins of Jorge Montt Fjord (main basin shown in Figure 4.1b). Gray circles indicate sediment core locations. For both figures, North is up.

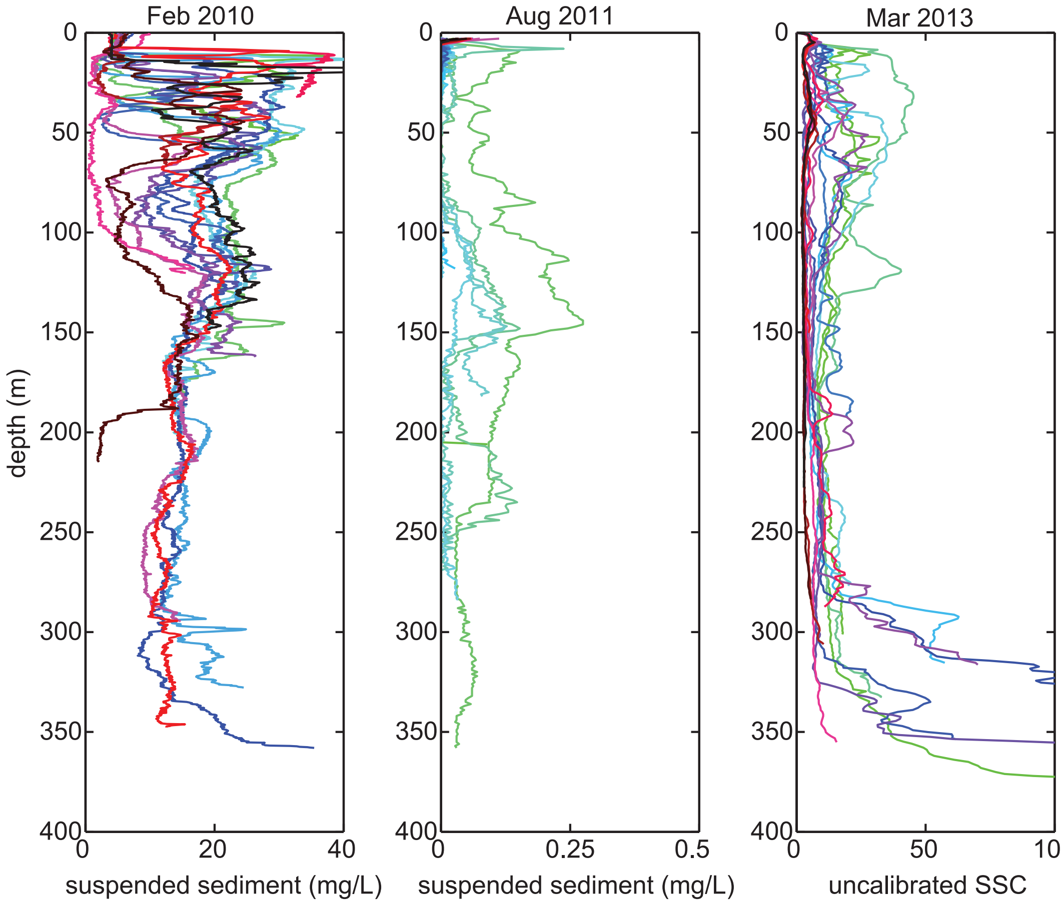

Figure 4.3. Jorge Montt Fjord Suspended Sediment Profiles
Profiles of suspended-sediment concentrations (SSC) from the main basin of Jorge Montt Fjord in austral summer (February and March) and austral winter (August). March 2013 values are uncalibrated, but are likely on the same order as February 2010.

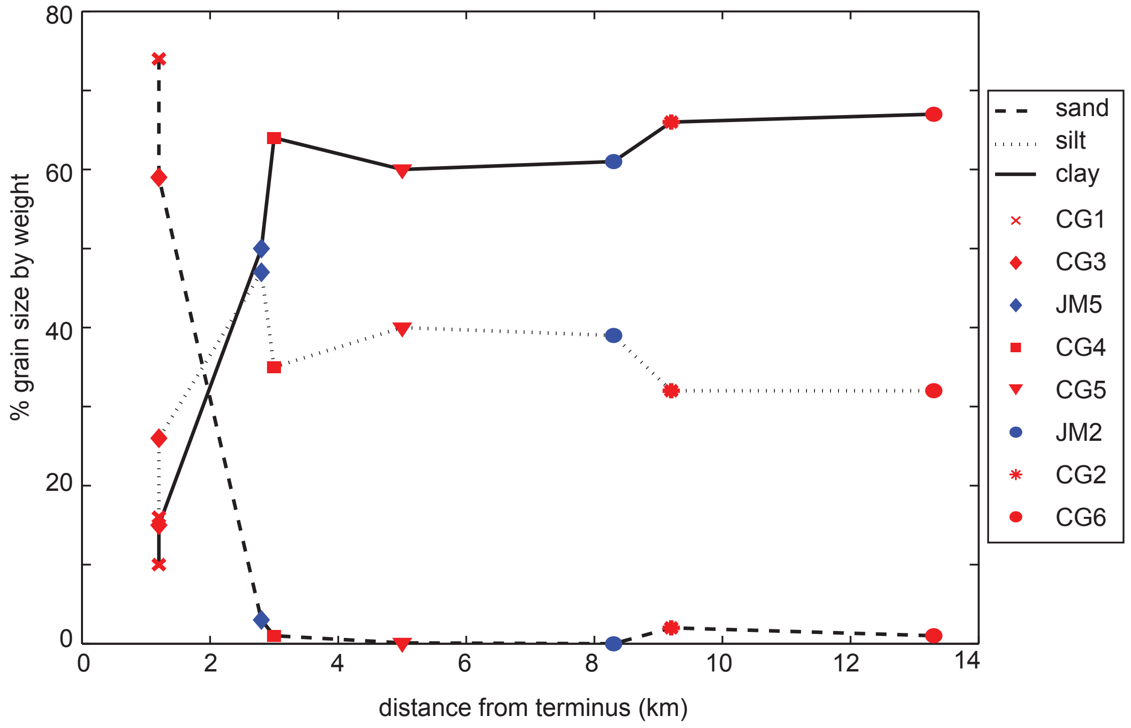

Figure 4.4. Grain Size Variation with Distance
Sediment grain-size distributions vary with distance from the glacier terminus, indicated by the portion of sand (black dashed line), silt (black dotted line), and clay (black solid line) for ~1-m-long cores from Columbia Fjord (CG, red markers), and Jorge Montt Fjord (JM, blue markers). Core numbers associated with each marker are indicated in the legend, and the corresponding core locations are shown in Figure 4.2.

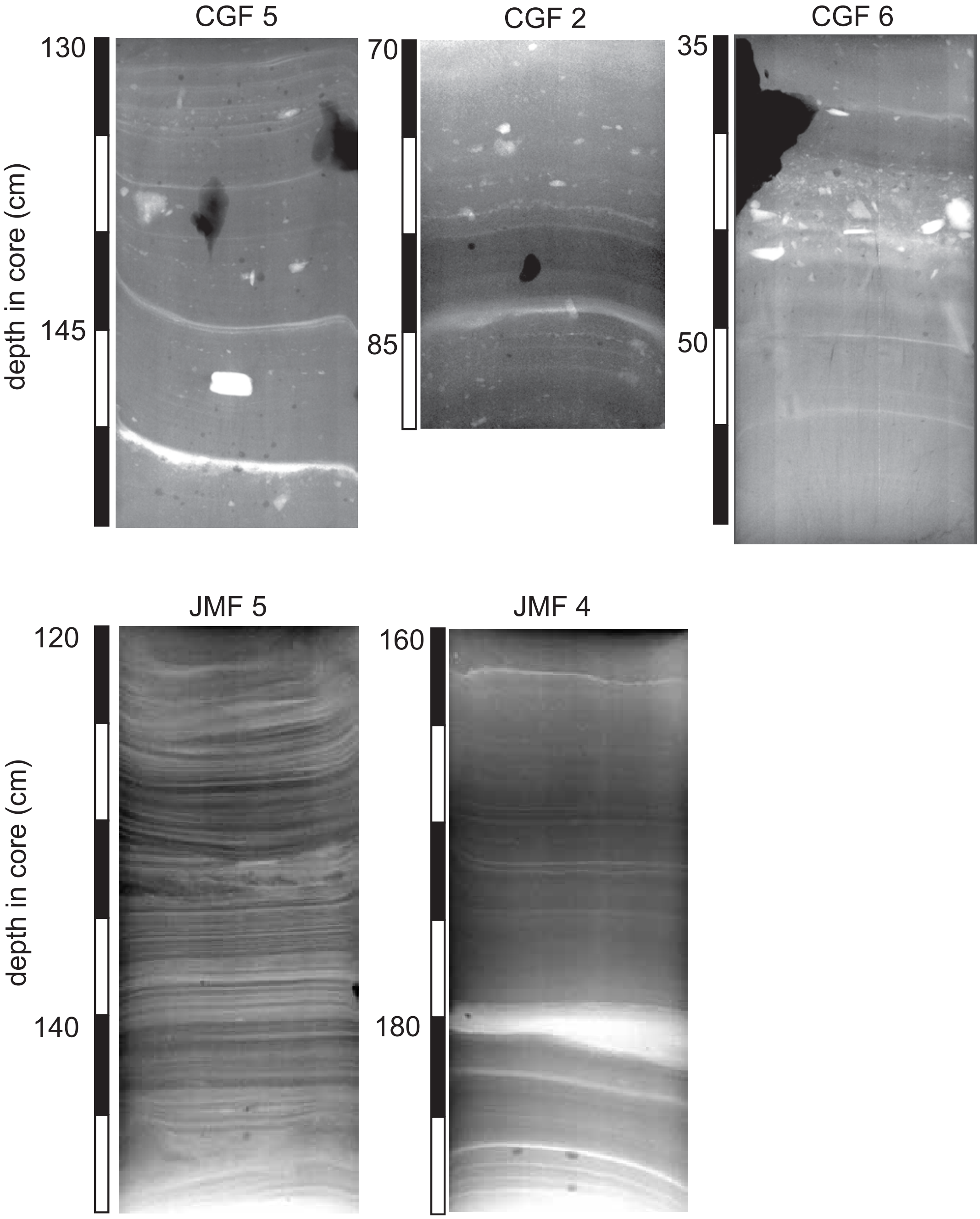

Figure 4.5. Sediment Core X-Radiographs
X-radiograph negatives of sediment cores collected from Columbia Fjord (top panel) and Jorge Montt Fjord (bottom panel). Core locations are shown in Figure 4.2. Light areas are relatively dense (coarser particles), and dark areas have lower bulk density (finer particles and higher porosity). Solid white particles are likely ice-rafted debris.

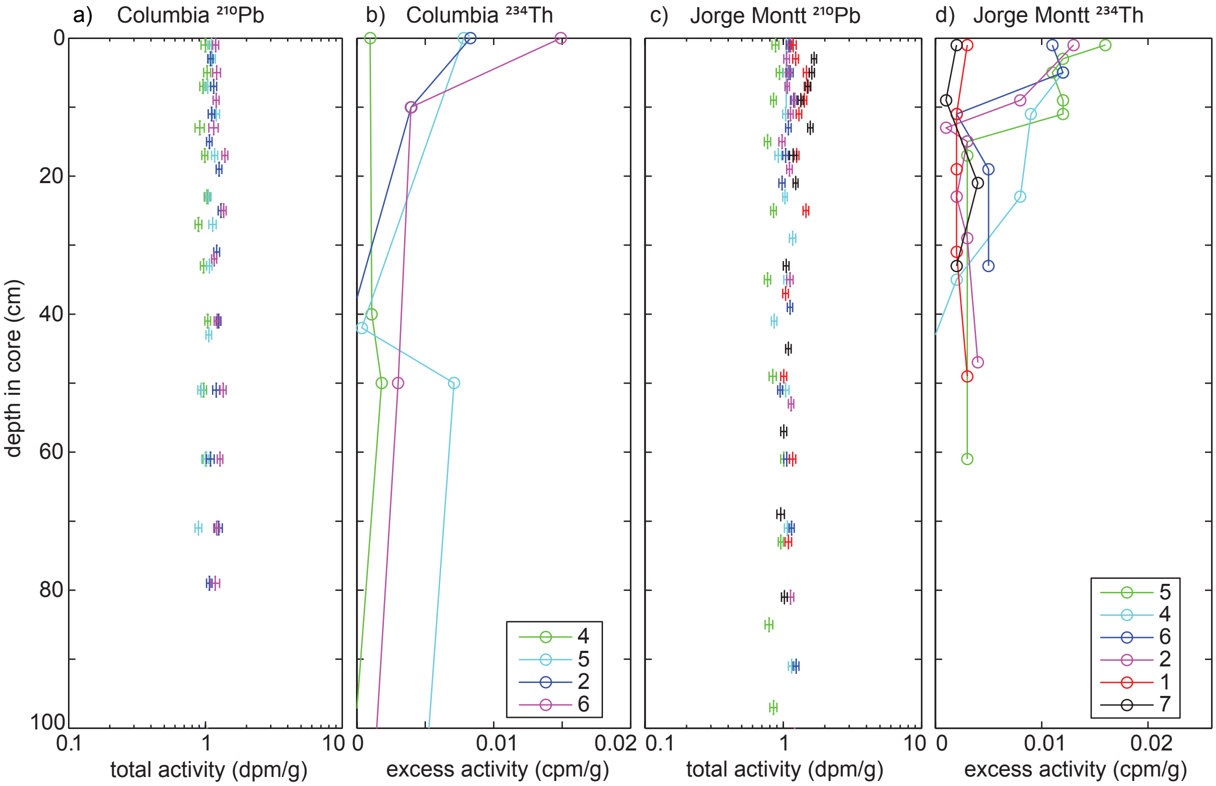

Figure 4.6. Sediment Core Radioisotope Profiles

Profiles of ^{210}Pb and ^{234}Th from Columbia Fjord (a and b) and Jorge Montt Fjord (c and d). Colors represent the same cores in both ^{210}Pb and ^{234}Th plots.

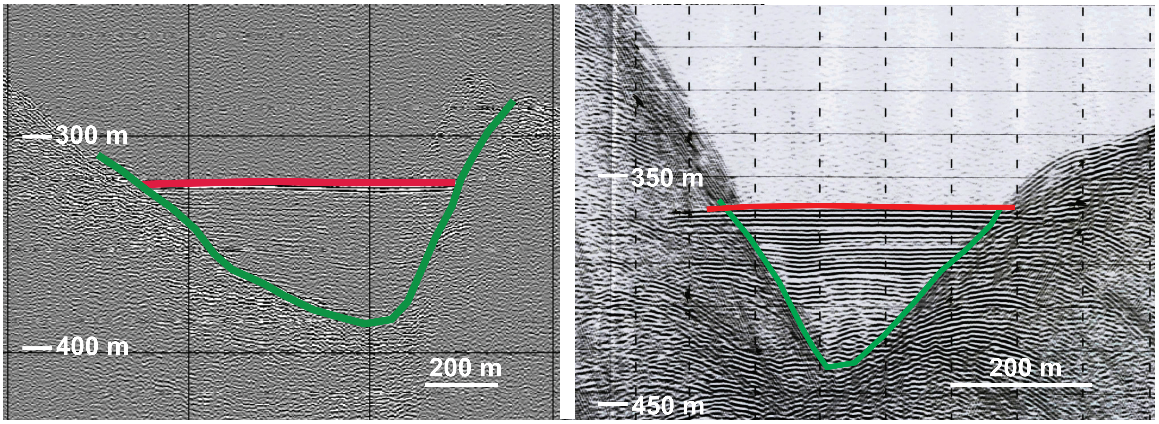

Figure 4.7. Fjord Seismic Profiles
Transverse seismic lines from Columbia Fjord, outer basin **(a)** and Jorge Montt Fjord, main basin **(b)**. Red and green lines indicate the top and base of the post-retreat sediment package.

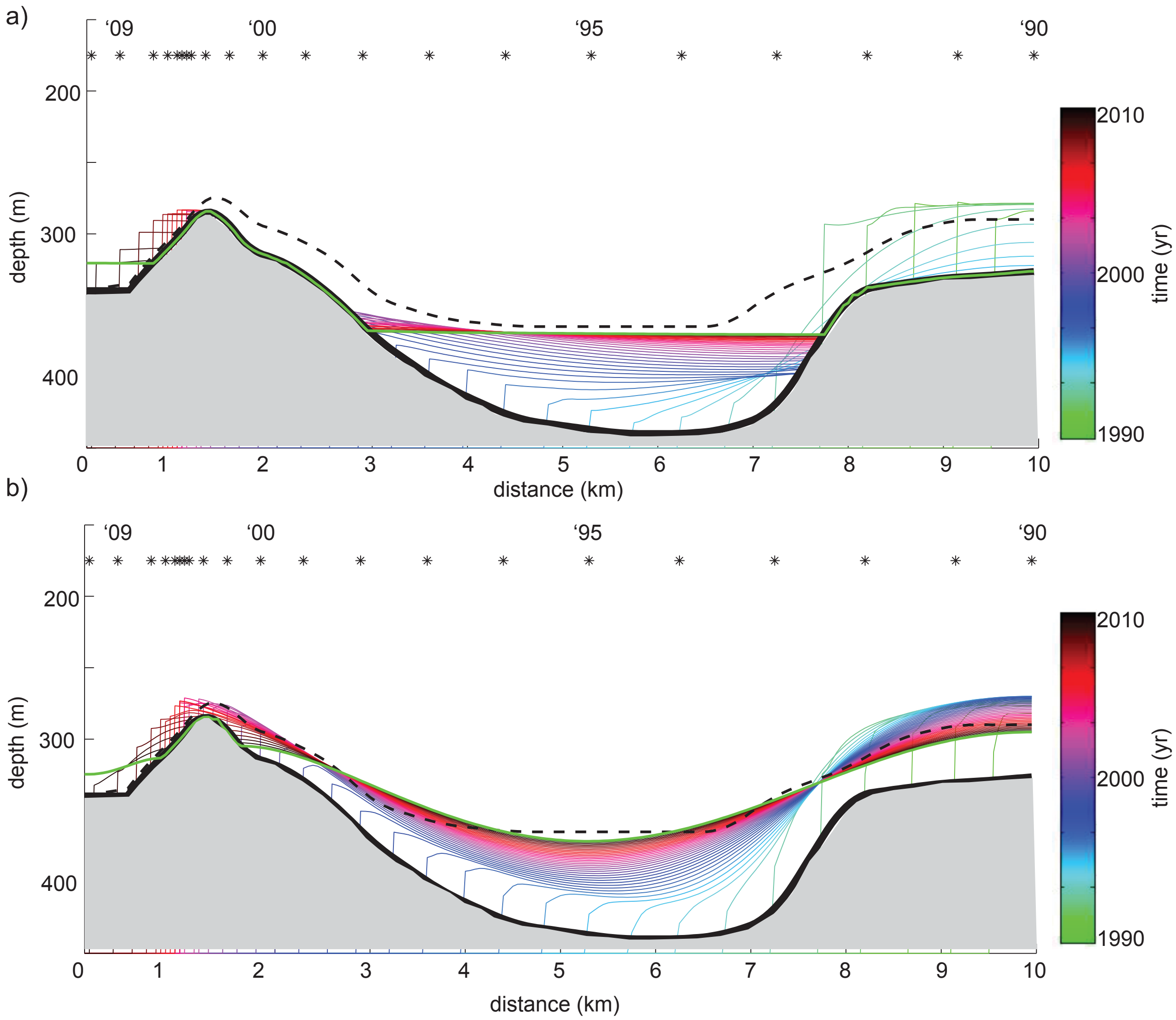

Figure 4.8. Modeled Sediment Basin for Jorge Montt

Two model simulations of the sediment basin created during the retreat of Jorge Montt Glacier using two values for the diffusivity: **(a)** 10^6 m^2 y^{-1}, and **(b)** 10^5 m^2 y^{-1}. In both figures, the gray shaded area is the material underlying the former glacier, the thick black line represents the interpreted base of the post-retreat sediment package, and the dashed black line is the measured fjord depth. The colored lines represent the evolution of the fjord seabed in the year indicated in the color bar, with the thick green line indicating the final model bathymetry in 2010. Any lines above the green line reflect sediment that has been post-depositionally redistributed in the basin.

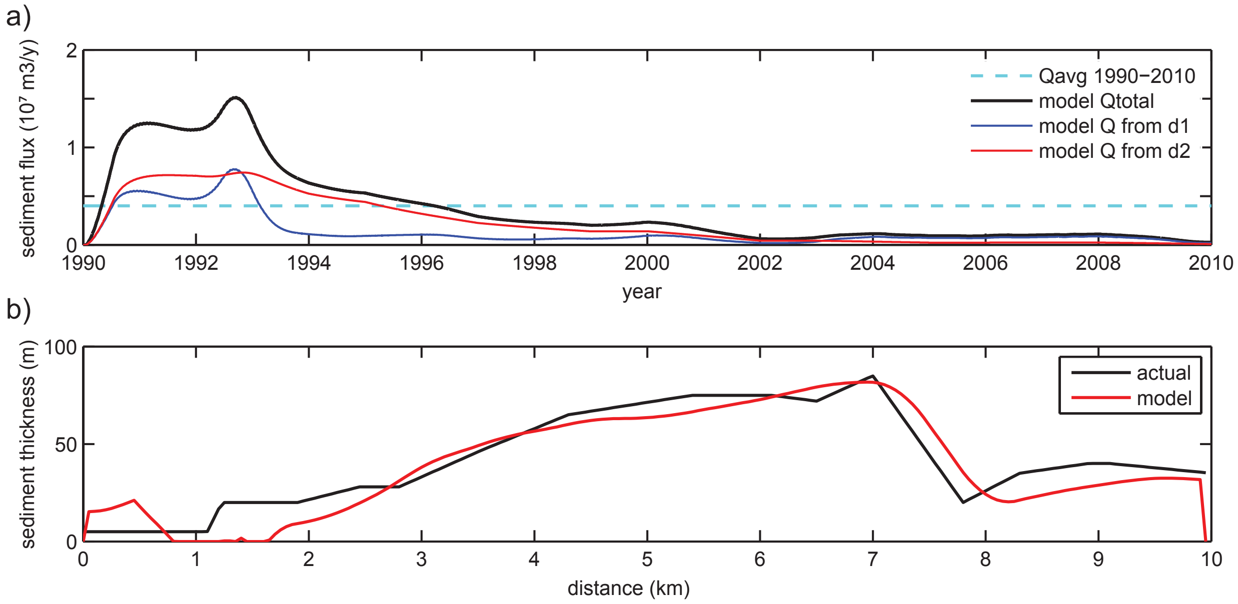

Figure 4.9. Jorge Montt Sediment-Flux History and Distribution
(a) Sediment flux history. The blue dashed line shows the mean flux for 1990-2010 estimated independently of the model from the calculated seismic volume. The thick black line shows the optimized, modeled sediment-flux history, and the blue and red lines indicate the contribution from proximal and distal accumulation (Equation 4.3), respectively. Due to the non-uniqueness of this inverse problem, a series of solutions exist that closely brackets the selected history (thick black line), similar to the output for Columbia Glacier (Figure 3.7). **(b)** Sediment thickness distribution, where the black line is the actual thickness measured from seismic profiles, and the red line is the final modeled sediment thickness distribution. Model results in both (a) and (b) were obtained with $\kappa=10^5$ m^2 y^{-1}.

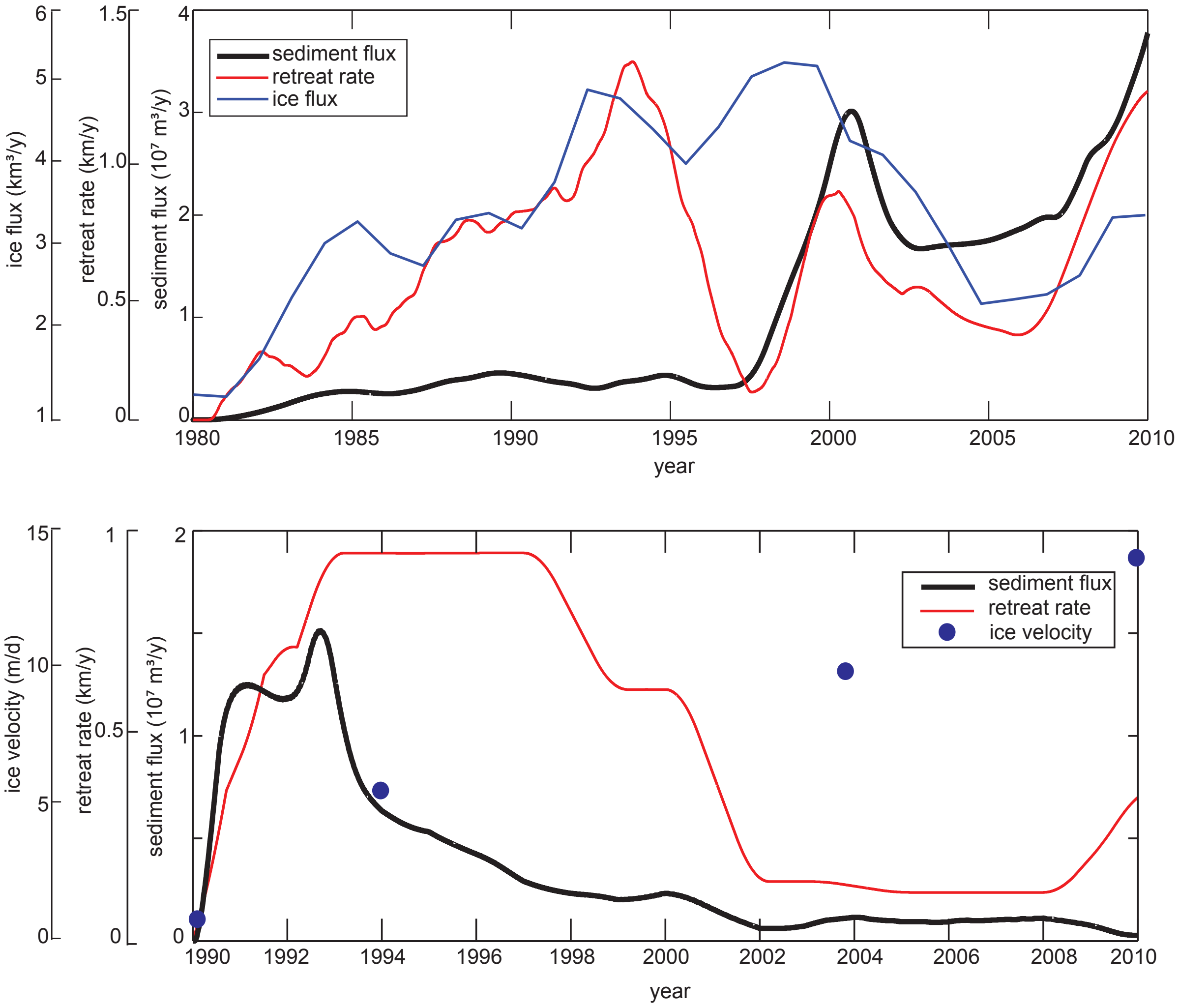

Figure 4.10. Sediment-Flux Histories Compared to Glacier Characteristics
(a) Temporal variations in the modeled sediment flux for Columbia Glacier (black), the retreat rate (red), and the interpolated ice flux (blue) (from O'Neel et al., 2013). The ice flux is used as a proxy for ice speed, assuming a constant cross-sectional area. **(b)** Modeled temporal variations in the sediment flux for Jorge Montt Glacier (black), the retreat rate (red) during the period of rapid retreat, and sparse velocity measurements (blue).

Chapter 5: Conclusions

Interpreting sediment records formed by glacial erosion requires an understanding of the processes controlling the production, transfer, and accumulation of these sediments. This thesis aims to shed light on the rates and processes of sediment accumulation in glacial fjords across a range of climates, and the glacial characteristics controlling the release of sediments into fjords. Rates of sediment accumulation are higher in settings with greater precipitation and meltwater availability, but the flux of sediment delivered to fjords is not a simple function of climate or glacier dynamics. In addition, the geometry of the surface and base of the glacier can control the sediment flux to fjords, and thus the resulting glacimarine stratigraphic record.

Observations of seabed and fjord water-column properties from Alaska, Patagonia, and the Antarctic Peninsula are used to determine sediment-accumulation rates and total sediment volumes delivered to fjords during retreat, and to assess the transport processes likely responsible for creating the deposits. A numerical model is developed to calculate the time-varying delivery of sediment to the temperate glacier fjords over the period of retreat such that the modeled sediment deposits and flux history, subject to the known retreat history, reproduce the observed sediment volume and the principal characteristics of the internal stratigraphic architecture. The sediment-flux histories are then interpreted in light of concurrent observations of glacial behavior to determine whether changes in the flux of sediment delivered to fjords are caused by concurrent changes in glacier dynamics.

In Chapter 2, modern rates of sediment accumulation in fjords along a climatic spectrum from temperate to subpolar are quantified. Profiles of naturally occurring radioisotope ^{210}Pb were determined from 21 cores in 12 fjords along a transect spanning from Chilean Patagonia to the

Antarctic Peninsula. Records from the Antarctic Peninsula cores indicate relatively constant sediment-accumulation rates of 1 to 7 mm yr^{-1} over the past century, despite the concurrent recent rapid warming in this area. The steady sediment accumulation in subpolar fjords is attributed to competing processes: a greater volume of sediment is delivered due to the increase in meltwater production caused by warming, while regional glacier retreat increases the distance between the sediment source and each of the core sites. Records from the South Shetland Islands, however, show that sediment accumulation has accelerated during recent decades, likely due to increasing air temperatures and more frequent precipitation events. In the temperate Chilean fjords, rates of sediment accumulation are >10's mm yr^{-1} near the ice front, and sediment tends to accumulate rapidly and during discrete events. The quantified increase in sediment accumulation from subpolar to temperate settings highlights the role of a warmer and wetter climate for increasing glacier motion, erosion, and the production of sediment.

Chapter 3 examines the history of sediment delivery to Columbia Fjord during the 30-year rapid retreat of Columbia Glacier. Due to the wealth of glaciological observations made through the glacier's retreat, temporal variations in sediment output can be compared closely to concurrent changes in ice behavior. During the retreat, 3.2×10^8 m^3 of sediment accumulated in the fjord, which corresponds to erosion of ~5 mm yr^{-1} averaged over the ~1000 km^2 glaciated area. A model developed to recreate the sediment-flux history from the glacier produces results consistent with the observed sediment thickness and stratigraphic architecture. Results show the sediment flux increased sixfold between 1997 and 2000, and was not caused by changes in glacier dynamics. A reconstructed history of the subglacial hydraulic potential based on existing glacier bed and surface profiles suggests that steep reverse-sloping sections (rising downglacier) of the glacier beds have impeded or prevented sediment transport through the subglacial system during early phases of the retreat. The dramatic increase in sediment flux beginning in ~1998 is attributed to an increase in the sediment-transport capacity of the subglacial hydraulic system, which was likely caused by the progressive steepening of the ice-surface slope over the downglacier portion of the subglacial basin as the glacier retreated. These results highlight the many factors affecting sediment delivery to fjords and the complexity of the preserved glacimarine sediment record.

Chapter 4 compares observations of fjord sediment accumulation and modeled sediment-flux histories for Columbia Fjord, Alaska to those for Jorge Montt Fjord, Patagonia. For both glacier-fjord systems, the volume of sediment delivered by the glaciers during their respective periods of retreat corresponds to erosion across the glaciated area of~4-5 mm yr^{-1}, despite significant differences in geography, tectonics, and the underlying lithology. Profiles of naturally occurring radioisotope ^{234}Th indicate sediment deposition rates of 0.2 to 0.4 cm d^{-1} kilometers away from the ice front in both fjords; profiles of ^{210}Pb are not long enough to permit measurement of sediment accumulation rates on decadal time scales but are consistent with rapid accumulation (~1 m yr^{-1}). Model results and sediment-core properties suggest different depocenters for coarse- and fine-grained sediment delivered to fjords. These results also stress the key role of diffusive gravity-driven processes for the delivery and transport of sediment in order to produce the observed sediment deposits and stratigraphic architecture. Similar to the results for Columbia Glacier and Fjord, the sediment-flux history from Jorge Montt Glacier does not correlate with observations of glacier dynamics; rather, the modeled sediment fluxes for both systems suggest that glacier-specific geometries control the storage of sediment subglacially, its eventual release into fjords, and its preservation in fjord sediment deposits.

The research presented here highlights the rich and complex nature of the connections between climate, glacier properties, and glacial sediment records. Importantly, temporal variations in the delivery to fjords of sediment stored subglacially can dominate the preserved sediment record. The simple model presented here has proven to be a powerful tool for inferring glacier-specific processes controlling the time-varying sediment flux to fjords, and for interpreting the processes controlling the distribution of glacial sediments within fjords. When present, large (km-scale), steep-sided subglacial basins can trap and store substantial volumes of glacially produced sediment for many decades. These sediments can be evacuated as the ice surface steepens across the down-glacier slope of the basin during glacier retreat, or as the basin shoals where sediments accumulate subglacially. This research points to the potentially important roles of glacial sediments, which are often overlooked and understudied, in ice-ocean interactions. Notably, fast sediment accumulation near the termini of temperate glaciers retreating in deepening water is perhaps the only known stabilizing influence on the demise of glaciers that reach the sea.

References

Abram, N.J., Mulvaney, R., Wolff, E.W., Triest, J., Kipfstuhl, S., Trusel, L.D., Vimeux, F., Fleet, L., Arrowsmith, C. (2013). Acceleration of snow melt in an Antarctic Peninsula ice core during the twentieth century. Nat. Geosci., 6(5), 404–411, doi:10.1038/ngeo1787.

Aller, R., Cochran, J. (1976). ^{234}Th/^{238}U disequilibrium in near-shore sediment: Particle reworking and diagenetic time scales. Earth Planet. Sci. Lett., 29, 37–50.

Aller, R.C., Benninger, L.K., Cochran, J.K. (1980). Tracking particle-associated processes in nearshore environments by use of ^{234}Th/^{238}U disequilibrium. Earth Planet. Sci. Lett., 47, 161–175, doi:10.1016/0012-821X(80)90034-5.

Alley R.B., Lawson, D.E., Larson, G.J., Evenson, E.B., Baker, G.S. (2003). Stabilizing feedbacks in glacier-bed erosion. Nature, 424(6950), 758–60, doi: 10.1038/nature01839.

Alley, R.B. (1991). Sedimentary processes may cause fluctuations of tidewater glaciers. Ann. Glaciol., 15, 119–124.

Alley, R.B., Anandakrishnan, S., Dupont, T., Parizek, B., Pollard, D. (2007). Effect of sedimentation on ice-sheet grounding line stability. Science, 315, 1838-1841, doi:10.1126/science.1138396.

Alley, R.B., Cuffey, K., Evenson, E., Strasser, J.C., Lawson, D.E., Larson, G.J. (1997). How glaciers entrain and transport basal sediment: physical constraints. Quat. Sci. Rev., 16, 1017–1038.

Anderson, J.B., Domack, E.W. (1991). Foreward, in Glacial Marine Sedimentation: Paleoclimatic Significance, edited by J.B. Anderson and G.M. Ashley, Geological Society of America, Boulder, CO, p. v-viii.

Anderson, J.B., Shipp, S., Lowe, A., Wellner, J.S., Mosola, A.B. (2002). The Antarctic Ice Sheet during the Last Glacial Maximum and its subsequent retreat history: a review. Quat. Sci. Rev., 21, 49–70.

Anderson, R.S., Anderson, S.P., Macgregor, K.R., Waddington, E.D., O'Neel, S., Riihimaki, C.A., Loso, M.G. (2004). Strong feedbacks between hydrology and sliding of a small alpine glacier. J. Geophy. Res., 109, 1-17, doi:10.1029/2004JF000120.

Andresen, C.S., Straneo, F., Ribergaard, M.H., Bjørk, A.A., Andersen, T.J., Kuijpers, A., Nørgaard-Pedersen, N., Kjær, K.H., Schjøth, F., Weckström, K., Ahlstrøm, A.P. (2011).

Rapid response of Helheim Glacier in Greenland to climate variability over the past century. Nat. Geosci., 5, 37–41. doi:10.1038/ngeo1349.

Appleby, P.G. (2002). Chronostratigraphic techniques in recent sediments, in Tracking Environmental Change Using Lake Sediments, edited by W.M. Last and J. P. Smol, Kluwer Academic Publishers, Dordrecht, The Netherlands, p. 189-219.

Arendt, A.A., Echelmeyer, K.A., Harrison, W.D., Lingle, C.S., Valentine, V.B. (2002). Rapid wastage of Alaska glaciers and their contribution to rising sea level. Science, 297(5580), 382-386, doi:10.1126/science.1072497.

Bartholomew, I., Nienow, P., Mair, D., Hubbard, A., King, M.A., Sole, A. (2010). Seasonal evolution of subglacial drainage and acceleration in a Greenland outlet glacier. Nat. Geosci., 3(6), 408-411, doi:10.1038/ngeo863.

Benn, D., Evans, D.J.A. (2010). Glaciers and Glaciation, 2nd Edition. Routledge, New York.

Benn, D., Hulton, N., Mottram, R. (2007). 'Calving laws','sliding laws' and the stability of tidewater glaciers, Ann. Glaciol., 46(1996), 123-130.

Bentley, S.J., Nittrouer, C.A., Sommerfield, C.K. (1996). Development of sedimentary strata in Eckernforde Bay, southwestern Baltic Sea. Geo-Mar. Lett., 16, 148–154.

Berger, A.L., et al. (2008). Quaternary tectonic response to intensified glacial erosion in an orogenic wedge. Nat. Geosci., 1(11), 793-799, doi:10.1038/ngeo334.

Berthier E., Schiefer, E., Clarke, G.K.C., Menounos, B., Remy, F. (2010). Contribution of Alaskan glaciers to sea-level rise derived from satellite imagery. Nat. Geosci., 3(2), 92–95, doi: 10.1038/ ngeo737.

Bindschadler, R.A., Rasmussen, L.A. (1983). Finite-difference model predictions of the drastic retreat of Columbia Glacier, Alaska. USGS Professional Paper, 1258: D1-D17.

Bogen, J. (1989). Glacial sediment production and development of hydro-electric power in glacierized areas. Ann. Glaciol., 13, 6–11.

Boldt, K.V., Nittrouer, C.A., Hallet, B., Koppes, M.N., Forrest, B.K., Wellner, J.S., Anderson, J.B. (2013). Modern rates of glacial sediment accumulation along a 15° S-N transect in fjords from the Antarctic Peninsula to southern Chile. J. Geophys. Res. Earth Surf., 118, 1–17. doi:10.1002/jgrf.20145.

Bornhold, B.D., Ren, P., Prior, D.B. (1994). High-frequency turbidity currents in British Columbia fjords. Geo-Mar. Lett. 14(4), 238-243.

Boyd, B., Anderson, J., Wellner, J., Fernández, R. (2008). The sedimentary record of glacial retreat, Marinelli Fjord, Patagonia: regional correlations and climate ties. Mar. Geol., 255(3-4), 165–178, doi:10.1016/j.margeo.2008.09.001.

Brown, C.S., Meier, M.F., Post, A. (1982). Calving speed of Alaska tidewater glaciers, with application to Columbia Glacier. USGS Professional Paper, 1258, C1-C13. 4 sheets, scale 1:250,000.

Brown, C.S., Rasmussen, L.A., Meier, M.F. (1986). Bed topography inferred from airborne radio-echo sounding of Columbia Glacier, Alaska. USGS Professional Paper, 1258: G1-G26.

Cai, J., Powell, R., Cowan, E., Carlson, P. (1997). Lithofacies and seismic-reflection interpretation of temperate glacimarine sedimentation in Tarr Inlet, Glacier Bay, Alaska. Mar. Geol. 143, 5–37.

Carlson, P. (1989). Seismic reflection characteristics of glacial and glacimarine sediment in the Gulf of Alaska and adjacent fjords. Mar. Geol. 85, 391–416.

Coakley, J.P., Syvitski, J.P.M. (1991). Sedigraph technique, in Principles, Methods, and Application of Particle Size Analysis, edited by J.P.M. Syvitski, Cambridge University Press, Cambridge, U.K, p. 129–142.

Cook, A., Fox, A., Vaughan, D., Ferrigno, J. (2005). Retreating glacier fronts on the Antarctic Peninsula over the past half-century. Science, 308(5721), 541.

Cowan, E., Powell, R., Smith, N.D. (1988). Rainstorm-induced event sedimentation at the tidewater front of a temperate glacier. Geol., 16, 409–412, doi:10.1130/0091-7613(1988)016<0409.

Cowan, E., Seramur, K., Cai, J., Powell, R.D. (1999). Cyclic sedimentation produced by fluctuations in meltwater discharge, tides and marine productivity in an Alaskan fjord. Sedimen., 46, 1109–1126.

Cowan, E.A., Cai, J., Powell, R.D., Clark, J.D., Pitcher J.N. (1997). Temperate glacimarine varves; an example from Disenchantment Bay, Southern Alaska. J. Sed. Res., 67(3), 536–549.

Cowan, E.A., Powell, R.D. (1990). Suspended sediment transport and deposition of cyclically interlaminated sediment in a temperate glacial fjord, Alaska, U.S.A, in Glacimarine

Environments: Processes and Sediments, edited by J. A. Dowdeswell and J. D. Scourse, Geological Society Special Publication, p. 75-89.

Cowan, E.A., Powell, R.D. (1991). Ice-proximal sediment accumulation rates in a temperate glacial fjord, southeastern Alaska, in Glacial Marine Sedimentation: Paleoclimatic Significance, edited by J. B. Anderson and G. M. Ashley, Geological Society of America, Boulder, CO, p. 61-73.

Cowan, E.A., Seramur, K.C., Powell, R.D., Willems, B.A., Gulick, S.P.S., Jaeger, J.M. (2010). Fjords as temporary sediment traps: History of glacial erosion and deposition in Muir Inlet, Glacier Bay National Park, southeastern Alaska. Geol. Soc. Am. Bull. 122, 1067–1080, doi:10.1130/B26595.1.

Cuffey, K.M., Conway, H., Hallet, B., Gades, A.M., Raymond, C.F. (1999). Interfacial water in polar glaciers and glacier sliding at −17°C. Geophy. Res. Lett., 26(6), 751-754, doi:10.1029/1999GL900096.

Cuffey, K.M., Paterson, W.S.B. (2010). The Physics of Glaciers, 4th edition. Elsevier, New York.

Curran, K.J., Hill, P.S., Milligan, T.G., Cowan, E.A., Syvitski, J.P.M., Konings, S.M. (2004). Fine-grained sediment flocculation below the Hubbard Glacier meltwater plume, Disenchantment Bay, Alaska. Mar. Geol., 203, 83–94, doi:10.1016/S0025-3227(03)00327-X.

DaSilva, J., Anderson, J., Stravers J. (1997). Seismic facies changes along a nearly continuous 24 latitudinal transect: the fjords of Chile and the northern Antarctic Peninsula. Mar. Geol., 143, 103-123.

De Woul, M., Hock, R. (2005). Static mass-balance sensitivity of Arctic glaciers and ice caps using a degree-day approach. Ann. Glaciol., 42, 217-224.

Degeest, A.L., Mullenbach, B.L., Puig, P., Nittrouer, C.A., Drexler, T.M., Durrieu de Madron, X., Orange, D.L. (2008). Sediment accumulation in the western Gulf of Lions, France: The role of Cap de Creus Canyon in linking shelf and slope sediment dispersal systems. Cont. Shelf Res., 28(15), 2031-2047, doi:10.1016/j.csr.2008.02.008.

DeMaster, D.J., McKee, B.A., Nittrouer, C.A., Jiangchu, Q., Guodong, C. (1985). Rates of sediment accumulation and particle reworking based on radiochemical measurements from continental shelf deposits in the East China Sea. Cont. Shelf Res., 4(1-2), 143-158, doi:10.1016/0278-4343(85)90026-3.

DeMaster, D.J., Nelson, T.M., Harden, S.L., Nittrouer, C.A. (1991). The cycling and accumulation of biogenic silica and organic carbon in Antarctic deep-sea and continental margin environments. Mar. Chem., 35(1-4), 489-502, doi:10.1016/S0304-4203(09)90039-1.

Denner, J.C., Lawson, D.E., Larson, G.J., Evenson, E.B., Alley, R.B., Strasser, J.C., Kopczynski, S. (1999). Seasonal variability in hydrologic-system response to intense rain events, Matanuska Glacier, Alaska, U.S.A. Ann. Glaciol., 28, 267–271, doi:10.3189/172756499781821715.

Dierssen, H.M., Smith, R.C., Vernet, M. (2002). Glacial meltwater dynamics in coastal waters west of the Antarctic Peninsula. Proc. Nat. Acad. Sci. USA, 99(4), 1790-5, doi:10.1073/pnas.032206999.

Domack, E., Foss, D. Syvitski, J. (1994). Transport of suspended particulate matter in an Antarctic fjord. Mar. Geol., 121, 161-170.

Domack, E., Leventer, A., Dunbar, R., Taylor, F., Brachfeld, S., Sjunneskog, C. (2001). Chronology of the Palmer Deep site, Antarctic Peninsula: a Holocene palaeoenvironmental reference for the circum-Antarctic. Holoc., 11(1), 1-9, doi:10.1191/095968301673881493.

Domack, E., Williams, C.R. (1990). Fine structure and suspended sediment transport in three Antarctic fjords. Ant. Res. Ser., 50, 71–89.

Domack, E.W., Ishman, S.E. (1993). Oceanographic and physiographic controls on modern sedimentation within Antarctic fjords. Geol. Soc. Am. Bull., 105(9), 1175–1189, doi:10.1130/0016-7606(1993)105<1175.

Domack, E.W., McClennen, C.E. (1996). Accumulation of glacial marine sediments in fjords of the Antarctic Peninsula and their use as late Holocene paleoenvironmental indicators. Ant. Res. Ser., 70, 135–154.

Ducklow, H.W., Baker, K., Martinson, D.G., Quetin, L.B., Ross, R.M., Smith, R.C., Stammerjohn, S.E., Vernet, M., Fraser, W. (2007). Marine pelagic ecosystems: the West Antarctic Peninsula. Phil. Trans. Royal Soc. Bio. Sci., 362(1477), 67-94, doi:10.1098/rstb.2006.1955.

Dukat, D.A., Kuehl, S.A. (1995). Non-steady-state ^{210}Pb flux and the use of ^{228}Ra/^{226}Ra as a geochronometer on the Amazon continental shelf. Mar. Geol., 125(3-4), 329-350, doi:10.1016/0025-3227(95)00018-T.

Dunbar, R.B., Anderson, J.B., Domack E.W. (1985). Oceanographic influences on sedimentation along the Antarctic continental shelf, in Oceanology of the Antarctic Continental Shelf, Antarctic Research Series, vol. 43, edited by S.S. Jacobs, pp. 291-312, AGU, Washington, D.C.

Egholm, D.L., Nielsen, S.B., Pedersen, V.K., Lesemann J.-E. (2009). Glacial effects limiting mountain height. Nature, 460(7257), 884-887, doi:10.1038/nature08263.

Elverhøi, A., Hooke, R.L.B., Solheim, A. (1998). Late Cenozoic erosion and sediment yield from the Svalbard–Barents Sea region: implications for understanding erosion of glacierized basins. Quat. Sci. Rev., 17(1-3), 209–241.

Enomoto, H., Abe, Y. (1983). Reconnaissance studies of meteorology and glaciology in Steffen and Jorge Montt Glaciers, Patagonia, in Naruse, R. (Ed.), Glaciological Studies in Patagonian Northern Icefield, 1984-1984. Japanese Soc. Snow Ice, p.7-14.

Fernandez, R.A., Anderson, J.B. Wellner, J.S., Hallet B. (2011). Timescale dependence of glacial erosion rates: A case study of Marinelli Glacier, Cordillera Darwin, southern Patagonia. J. Geophy. Res., 116(F1), 1-18, doi:10.1029/2010JF001685.

Fountain, A.G., Walder, J.S. (1998). Water flow through temperate glaciers. Rev. Geophy., 36, 299-328.

Fu-Xing, H., Jian-Guo, S., Kun, W. (2012). The influence of sea water velocity variation on seismic traveltimes, ray paths, and amplitude. Appl. Geophy., 9(3), 319-325, doi: 10.1007/s11770-012-0344-2.

Fudge, T., Humphrey, N., Harper, J., Pfeffer, W.T. (2008). Diurnal fluctuations in borehole water levels: configuration of the drainage system beneath Bench Glacier, Alaska, USA. J. Glaciol., 54(185), 297-306.

Gardner, A.S., et al. (2013). A reconciled estimate of glacier contributions to sea level rise: 2003 to 2009. Science, 340(6134), 852–857, doi: 10.1126/science.1234532.

Gilbert, R., Chong, Å., Dunbar, R.B., Domack, E.W. (2003). Sediment Trap Records of Glacimarine Sedimentation at Müller Ice Shelf, Lallemand Fjord, Antarctic Peninsula. Arc. Antarc. Alp. Res., 35(1), 24-33, doi:10.1657/1523-0430(2003)035.

Gilbert, R., Domack, E.W. (2003). Sedimentary record of disintegrating ice shelves in a warming climate, Antarctic Peninsula. Geochem. Geophy. Geosys., 4(4), 1-12, doi:10.1029/2002GC000441.

Goff, J.A., Lawson, D.E., Willems, B.A., Davis, M., Gulick, S.P.S. (2012). Morainal bank progradation and sediment accumulation in Disenchantment Bay, Alaska: Response to advancing Hubbard Glacier. J. Geophys. Res., 117(F2), F02031, doi:10.1029/2011JF002312.

Griffith, T.W., Anderson, J.B. (1989). Climatic control of sedimentation in bays and fjords of the northern Antarctic Peninsula. Mar. Geol., 85(2-4), 181–204.

Hallet, B. (1979). A theoretical model of glacial abrasion. J. Glaciol., 23, 39-50.

Hallet, B. (1996). Glacial quarrying: a simple theoretical model, Ann. Glaciol., 22, 1-8.

Hallet, B., Hunter, L., Bogen, J. (1996). Rates of erosion and sediment evacuation by glaciers: A review of field data and their implications. Glob. Planet. Change, 12(1-4), 213–235, doi: 10.1016/0921-8181(95)00021-6.

Harbor, J. (1992). Numerical modeling of the deveopment of U-shaped valleys by glacial erosion. Geol. Soc. Am. Bull., 104, 1364-1375, doi: 10.1130/0016-7606(1992)104<1364.

Harden, S.L., DeMaster, D., Nittrouer, C. (1992). Developing sediment geochronologies for high-latitude continental shelf deposits: a radiochemical approach. Mar. Geol., 103, 69-97.

Harper, J.T., Humphrey, N.F., Pfeffer, W., Fudge, T., O'Neel, S. (2005). Evolution of subglacial water pressure along a glacier's length. Ann. Glaciol., 40, 31-36.

Harris, P., Domack, E., Manley, P., Gilbert, R. (1999). Andvord drift: a new type of inner shelf, glacial marine deposystem from the Antarctic Peninsula. Geology, doi:10.1130/0091-7613(1999)027<0683.

Hay, W., Sloan, J.L.I., Wold, C.N. (1988). Mass/age distribution and composition of sediments on the ocean floor and the global rate of sediment subduction. J. Geophy. Res., 93, 14933-14940.

Headley, R.M., Enkelmann, E., Hallet, B. (2013). Examination of the interplay between glacial processes and exhumation in the Saint Elias Mountains, Alaska. Geosphere, 9(2), 229–241, doi: 10.1130/GES00810.1.

Hill, P.S., Syvitski, J.P., Cowan, E.A., Powell, R.D. (1998). In situ observations of floc settling velocities in Glacier Bay, Alaska. Mar. Geol., 145, 85–94.

Holland, D.M., Thomas, R.H., de Young, B., Ribergaard, M.H., Lyberth, B. (2008). Acceleration of Jakobshavn Isbræ triggered by warm subsurface ocean waters. Nat. Geosci., 1, 659–664, doi:10.1038/ngeo316.

Holland, M.M., Bitz, C.M. (2003). Polar amplification of climate change in coupled models. Clim. Dyn., 21(3-4), 221-232, doi:10.1007/s00382-003-0332-6.

Hooke, R. (1991). Positive feedbacks associated with erosion of glacial cirques and overdeepenings. Geol. Soc. Am. Bull., 103(8), 1104–1108, doi: 10.1130/0016-7606(1991)103<1104.

Hooke, R., Elverhøi, A. (1996). Sediment flux from a fjord during glacial periods, Isfjorden, Spitsbergen. Glob. Planet. Change, 12, 237-249.

Howat, I.M., Joughin, I., Scambos, T.A. (2007). Rapid changes in ice discharge from Greenland outlet glaciers. Science, 315, 1559–1561, doi: 10.1126/science.1138478.

Hulton, N., Purves, R., McCulloch, R., Sugden, D.E., Bentley, M.J. (2002). The last glacial maximum and deglaciation in southern South America. Quat. Sci. Rev., 21, 233-241.

Humphrey, N., Kamb, B., Fahnestock, M. (1993). Characteristics of the bed of the lower Columbia Glacier, Alaska. J. Geophys. Res., 98, 837–846.

Humphrey, N.F., Raymond, C. (1994). Hydrology, erosion and sediment production in a surging glacier: Variegated Glacier, Alaska, 1982-83. J. Glaciol., 40(136), 539–552.

Hunter, L., Powell, R.D., Lawson, D.E. (1996a). Flux of debris transported by ice at three Alaskan tidewater glaciers. J. Glaciol., 42(140), 123–135.

Hunter, L., Powell, R.D., Lawson, D.E. (1996b). Morainal-bank sediment budgets and their influence on the stability of tidewater termini of valley glaciers entering Glacier Bay, Alaska, USA. Ann. Glaciol., 22, 211–216.

Iken, A., Bindschadler, R.A. (1986). Combined measurements of subglacial water-pressure and surface velocity of Findelengletscher, Switzerland - conclusions about drainage system and sliding mechanism. J. Glaciol., 32(110), 101-119.

IPCC, (2013). Climate change 2013: the physical science basis. Intergovermental Panel on Climate Change, Working Group I, Contribution to the IPCC Fifth Assessment Report, Final Draft.

Iverson, N.R. (1991). Potential effects of subglacial water-pressure fluctuations on quarrying. J. Glaciol., 37(125), 27-36.

Iverson, N.R. (2012). A theory of glacial quarrying for landscape evolution models, Geology, 40(8), 679-682, doi:10.1130/G33079.1.

Jacob, T., Wahr, J., Pfeffer, W.T., Swenson, S. (2012). Recent contributions of glaciers and ice caps to sea level rise. Nature, 482(7386), 514-518, doi:10.1038/nature10847.

Jacobs, S.S., Jenkins, A., Giulivi, C.F., Dutrieux, P. (2011). Stronger ocean circulation and increased melting under Pine Island Glacier ice shelf. Nat. Geosci. 4, 519–523, doi:10.1038/ngeo1188.

Jaeger, J.M., Nittrouer, C.A. (1999a). Sediment deposition in an Alaskan fjord; controls on the formation and preservation of sedimentary structures in Icy Bay. J. Sed. Res., 69(5), 1011–1026.

Jaeger, J.M., Nittrouer, C.A. (1999b). Marine record of surge-induced outburst floods from the Bering Glacier, Alaska. Geology, 27(9), 847-850, doi:10.1130/0091-7613(1999)027<0847.

Jaeger, J.M., Nittrouer, C.A., Scott, N.D., Milliman, J.D. (1998). Sediment accumulation along a glacially impacted mountainous coastline: north-east Gulf of Alaska. Basin Res., 10, 155-173.

Jenkins, A. (2011). Convection-Driven Melting near the Grounding Lines of Ice Shelves and Tidewater Glaciers. J. Phys. Oceanogr., 41(12), 2279–2294, doi: 10.1175/JPO-D-11-03.1.

Joughin, I., Alley, R.B., Holland, D.M. (2012). Ice-sheet response to oceanic forcing. Science, 338, 1172–1176, doi:10.1126/science.1226481.

Joughin, I., Howat, I.M., Alley, R.B., Ekstrom, G., Fahnestock, M., Moon, T., Nettles, M., Truffer, M., Tsai, V.C. (2008). Ice-front variation and tidewater behavior on Helheim and Kangerdlugssuaq Glaciers, Greenland. J. Geophy. Res., 113(F1), 1-11, doi:10.1029/2007JF000837.

Joughin, I., Smith, B.E., Medley, B. (2014). Marine ice sheet collapse potentially underway for the Thwaites Glacier Basin, West Antarctica. Science, 344, 735-738, doi:10.1126/science/1249055.

Kamb, B., Engelhardt, H., Fahnestock, M. (1994). Mechanical and hydrologic basis for the rapid motion of a large tidewater glacier 2. Interpretation. J. Geophys. Res., 99(B8), 15231–15244.

King, J.C., Turner, J., Marshall, G.J., Connolley, W.M., Lachlan-Cope, T.A. (2003). Antarctic Peninsula climate variability and its causes revealed by analysis of instrumental records, in

Antarctic Peninsula Climate Variability, Antarctic Research Series, vol. 79, edited by E. Domack, A. Leventer, A. Burnett, R. Bindschadler, P. Convey, and M. Kirby, pp. 17-30, Antarctic Research Series, AGU, Washington, D.C.

Koppes, M., Conway, H., Rasmussen, L.A., Chernos, M. (2011). Deriving mass balance and calving variations from reanalysis data and sparse observations, Glaciar San Rafael, northern Patagonia, 1950–2005. Cryosph., 5, 791–808, doi:10.5194/tc-5-791-2011.

Koppes, M.N. (2007). Glacier erosion and response to climate, from Alaska to Patagonia, PhD Thesis, Dept. of Earth and Space Sci., Univ. of Washington, Seattle, WA, USA.

Koppes, M.N. (2012). Climate-driven variability of glacier erosion and its impact on mountain evolution. Abstract EP012-0107 presented at 2012 Fall Meeting, AGU, San Francisco, Calif., 3-7 Dec.

Koppes, M.N., Hallet, B. (2002). Influence of rapid glacial retreat on the rate of erosion by tidewater glaciers. Geology, 30(1), 47, doi: 10.1130/0091-7613(2002)030<0047:IORGRO>2.0.CO;2.

Koppes, M.N., Hallet, B. (2006). Erosion rates during rapid deglaciation in Icy Bay, Alaska. J. Geophys. Res., 111(F2), 1–11, doi: 10.1029/2005JF000349.

Koppes, M.N., Hallet, B. (2010). Glacier erosional response to transient climate. Abstract EP52A-03 presented at 2010 Fall Meeting, AGU, San Francisco, Calif., 13-17 Dec.

Koppes, M.N., Hallet, B., Anderson, J.B. (2009). Synchronous acceleration of ice loss and glacial erosion, Glaciar Marinelli, Chilean Tierra del Fuego. J. Glaciol., 55, 207–220, doi:10.3189/002214309788608796.

Koppes, M.N., Montgomery, D.R. (2009). The relative efficacy of fluvial and glacial erosion over modern to orogenic timescales. Nat. Geosci., 2, 644–647, doi:10.1038/ngoe616.

Koppes, M.N., Sylwester, R., Rivera, A., Hallet, B. (2010). Variations in sediment yield over the advance and retreat of a calving glacier, Laguna San Rafael, North Patagonian Icefield. Quat. Res., 73, 84–95, doi:10.1016/j.yqres.2009.07.006.

Krimmel, R.M. (2001). Photogrammetric data set, 1957-2000, and bathymetric measurements for Columbia Glacier, Alaska. USGS Water-Resources Investig. Rep., 01-4089, 46 pp.

Kuehl, S.A., Hariu, T.M., Moore, W.S. (1989). Shelf sedimentation off the Ganges-Brahmaputra system: Evidence for sediment bypassing to the Bengal fan. Geology, 17(12), 1132-1135.

Ledford-Hoffman, P., DeMaster, D., Nittrouer, C. (1986). Biogenic-silica accumulation in the Ross Sea and the importance of Antarctic continental-shelf deposits in the marine silica budget. Geoch. et Cosmoch. Acta, 50, 2099-2110.

Lemke, P., et al. (2007). Observations: Changes in Snow, Ice and Frozen Ground, in Climate Change 2007: The Physical Science Basis. Contribution of Working Group I to the Fourth Assessment Report of the Intergovernmental Panel on Climate Change, edited by S. Solomon, D. Qin, M. Manning, Z. Chen, M. Marquis, K. B. Averyt, M. Tignor and H. L. Miller, Cambridge University Press, New York.

Leventer, A., Domack, E.W., Ishman, S.E., Brachfeld, S., McClennen, C.E., Manley, P. (1996). Productivity cycles of 200–300 years in the Antarctic Peninsula region: Understanding linkages among the sun, atmosphere, oceans, sea ice, and biota. Geol. Soc. Am. Bull., 108, 1626-1644, doi:10.1130/0016-7606(1996)108<1626.

Luckman, A., Murray, T., de Lange, R., Hanna, E. (2006). Rapid and synchronous ice-dynamic changes in East Greenland. Geophys. Res. Lett., 33(3), 2–5 (doi: 10.1029/2005GL025428)

Mackiewicz, N.E., Powell, R.D., Carlson, P.R., Molnia, B.F. (1984). Interlaminated ice-proximal glacimarine sediments in Muir Inlet, Alaska. Mar. Geol., 57, 113–147.

Majewski, W., Wellner, J.S., Szczucinski, W., Anderson, J.B. (2012). Holocene oceanographic and glacial changes recorded in Maxwell Bay, West Antarctica. Mar. Geol., 326, 67-79, doi: 10.1016/j.margeo.2012.08.009.

McCave, I.N., Bryant, R.J., Cook, H.F., Coughanowr, C.A. (1986). Evaluation of a laser-diffraction-size analyzer for use with natural sediments. J. Sed. Pet., 56, 561–564.

McClintic, M.A., DeMaster, D.J. Thomas, C.J. and Smith, C.R. (2008). Testing the FOODBANCS hypothesis: Seasonal variations in near-bottom particle flux, bioturbation intensity, and deposit feeding based on ^{234}Th measurements. Deep Sea Res. Part II: Top. Studies in Oceanogr., 55(22-23), 2425-2437, doi:10.1016/j.dsr2.2008.06.003.

McKee, B., DeMaster, D., Nittrouer, C. (1986). Temporal variability in the partitioning of thorium between dissolved and particulate phases on the Amazon shelf: implications for the scavenging of particle-reactive species. Cont. Shelf Res., 6, 87–106.

McKee, B., Nittrouer, C., DeMaster, D. (1983). Concepts of sediment deposition and accumulation applied to the continental shelf near the mouth of the Yangtze River. Geology, 11, 631–633, doi:10.1130/0091-7613(1983)11<631.

McNabb, R., Hock, R. (2014). Alaska tidewater glacier terminus positions, 1948–2012. J. Geophys. Res. Earth Surf., 119, 153–167, doi:10.1002/2013JF002915.

McNabb, R.W., Hock, R., O'Neel, S., Rasmussen, L.A., Ahn, Y., Braun, M., Conway, H., Herreid, S., Joughin, I., Pfeffer, W.T., Smith, B.E., Truffer, M. (2012). Using surface velocities to calculate ice thickness and bed topography: a case study at Columbia Glacier, Alaska, USA. J. Glaciol., 58, 1151–1164, doi:10.3189/2012JoG11J249.

Meier, M., Lundstrom, S., Stone, D., Kamb, B., Engelhardt, H., Humphrey, N.F., Dunlap, W.W., Fahnestock, M., Krimmel, R.M., Walters, R. (1994). Mechanical and hydrologic basis for the rapid motion of a large tidewater glacier, 1. Observations. J. Geophys. Res. 99, 15219–15229.

Meier, M.F., Dyurgerov, M.B., Rick, U.K., O'neel, S., Pfeffer, W.T., Anderson, R.S., Anderson, S.P., Glazovsky, A.F. (2007). Glaciers dominate eustatic sea-level rise in the 21st century. Science, 317(5841), 1064-1067, doi:10.1126/science.1143906.

Meier, M.F., Post, A. (1987). Fast tidewater glaciers. J. Geophys. Res., 92(B9), 9051–9058.

Meier, M.F., Rasmussen, L.A., Krimmel, R.M., Olsen, R.W., Frank, D. (1985). Photogrammetric determination of surface altitude, terminus position, and ice velocity of Columbia Glacier, Alaska. USGS Professional Paper, 1258: F1-F41. 7 sheets, scale 1:50,000.

Meier, M.F., Rasmussen, L.A., Miller, D.S. (1985). Columbia Glacier in 1984: Disintegration underway. USGS Open File Rep., 85-81, 21 pp.

Merrand, Y., Hallet, B. (1996). Water and sediment discharge for a large surging glacier: Bering Glacier, Alaska, summer 1994. Ann. Glaciol., 22, 233-240.

Michalchuk, B.R., Anderson, J.B., Wellner, J.S., Manley, P.L., Majewski, W., Bohay, S. (2009). Holocene climate and glacial history of the northeastern Antarctic Peninsula: the marine sedimentary record from a long SHALDRIL core. Quat. Sci. Rev., 29, 3049-3065, doi: 10.1016/j.quascirev.2009.08.012.

Milliken, K.T., Anderson, J.B., Wellner, J.S., Bohaty, S.M., Manley, P.L. (2009). High-resolution Holocene climate record from Maxwell Bay, South Shetland Islands, Antarctica. Geol. Soc. Am. Bull., 121(11-12), 1711–1725, doi: 10.1130/B26478.1.

Moffat, C. (2014). Wind-driven modulation of warm water supply to a proglacial fjord, Jorge Montt Glacier, Patagonia. Geophys. Res. Lett., Accepted.

Moffat, C., et al., in prep. Seasonal evolution of the circulation and hydrography in a proglacial fjord in Chilean Patagonia.

Molnar, P., England, P. (1990). Late Cenozoic uplift of mountain ranges and global climate change: chicken or egg? Nature, 346, 29-34.

Molnia, B. (1983). Subarctic glacial-marine sedimentation: a model, in Glacial-Marine Sedimentation, edited by B. Molnia, pp. 95-477, Plenum Press, New York.

Molnia, B.F. (1979). Sedimentation in coastal embayments in the northern Gulf of Alaska. Proceedings of the Offshore Technology Conference. 11, 665-676.

Monien P., Schnetger, B., Brumsack, H.-J., Hass, H.C., Kuhn, G. (2011). A geochemical record of late Holocene palaeoenvironmental changes at King George Island (maritime Antarctica). Antarc. Sci., 23, 255-267, doi:10.1017/S095410201100006X.

Motyka, R.J., Dryer, W.P., Amundson, J., Truffer, M., Fahnestock, M. (2013). Rapid submarine melting driven by subglacial discharge, LeConte Glacier, Alaska. Geophys. Res. Lett. 40, 5153–5158, doi:10.1002/grl.51011.

Motyka, R.J., Hunter, L., Echelmeyer, K. (2003). Submarine melting at the terminus of a temperate tidewater glacier, LeConte Glacier, Alaska, USA. Ann. Glaciol., 36, 57-65.

Motyka, R.J., Truffer, M., Fahnestock, M., Mortensen, J., Rysgaard, S., Howat I. (2011). Submarine melting of the 1985 Jakobshavn Isbræ floating tongue and the triggering of the current retreat. J. Geophy. Res., 116(F1), 1-17, doi:10.1029/2009JF001632.

Motyka, R.J., Truffer, M., Kuriger, E.M., Bucki, A.K. (2006). Rapid erosion of soft sediments by tidewater glacier advance: Taku Glacier, Alaska, USA. Geophys. Res. Lett., 33(24), 1–5, doi: 10.1029/2006GL028467.

Mugford, R.I., Dowdeswell, J.A. (2011). Modeling glacial meltwater plume dynamics and sedimentation in high-latitude fjords. J. Geophys. Res., 116(F1), 1–20, doi: 10.1029/2010JF001735.

Mulder, T., Alexander, J. (2001). The physical character of subaqueous sedimentary density flows and their deposits. Sediment., 48, 269-299.

Mulder, T., Syvitski, J.P.M. (1995). Turbidity currents generated at river mouths during exceptional discharges to the world oceans. J. Geol., 103(3), 285–299.

Mulder, T., Syvitski, J.P.M., Migeon, S., Faugeres, J.-C., Savoye, B. (2003). Marine hyperpycnal flows: initiation, behavior and related deposits. A review. Mar. Pet. Geol. 20, 861–882, doi:10.1016/j.marpetgeo.2003.01.003.

Mullenbach, B.L., Nittrouer, C.A. (2000). Rapid deposition of fluvial sediment in the Eel Canyon, northern California. Cont. Shelf Res., 20(16), 2191-2212, doi:10.1016/S0278-4343(00)00067-4.

Murray, T., et al. (2010). Ocean regulation hypothesis for glacier dynamics in southeast Greenland and implications for ice sheet mass changes. J. Geophys. Res., 115(F3), 1-15, doi:10.1029/2009JF001522.

Nick, F.M., van der Veen, C.J., Oerlemans, J. (2007). Controls on advance of tidewater glaciers: Results from numerical modeling applied to Columbia Glacier. J. Geophys. Res., 112(F3), 1–11, doi: 10.1029/2006JF000551.

Nienow, P., Sharp, M., Willis, I. (1998). Seasonal changes in the morphology of the subglacial drainage system, Haut Glacier d'Arolla, Switzerland. Ear. Surf. Proc. Landf., 23, 825-843.

Nittrouer, C.A., DeMaster, D., McKee, B.A., Cutshall, N.H., Larsen, I.L. (1984). The effect of sediment mixing on Pb-210 accumulation rates for the Washington continental shelf. Mar. Geol., 54, 201-221.

Nittrouer, C.A., Sternberg, R., Carpenter, R. (1979). The use of Pb-210 geochronology as a sedimentological tool: application to the Washington continental shelf. Mar. Geol., 31, 297–316.

Noll, G.T. (2005). Report of equipment and methods to accompany data from Project OPR-P132-RA-05, Eastern Prince William Sound, AK. National Oceanographic and Atmospheric Administration. National Geophysical Data Center, National Ocean Service, Boulder, CO. Columbia Bay Hydrographic Survey RAP Sheets H11493/H11494.

O'Neel, S., Joughin, I.R., March, R.S., Burgess, E.W., Welty, W., Pfeffer, W.T., Larsen, C.F. (2013). High space-time resolution analysis of ice motion at a rapidly retreating tidewater glacier. Abstract C42B-05, presented at 2013 Fall Meeting, AGU, San Francisco, Calif., 9–13 Dec.

O'Neel, S., Marshall, H.P., McNamara, D.E., Pfeffer, W.T. (2007). Seismic detection and analysis of icequakes at Columbia Glacier, Alaska. J. Geophys. Res., 112(F3), 1–14, doi: 10.1029/2006JF000595.

O'Neel, S., Pfeffer, W.T., Krimmel, R.M., Meier, M. (2005). Evolving force balance at Columbia Glacier, Alaska, during its rapid retreat. J. Geophys. Res., 110(F3), 1–18, doi: 10.1029/2005JF000292.

Oerlemans, J. (2005). Extracting a climate signal from 169 glacier records. Science, 308(5722), 675-677, doi:10.1126/science.1107046.

Palinkas, C.M., Nittrouer, C.A. (2006). Clinoform sedimentation along the Apennine shelf, Adriatic Sea. Mar. Geol., 234, 245-260.

Pearce, J.T., Pazzaglia, F.J., Evenson, E.B., Lawson, D.E., Alley, R.B., Germanoski, D., Denner, J.D. (2003). Bedload component of glacially discharged sediment: Insights from the Matanuska Glacier, Alaska. Geology, 31, 7-10, doi:10.1130/0091-7613(2003)031<0007:BCOGDS>2.0.CO;2.

Pelto, M.S., Warren, C. (1991). Relationship between tidewater glacier calving velocity and water depth at the calving front. Ann. Glaciol., 15, 115–118.

Pfeffer, W.T. (2007). A simple mechanism for irreversible tidewater glacier retreat. J. Geophy. Res., 112(F3), 1-12, doi:10.1029/2006JF000590.

Pfeffer, W.T., Cohn, J., Meier, M. (2000). Alaskan glacier beats a dramatic retreat. EOS, Trans. Am. Geophys. Union, 81, 577–584.

Pfeffer, W.T., Harper, J.T., O'Neel, S. (2008). Kinematic constraints on glacier contributions to 21st-century sea-level rise. Science, 321(5894), 1340-1343, doi:10.1126/science.1159099.

Pollard, D., DeConto, R. (2007). A coupled ice-sheet/ice-shelf/sediment model applied to a marine-margin flowline: forced and unforced variations, in Glacial Sedimentary Processes and Products, edited by M.J. Hambrey, P. Christoffersen, N.F. Glaser, and B. Hubbard, International Association of Sedimentologists Special Publication, p. 35-52.

Post, A., O'Neel, S., Motyka, R., Streveler, G. (2011). A complex relationship between calving glaciers and climate. EOS, Trans. Am. Geophys. Union, 92(37), 305-306.

Powell, R.D. (1981). A model for sedimentation by tidewater glaciers. Ann. Glaciol., 2(1), 129–134.

Powell, R.D. (1991). Grounding-line systems as second-order controls on fluctuations of tidewater termini of temperate glaciers, in Glacial Marine Sedimentation: Paleoclimatic Significance, edited by J.B. Anderson and G.M. Ashley, Geological Society of America Special Paper 261, Boulder, CO, p. 75–93.

Powell, R.D., Dawber, M., McInnes, J.N., Pyne, A.R. (1996). Observations of the grounding-line area at a floating glacier terminus. Ann. Glaciol., 22, 217-223.

Powell, R.D., Molnia, B.F. (1989). Glacimarine sedimentary processes, facies and morphology of the south-southeast Alaska shelf and fjords. Mar. Geol., 85(2-4), 359–390.

Powell, R.D., Molnia, B.F. (1989). Glacimarine sedimentary processes, facies and morphology of the south-southeast Alaska shelf and fjords. Mar. Geol., 85, 359–390.

Prior, D.B., Bornhold, B.D., Wiseman, W.J., Lowe, D.R. (1987). Turbidity current activity in a British Columbia fjord. Science, 237, 1330–1333, doi:10.1126/science.237.4820.1330.

Pritchard, H.D., Arthern, R.J., Vaughan, D.G., Edwards, L.A. (2009). Extensive dynamic thinning on the margins of the Greenland and Antarctic ice sheets. Nature, 461(7266), 971–5, doi: 10.1038/nature08471.

Pritchard, H.D., Vaughan, D.G. (2007). Widespread acceleration of tidewater glaciers on the Antarctic Peninsula. J. Geophys. Res., 112(F3), 1-10, doi:10.1029/2006JF000597.

Radić, V., Hock, R. (2011). Regionally differentiated contribution of mountain glaciers and ice caps to future sea-level rise. Nat. Geosci., 4(2), 91–94, doi: 10.1038/ngeo1052.

Rasmussen, L.A. (1989). Surface velocity variations of the lower part of Columbia Glacier, Alaska, 1977-1981. USGS Professional Paper, 1258: H1-H52.

Rasmussen, L.A., Conway, H., Krimmel, R.M., Hock, R. (2011). Surface mass balance, thinning and iceberg production, Columbia Glacier, Alaska, 1948-2007. J. Glaciol., 57(203), 431–440.

Rasmussen, L.A., Meier, M.F. (1982), Continuity equation model of the predicted drastic retreat of Columbia Glacier, Alaska. USGS Professional Paper, 1258: A1-A23.

Rasmussen, L.A., Meier, M.F. (1985). Surface topography of the lower part of Columbia Glacier, Alaska. USGS Professional Paper, 1258: E1-E63.

Rau, F., Braun, M. (2002). The regional distribution of the dry-snow zone on the Antarctic Peninsula north of 70S. Ann. Glaciol., 34, 95-100.

Reynolds, J.M. (1981). The distribution of mean annual temperatures in the Antarctic Peninsula. Brit. Antarc. Sur. Bull., 54(1), 123–133.

Rignot, E., Kanagaratnam, P. (2006). Changes in the velocity structure of the Greenland Ice Sheet. Science, 311(5763), 986–990, doi: 10.1126/science.1121381.

Rignot, E., Koppes, M.N., Velicogna, I. (2010). Rapid submarine melting of the calving faces of West Greenland glaciers. Nat. Geosci., 3, 1–5, doi:10.1038/ngeo765.

Rignot, E., Mouginot, J., Larsen, C.F., Gim, Y., Kirchner, D. (2013). Low-frequency radar sounding of temperate ice masses in Southern Alaska. Geophys. Res. Lett., 40, 5399-5405, doi: 10.1002/2013GL057452.

Rignot, E., Mouginot, J., Morlighem, M., Seroussi, H., Scheuchl, B. (2014). Widespread, rapid grounding line retreat of Pine Island, Thwaites, Smith, and Kohler glaciers, West Antarctica, from 1992 to 2011. Geophys. Res. Lett., 1–8, doi:10.1002/2014GL060140.

Rignot, E., Rivera, A., Casassa, G. (2003). Contribution of the Patagonia Icefields of South America to sea level rise. Science, 302, 434–437, doi:10.1126/science.1087393.

Rignot, E., Velicogna, I., van den Broeke, M.R., Monaghan, A., Lenaerts, J. (2011). Acceleration of the contribution of the Greenland and Antarctic ice sheets to sea level rise. Geophys. Res. Lett., 38, 1–5, doi:10.1029/2011GL046583.

Riihimaki, C.A., Macgregor, K.R., Anderson, R.S., Anderson, S.P, Loso, M.G. (2005). Sediment evacuation and glacial erosion rates at a small alpine glacier. J. Geophys. Res., 110, 1–17, doi: 10.1029/2004JF000189.

Rivera, A., Corripio, J., Bravo, C., Cisternas, S. (2012a). Glaciar Jorge Montt (Chilean Patagonia) dynamics derived from photos obtained by fixed cameras and satellite image feature tracking. Ann. Glaciol., 53, 147–155, doi:10.3189/2012AoG60A152.

Rivera, A., Koppes, M.N., Bravo, C., Aravena, J.C. (2012b). Little Ice Age advance and retreat of Glaciar Jorge Montt, Chilean Patagonia. Clim. Past, 8, 403–414, doi:10.5194/cp-8-403-2012.

Rothlisberger, H. (1972). Water pressure in intra- and subglacial channels. J. Glaciol., 11(62), 177–203.

Rückamp, M., Blindow, N. (2011). King George Island ice cap geometry updated with airborne GPR measurements. Earth System Science Data Discussions, 4(1), 123-139, doi:10.5194/essdd-4-123-2011.

Salcedo-Castro, J., Bourgault, D., Bentley, S.J., deYoung, B. (2013). Non-hydrostatic modeling of cohesive sediment transport associated with a subglacial buoyant jet in glacial fjords: A process-oriented approach. Ocean Model., 63, 30–39, doi:10.1016/j.ocemod.2012.12.005.

Schjøth, F., Andresen, C., Straneo, F., Murray, T., Scharrer, K., Korablev, A. (2012). Campaign to map the bathymetry of a major Greenland fjord. EOS, Trans. Am. Geophys. Union, 93.

Schoof, C. (2007). Ice sheet grounding line dynamics: Steady states, stability, and hysteresis. J. Geophys. Res., 112(F3), F03S28, doi: 10.1029/2006JF000664.

Schoof, C. (2010). Ice-sheet acceleration driven by melt supply variability. Nature, 468(7325), 803-6, doi:10.1038/nature09618.

Seramur, K.C., Powell, R.D., Carlson, P.R. (1997). Evaluation of conditions along the grounding line of temperate marine glaciers: an example from Muir Inlet, Glacier Bay, Alaska. Mar. Geol., 140(704), 307–327.

Sheaf, M.A., Serpa, L., Pavlis, T.L. (2003). Exhumation rates in the St. Elias Mountains, Alaska. Tectonophysics, 367(1-2), 1-11, doi: 10.1016/S0040-1951(03)00124-0.

Shepherd, A., et al. (2012). A reconciled estimate of ice-sheet mass balance. Science, 338, 1183–9, doi:10.1126/science.1228102.

Shreve, R. (1972). Movement of water in glaciers. J. Glaciol., 11(62), 205–214.

Sikonia, W.G. (1982). Finite element glacier dynamics model applied to Columbia Glacier, Alaska. USGS Professional Paper, 1258: B1-B74.

Simms, A.R., Milliken, K.T., Anderson, J.B., Wellner, J.S. (2011). The marine record of deglaciation of the South Shetland Islands, Antarctica since the Last Glacial Maximum. Quat. Sci. Rev., 30(13-14), 1583-1601, doi:10.1016/j.quascirev.2011.03.018.

Smith, L., Alexander, C., Jennings, A. (2002). Accumulation in East Greenland Fjords and on the continental shelves adjacent to the Denmark Straight over the last century based on ^{210}Pb Geochronology. Arctic, 55(2), 109-122.

Sommerfield, C.K., Nittrouer, C.A. (1999). Modern accumulation rates and a sediment budget for the Eel shelf: a flood-dominated depositional environment. Mar. Geol., 154, 227-241.

Stoker, M.S., Pheasant, J.B., Josenhans, H. (1997). Seismic methods and interpretation, in Glaciated Continental Margins: An Atlas of Acoustic Images, edited by T.A. Davis et al., CRC Press, Boca Raton, FL, p. 9–26.

Straneo, F., et al. (2013). Challenges to Understanding the Dynamic Response of Greenland's Marine Terminating Glaciers to Oceanic and Atmospheric Forcing. Bull. Am. Meteorol. Soc., 94(8), 1131–1144, doi:10.1175/BAMS-D-12-00100.1.

Straneo, F., Curry, R.G., Sutherland, D.A., Hamilton, G.S., Cenedese, C., Våge, K., Stearns, L.A. (2011). Impact of fjord dynamics and glacial runoff on the circulation near Helheim Glacier. Nat. Geosci., 4, 322-327, doi:10.1038/ngeo1109.

Straneo, F., Hamilton, G., Sutherland, D.A., Stearns, L.A., Davidson, F., Hammil, M.O., Stenson, G.B., Rosing-Asvid, A. (2010). Rapid circulation of warm subtropical waters in a major glacial fjord in East Greenland. Nat. Geosci., 3, 1–5, doi:10.1038/ngeo764.

Sutherland, D.A., Straneo, F. (2012). Estimating ocean heat transports and submarine melt rates in Sermilik Fjord, Greenland, using lowered acoustic Doppler current profiler (LADCP) velocity profiles. Ann. Glac., 53(60), 50–58, doi:10.3189/2012AoG60A050.

Sutherland, D.A., Straneo, F., Stenson, G.B., Davidson, F.J.M., Hammill, M.O., Rosing-Asvid, A. (2013). Atlantic water variability on the SE Greenland continental shelf and its relationship to SST and bathymetry. J. Geophys. Res. Ocean., 118, 847–855, doi:10.1029/2012JC008354.

Swift, D., Nienow, P., Spedding, N. (2002). Geomorphic implications of subglacial drainage configuration: rates of basal sediment evacuation controlled by seasonal drainage system evolution. Sed. Geol., 149, 5 - 19.

Swift, D.A., Nienow, P.W., Hoey, T.B. (2005). Basal sediment evacuation by subglacial meltwater: suspended sediment transport from Haut Glacier d'Arolla, Switzerland. Earth Surf. Process. Landforms, 30, 867–883, doi:10.1002/esp.1197.

Syvitski, J. (1989). On the deposition of sediment within glacier-influenced fjords: oceanographic controls. Mar. Geol., 85, 301–329.

Syvitski, J.M., Burrell, D.C., Skei, J.M. (1987). Fjords: Processes and Products. Springer, New York.

Syvitski, J.P.M. (1991). Towards an understanding of sediment deposition on glaciated continental shelves. Cont. Shelf Res., 11, 897-937.

Szczucinski, W., Zajaczkowski, M. (2012). Factors controlling downward fluxes of particulate matter in glacier-contact and non-glacier contact settings in a subpolar fjord (Billefjorden, Svalbard), in Sediments, Morphology and Sedimentary Processes on Continental Shelves, vol. 44, edited by M.Z. Li, C.R. Sherwood, and P.R. Hill, International Association of Sedimentologists, Wiley-Blackwell, Oxford, UK, p. 369-386.

Szczucinski, W., Zajaczkowski, M., Scholten, J. (2009). Sediment accumulation rates in subpolar fjords – Impact of post-Little Ice Age glaciers retreat, Billefjorden, Svalbard. Estuar. Coast. Shelf Sci., 85(3), 345-356, doi:10.1016/j.ecss.2009.08.021.

Thomson, S.N., Brandon, M.T., Tomkin, J.H., Reiners, P.W., Vásquez, C., Wilson, N.J. (2010). Glaciation as a destructive and constructive control on mountain building. Nature, 467(7313), 313-7, doi:10.1038/nature09365.

Turekian, K.K., Cochran, J.K. (1978). Determination of marine chronologies using natural radionuclides, in Riley, J.P. (Ed.), Chemical Oceanography. Volume 7: New York, Academic Press, p. 313-360.

Turner, J., Colwell, S.R., Harangozo, S. (1997). Variability of precipitation over the coastal western Antarctic Peninsula from synoptic observations. J. Geophy. Res., 102(D12), 13999-14007, doi:10.1029/96JD03359.

Turner, J., Lachlan-Cope, T., Colwell, S., Marshall, G. J. (2005). A positive trend in western Antarctic Peninsula precipitation over the last 50 years reflecting regional and Antarctic-wide atmospheric circulation changes. Ann. Glaciol., 41(1), 85-91.

Turner, J., Lachlan-Cope, T., Marshall, G., Morris, E., Mulvaney, R., Winter, W. (2002). Spatial variability of Antarctic Peninsula net surface mass balance. J. Geophys. Res., 107, 1-18.

Van den Broeke, M., Bamber, J., Ettema, J., Rignot, E., Schrama, E., van den Berg, W.J., van Mejgaard, E., Velicogna, I., Wouters, B. (2009). Partitioning recent Greenland mass loss. Science, 326, 984–986, doi: 10.1126/science.1178176.

van der Veen, C.J. (1996). Tidewater calving. J. Glaciol., 42(141), 375–385.

van der Veen, C.J. (2002). Calving glaciers. Prog. Phys. Geog., 26(1), 96-122, doi:10.1191/0309133302pp327ra.

Vaughan, D.G., Marshall, G.J., Connolley, W.M., Parkinson, C., Mulvaney, R., Hodgson, D.A., King, J.C., Pudsey, C.J., Turner, J. (2003). Recent rapid regional climate warming on the Antarctic Peninsula. Clim. Change, 60(3), 243–274.

Vieli, A., Nick, F.M. (2011). Understanding and modeling rapid dynamical changes of tidewater outlet glaciers: issues and implications. Surv. Geophys., 32(4-5), 437–458, doi:10.1007/s10712-011-9132-4.

Vorren, T.O., Richardsen, G., Knutsen, S.-M., Henriksen, E. (1991). Cenozoic erosion and sedimentation in the western Barents Sea. Mar. Petro. Geol., 8, 317-340.

Walter, F., O'Neel, S., McNamara, D., Pfeffer, W.T., Bassis, J.N., Fricker, H.A. (2010). Iceberg calving during transition from grounded to floating ice: Columbia Glacier, Alaska. Geophys. Res. Lett., 37(15), 1–5, doi: 10.1029/2010GL043201.

Willems, B.A., Powell, R.D., Cowan, E.A., Jaeger, J.M. (2011). Glacial outburst flood sediments within Disenchantment Bay, Alaska: Implications of recognizing marine jökulhlaup deposits in the stratigraphic record. Mar. Geol., 284(1-4), 1–12, doi: 10.1016/j.margeo.2011.03.004.

Willis, M.J., Melkonian, A.K., Pritchard, M.E., Rivera, A. (2012). Ice loss from the Southern Patagonian Ice Field, South America, between 2000 and 2012. Geophys. Res. Lett. 39, L17501, doi:10.1029/2012GL053136.

Yilmaz, O. (2001). Seismic data analysis: processing, inversion, and interpretation of seismic data. Society of Exploration Geophysicists, Tulsa, OK.

Yoon, H., Park, B., Domack, E. (1998). Distribution and dispersal pattern of suspended particulate matter in Maxwell Bay and its tributary, Marian Cove, in the South Shetland Islands, West Antarctica. Mar. Geol., 152, 261-275.

Yoon, H., Park, B., Kim, Y. (2000). Glaciomarine sedimentation and its paleoceanographic implications along the fjord margins in the South Shetland Islands, Antarctica during the last 6000 years. Palaeogeog., Palaeoclim., Paleoeco., 157, 189-211.

Yoon, H.I., Yoo, K.-C., Bak, Y.-S., Lim, H.S., Kim, Y., Lee, J.I. (2010). Late Holocene cyclic glaciomarine sedimentation in a subpolar fjord of the South Shetland Islands, Antarctica, and its paleoceanographic significance: Sedimentological, geochemical, and paleontological evidence. Geol. Soc. Am. Bull., 122(7-8), 1298-1307, doi:10.1130/B30178.1.

Zhang, P., Molnar, P., Downs, W.R. (2001). Increased sedimentation rates and grain sizes 2-4 Myr ago due to the influence of climate change on erosion rates. Nature, 410(6831), 891-7, doi:10.1038/35073504.

VITA

Katherine V. Boldt was born and grew up outside of Cleveland, Ohio. She received a Bachelor of Arts in Earth Sciences, *cum laude*, from Dartmouth College in Hanover, New Hampshire in 2008. At the University of Washington in Seattle, WA, she earned a Masters of Science in Geological Oceanography in 2010, and a Doctor of Philosophy in Geological Oceanography in 2014.